FEDERAL UNIVERSITY OF OURO PRETO

GRADUATE PROGRAMME ON MATERIALS ENGINEERING

Master's Thesis

"Effect of Ti and Nb Additions on the Formation of Craters for IF Steel Galvanneal Coatings"

Author: Breno Storch

Supervisors: Dr Fernando Gabriel S. Araújo

Dr Joseph McDermid

November, 2009

FEDERAL UNIVERSITY OF OURO PRETO

GRADUATE PROGRAMME ON MATERIALS ENGINEERING

Breno Storch

EFFECT OF Ti AND Nb ADDITIONS ON THE FORMATION OF CRATERS FOR IF STEEL GALVANNEAL COATINGS

Master's Thesis presented to the Materials Engineering Graduate Programme at the Federal University of Ouro Preto, Brazil

Research Area: Coating Developments
Supervisors: Dr Fernando Gabriel S. Araújo
Dr Joseph McDermid

Ouro Preto, Brazil
Federal University of Ouro Preto
2009

MASTER'S THESIS TABLE OF CONTENTS

List of Figures 5

List of Tables 7

Abstract 8

1. INTRODUCTION 9

2. LITERATURE BACKGROUND 10

2.1. INFLUENCE OF ALLOYING ELEMENTS ON IF STEELS 10

2.2. C, N, S AND P STABILIZATION IN IF STEELS 11

2.3. MICROSTRUCTURE OF IF STEELS 13

2.4. CONTINUOUS GALVANIZING AND GALVANNEALING 14

2.4.1. FORMATION OF GALVANNEALED COATINGS 16

2.4.2. GROWTH OF Fe-Zn INTERMETALLIC COMPOUNDS 30

2.4.3. CRATER FORMATION 49

2.4.4. EFFECT OF IF STEEL ALLOYING ELEMENTS ON GALVANNEALED COATING STRUCTURE 53

3. EXPERIMENTAL PROCEDURE 62

3.1. MATERIALS 62

3.2. TESTS PERFORMED 64

3.3. METALLOGRAPHIC CHARACTERIZATION OF AS-RECEIVED SAMPLES. 65

3.4. IF STEEL GA SAMPLES WITH STREAKS 65

3.5. HOT-DIP PROCESS SIMULATOR 66

3.5.1. DEFINITION OF HEAT TREATMENT CYCLES FOR Ti- AND DUAL-STABILIZED IF STEEL GRADES 67

3.5.2. INTERRUPTED CYCLES FOR IF STEEL BARE SAMPLES 68

3.5.3. Ti-STABILIZED IF STEEL GRADE 69

3.5.4. DUAL-STABILIZED IF STEEL GRADE 69

3.5.5. POST-PROCESSING AND STORAGE OF EXPERIMENTAL COUPONS 70
3.6. SAMPLE ANALYSIS TECHNIQUES 70
4. RESULTS AND DISCUSSION 74
4.1. MICROSTRUCTURE CHARACTERIZATION 74
4.2. CHEMICAL PROFILES ON Ti- AND DUAL-STABILIZED IF STEEL BARE AND COATED SAMPLES 75
4.3. CRATER ANALYSIS ON TOP OF GA COATINGS 88
4.3.1. CRATER ANALYSIS ON LIGHT AND DARK STREAKED AREAS FOR AS-RECEIVED GA COATINGS 88
4.3.2. SAMPLES RUN UNDER SPECIAL COOLING CONDITIONS AT THE HOT-DIP PROCESS SIMULATOR 90
4.4. STEEL SUBSTRATE REACTIVITY ALONG FERRITE GRAIN BOUNDARIES ON Ti- AND DUAL-STABILIZED IF STEEL SUBSTRATES: 92
4.4.1. REGIONS OF HIGH REACTIVITY AND FORMATION OF OUTBURSTS 93
4.4.2. REGIONS OF HIGH REACTIVITY AND FORMATION OF CRATERS ON LIGHT AND DARK STREAKED AREAS 93
4.5. THE EFFECT OF THE DIFFUSION OF IF STEEL ALLOYING ELEMENTS TOWARDS THE INTERFACE BETWEEN IF STEEL SUBSTRATES AND GA COATINGS ON CRATER FORMATION 94
4.5.1. Ti DEPLETION AT THE STEEL SUBSTRATE-GA COATING INTERFACE; 94
4.5.2. Nb ENRICHMENT AT THE STEEL SUBSTRATE-GA COATING INTERFACE 95
4.5.3. EFFECT OF Ti AND Nb SURFACE SEGREGATION ON CRATER FORMATION 98
5. CONCLUSIONS 100
6. ACKNOWLEDGEMENTS 101
7. BIBLIOGRAPHY 102

List of Figures

Figure 1. Flowchart of the steps carried out by this research project. 64
Figure 2. Thermal profiles set up for both IF steel grades at the HDP simulator. The markers show sampling conditions. 69
Figure 3. Thermal sequence for sampling with interrupted GA thermal cycles for both IF steel grades at the HDP simulator. 73
Figure 4. Micrograph featuring typical microstructures found for the as-received (as-cold-rolled) samples for Ti-stabilized IF steel substrate (optical microscope, magnification: 100X) 74
Figure 5. Micrograph featuring typical microstructure found for the as-received (as-cold-rolled) sample for dual-stabilized IF steel substrate (optical microscope, magnification: 100X). 75
Figure 6. SEM images at 2100x and 2020x featuring the GA coating cross section for the Ti-stabilized IF steel grade (left-hand side) and the dual-stabilized IF steel grade (right-hand side). 76
Figure 7. Spots chosen along the Ti-stabilized IF steel thermal profile. Region within the solid red square feature the prior condition to sample dipping into the Zn bath. 77
Figure 8. Spots chosen along the dual-stabilized IF steel thermal profile. Region within the solid red square feature the prior condition to sample dipping into the Zn bath. 77
Figure 9. Ti outermost surface concentration along the spots where bare steel samples were taken out of Ti-stabilized IF steel thermal profiles. (S1 to 12 => temperature vs. time condition) 78
Figure 10. Nb outermost surface concentration along the spots where bare steel samples were taken out of Ti-stabilized IF steel thermal profiles. (S1 to 12 => temperature vs. time condition) 79
Figure 11. Ti outermost surface concentration along the spots where bare steel samples were taken out of dual-stabilized IF steel thermal profiles. (S1 to 12 => temperature vs. time condition)..... 80
Figure 12. Nb outermost surface concentration along the spots where bare steel samples were taken out of dual-stabilized IF steel thermal profiles. (S1 to 12 => temperature vs. time condition)..... 81

Figure 13. Ti surface concentration at specific depths results along the thermal cycle set up for the Ti-stabilized IF steel grade (Ti bulk concentration is 0.062%). 82
Figure 14. Nb surface concentration results at 0.02 and 0.10µm depth along the thermal cycle set up for the dual-stabilized IF steel grade (Nb bulk concentration is 0.029%)..... 83
Figure 15. XPS surface analysis results for the dual-stabilized IF steel grade, featuring a Nb 3d3/2 peak whose binding energy is 207.4 eV), which corresponds to Nb2O5. 84
Figure 16. GD-OES Zn, Fe and Al atomic concentration across GA coating for a Ti-stabilized IF steel substrate..... 85
Figure 17. GD-OES Zn, Fe and Al atomic concentration across GA coating for a dual-stabilized IF steel substrate..... 86
Figure 18. Ti and Nb concentrations along a 30 µm-thick GA coating on top of a Ti-stabilized IF steel substrate..... 87
Figure 19. Ti and Nb concentrations along a 12 µm-thick GA coating on top of a dual-stabilized IF steel substrate..... 88
Figure 20. Stereoscope micrographs featuring light and dark streaked areas on top of GA coatings for Ti-stabilized IF steels. Magnification: 6.5 x. 89
Figure 21. SEM micrographs featuring light (right-hand side) and dark (light-hand side) streaked areas on top of GA coatings for Ti-stabilized IF steels. Magnification: 573 x. 89
Figure 22. SEM images at 2300x featuring typical microstructures for a dark streaked area (left-hand side), whose EDS chemistry taken from the bottom matches a Γ phase, and light streaked area (right-hand side), whose chemistry is typical of a δ phase..... 90
Figure 23. Pictures feature the overall outlook of Ti- (left-hand side) and dual-stabilized (right-hand side) IF steel panels that run interrupted GA thermal cycles under faster cooling rates. 91
Figure 24. SEM images and EDS chemistries for craters on bottom of light streaked areas at GA coatings on top of Ti-stabilized IF steel panels after running interrupted GA thermal cycles under faster cooling rates..... 91
Figure 25. SEM images and EDS chemistries for craters on bottom of dark streaked areas at GA coatings on top of Ti-stabilized IF steel panels after running interrupted GA thermal cycles under faster cooling rates..... 92

List of Tables

Table 1. Features of Fe-Zn intermetallic compounds. 30
Table 2. Usual chemistry range of Fe-Zn intermetallic compounds. 31
Table 3. IF Steel substrates and conditions tested. 62
Table 4. Chemistries for the Ti-stabilized IF steel grade and the dual-stabilized IF steel grade. 63
Table 5. Tests performed on the IF steels. 64
Table 6. HDG operating parameters carried out for setting up thermal cycles run on both IF steel grades during HDG simulations. 68
Table 7. Ferrite average grain sizes of the IF steels studied before and after galvannealing. 75

Abstract

Interstitial Free steels feature alloying elements present in an ultra low C matrix that account for C stabilization and consequently a high number of C free interstitials in a ferrite matrix that give these steels the ideal texture, low yield point, favorable plastic strain ratios, high elongation and n-value necessary for an ideal performance on forming press, drawing and stamping operations especially for automotive body part applications.

This Master's thesis indicates that Ti-stabilized IF steel substrates are more reactive than dual-stabilized IF steel substrates probably due to the presence of islands of Nb oxides at the interface between the steel substrate and the GA coating. These Nb oxides may block the Fe-Zn interdiffusion along the ferrite grain boundaries. Hence, higher reactivity rates for Ti-stabilized IF steel grades mean that this substrate is more prone than a dual-stabilized IF steel to the formation of outbursts and consequently the formation of craters, which are morphologically characterized as clusters of outbursts, whose formation mechanisms are based on capillarity effects accounting for amounts of liquid Zn being drained away from these spots. Besides, this work has also explored the typical chemistry and morphology features of craters on top of dark and light streaked areas on GA coatings, showing that there are δ crystals on the bottom of craters on light streaked areas, whereas Γ phase was found on the bottom of craters on dark streaked areas. Also, it turns out that craters on dark streaked regions are deeper than those on light streaked areas. On top of that, the crater coverage on dark streaked regions is larger than on light streaked areas.

1. INTRODUCTION

Interstitial Free or IF steels have been the cornerstone of the steel industry for forming, drawing and stamping applications for a number of years due to their low yield strength, favorable plastic strain ratios and high uniform elongation.

The industry uses Ti-, Nb- and Ti-Nb-stabilized IF grades for a variety of applications. These grades are easy to galvanize as the bulk of the substrate is ferrite and preparation of the substrate surfaces is such that their wettability by liquid Zn-Al alloys becomes trivial. However, it has been noticed that Ti-containing grades do not behave as well as Nb-bearing grades when manufacturing galvannealed coatings. The former usually exhibit features of decreased coating integrity (i.e. decreased coating adherence) and a surface defect whose appearance is crater-like, which can be characterized as a discontinuity on the surface of galvanneal coatings and results in poor coating appearance.

These problems are not commonly seen on the surface of Nb-stabilized IF steel coatings. However, Nb-bearing grades do not generally have the same desirable mechanical properties (particularly with respect to formability) found in Ti containing grades. The former are generally prone to have higher alloying costs requiring higher power to recrystallize anneal and galvanneal. Therefore, Ti-Nb-stabilized IF steel grades were developed as a compromise between these two behaviors.

It is worth pointing out that the differences between these two grades in the galvannealing process are remarkable considering the rather low level of alloying elements in these steels and the fact that the Ti and Nb additions are ‘tied up’ as carbides and nitrides to a large extent.

It is also worth mentioning that modeling work on the chemical development (i.e. Fe content) of galvanneal coatings on IF steel substrates has been performed by some researchers. Some authors have also examined the influence of microstructural and process variables on the structural formation of metallic coatings on IF steels. However, it is

believed that the fundamental origin of the differences between the process behavior of these steel substrates lies in a reasonable comprehension of the effect of substrate reactivity upon the formation, growth and breakdown of the inhibition layer in the galvanizing bath.

The purpose of this project is to assess the cratering formation mechanism on GA coatings and its relation with IF steel reactivities whose main influence depend upon the segregation of Ti and Nb compounds at the ferrite grain boundaries.

2. LITERATURE BACKGROUND

2.1. INFLUENCE OF ALLOYING ELEMENTS ON IF STEELS

The chemical elements Ti and Nb are very effective as microalloying elements in IF steels, influencing the microstructure by both solute drag effect and the formation of nitrides and carbides. Since the solubility product and the physical properties of each element and each compound are different, there exist characteristic differences which cause each of these elements to have specific merits.

Titanium forms nitrides, which are stable at high temperatures, and these Ti nitrides provide control of the austenite grain size at the reheating temperature before hot working and also in the welding, in particular in the heat affected zone close to the fusion boundary. The elimination of free N due to the formation of TiN is positive for the toughness and indirectly makes Nb more effective. Furthermore, the influence of Ti on sulphide shape control had been widely used at a time, when the production of low S contents was not standard.

Niobium is reported by some authors as the most effective microalloying element for grain refinement by controlling the austenite grain size during the reheating processes for heat treatments like normalizing, quenching or carburizing, acting additionally to the traditional AlN technology. Moreover, it has an outstanding status in retarding recrystallization during austenite processing via thermomechanical rolling, resulting in grain refinement, which cannot be obtained by any heat treatment process. Other outstanding effects of Nb, such

as lowering the austenite-ferrite transformation temperature by a solute drag effect of the effective precipitation hardening potential can be used only to a certain extent due to its limited solution in austenite. As a result, the combined usage of microalloying elements is often the optimum solution.

2.2. C, N, S AND P STABILIZATION IN IF STEELS

Interstitial Free (IF) steels are ultra low carbon steels where all the interstitials, generally C and N, have been completely combined with alloying elements and are characterized by low yield strength and excellent formability i.e. high elongation and n-value even when produced through continuous annealing and galvanizing lines.[1]

Therefore, Interstitial Free (IF) steel grain boundaries are essentially C free due to the precipitation of Ti and Nb carbides within the grains.[2]

Regarding to Ti-stabilized IF steels, the more traditional approach is that Ti additions are made to combine with N and S, while Nb additions are made to account for C, as shown by the following relationships:

- $Ti_{stabilize} = 3.42N + 1.5S$;
- $Nb_{stabilize} = 7.74C$.

According to this same traditional approach, the predominant precipitates would be TiN, TiS, $Ti_4C_2S_2$ and NbC, with the amount of each primarily depending upon composition. Recent work has shown that Nb may also be present in a complex carbo-sulfide $(Ti,Nb)_4C_2S_2$.[2]

It has been noticed that, depending upon the Ti level, a substantial amount of Nb may remain in solid solution. In such cases, the solute Nb may be beneficial for property development, especially with respect to hot-dip galvanneal coatings.

Osman et al. [3] mentioned that Nb additions are typically made to stabilize interstitial species. However, there are cases where solute Nb will be desired for property development. Nb additions to these grades may be made to enhance other properties. This

solute Nb has been shown to segregate to grain boundaries, to subgrain boundaries, and to free surfaces. Hook et al. apud Osman et al.[3] showed that a strong relationship between the solute Nb to the grain boundaries will become important in the microstructural development of galvanneal coatings as well as cold work embrittlement resistance.

In these grades, interstitial stabilization primarily occurs through precipitation with Ti, similar to that found in Ti-stabilized steels. The traditionally accepted precipitation sequence in Ti-stabilized steels with atomic ratio S:C:N 1:1:1 is TiN, TiS, $Ti_4C_2S_2$ and TiC, as the temperature decreases. The amount of Ti required to fully stabilize IF steels was expressed as (wt%): $Ti_{stabilize} = 3.42N + 1.5S + 4C$.[3]

Bhattacharya et al. [1] carried out studies on the behavior of Nb additions upon galvanneal coatings. It has been stressed that Nb is also added to IF steels in order to produce 'high strength' IF steels where Nb addition imports strengthening by grain refinement and by precipitation hardening of NbC or Nb(CN). One effect of Nb, which has been well established, is its effect on crystallographic texture. It is known that Nb additions improve the r_{45} value and reduces Δr compared to Ti-IF steels. The other well-known and interesting effect of Nb is the improvement of the galvannealing behavior of IF steels. The work of Tokunaga and Kato apud Bhattacharya et al. [1]showed that the powdering tendency of Ti-Nb-stabilized IF steels is superior to Ti-stabilized IF steels. Moreover, recent work by Cheng apud Bhattacharya et al. [1] has shown that while under certain conditions, the galvannealing rates of Ti-IF and Ti-Nb-IF steels are comparable, it is more consistent in Ti-Nb-IF than in Ti-IF steels.

It is also worth noting that Nb concentration at the surface of annealed Ti-Nb-IF steel sample is about three times of that for Ti-IF sample. Some GD-OES results clearly showed that Nb segregates to the surface both at higher concentrations and to a higher depth in Ti-Nb-IF steels. Through elemental profiles obtained by ESCA, below the outer layer of contaminants (C and O), the segregation of Nb was easily detected in significant amounts in Ti-Nb-IF steels and to a much lesser extent in Ti-IF steels.[1]

Feliu et al [4], in a study oriented to characterize oxides on the surface of galvanneal coatings, observed that a slight increase in the number of white precipitates (Ti nitrides and

sulfides) was seen on the Ti-stabilized IF steels, compared with those observed on the dual stabilized IF steel. However, they mentioned that there had been no correlation yet between those precipitates and any relevant substrate differences.

2.3. MICROSTRUCTURE OF IF STEELS

The interstitial atoms such as C and N feature an important effect upon the deformation behavior of steels. Indeed, discontinuous yielding in steels is strongly related to interstitial species[5,6].

In fact, it has been pointed out that a yield point is bound to stand still even with an interstitial C content of 10 ppm. Furthermore, solute C and N may also minimize the formability, especially work hardening, of steels[7].

Moreover, discontinuous yielding can lead to Lüders bands formation that are detrimental of surface aesthetics, and may also result in premature breakage during forming or even non-uniform springback after deformation.

Therefore, in order to solve those detrimental effects of interstitial species as stated above, Interstitial Free Steels have been developed whose microstructure is nearly free of solute C and N.

Besides, these IF steels predominantly rely on the solid state precipitation of carbides, nitrides, and carbo-sulfide especially in order to reduce the solute interstitial content as shown on a previous session.

Additionally, the total C and N contents are reduced to extremely low levels, typically less than 50 ppm wt C and less than 60 ppm wt N through the use of modern steelmaking techniques at the steelmaking shop such as the circulation-type vacuum degassing process[3].

2.4. CONTINUOUS GALVANIZING AND GALVANNEALING

Hot-dip galvanizing is the immersion of a steel article in a liquid bath of Zn or a Zn alloy, by batch or continuous process.[8]

Hot-dip galvanneal coatings are Fe-Zn alloy coatings, which typically contain between 8 and 12 wt% Fe.[3] They are essentially diffusion coatings that expose the Zn galvanized steel to an annealing temperature around 500 ^{0}C to produce a fully alloyed coating containing Fe-Zn intermetallic phases. This is accomplished by inserting heating and cooling capacity above the liquid Zn pot in order for the galvannealing process to be continuous.[8]

Since galvanneal is the process that converts pure Zn in coating into Fe-Zn intermetallic compounds through diffusion between Zn and substrate steel, the phase evolution of coating upon galvannealing strongly depends on the alloy layer formed first between molten Zn and steel substrate.[9]

Galvanneal steel sheets are important for automotive and other applications because they offer excellent corrosion resistance, good weldability, and good formability.[10] Furthermore, hot-dip galvanneal coating products are becoming particularly popular among car-makers because of their moderate production costs, easy fabrication and good in-service performances. Its sticking-free stamping capability, good spot weldability, and outstanding perforation and cosmetic corrosion resistances are especially worth mentioning. In the case of car body panels, particularly for exposed parts, coating adhesion is of prime importance.[11]

Additionally, it is well know that galvannealed material offers a number of advantages over galvanized sheet: better spot weldability and paint adhesion and less risk for sticking during press forming.[12]

Usually an annealing thermal cycle is required prior to galvannealing. Many studies have been published in which annealing cycles lasting up to several hours have been used to reveal the segregation mechanisms of small alloying element contents towards the surface of steels. These long annealing times are necessary to obtain a sufficient amount of precipitates on the steel surface in order to characterize them by conventional techniques. Far fewer researchers use annealing cycles that are similar (close to 1 minute) to those commonly used during galvanizing in commercial lines.[4]

During galvanneal processing, it was observed that the development of the coating microstructure can be divided into at least four distinct stages, as follows:

- Formation of the Fe-Al inhibition layer;
- Breakdown of the inhibition layer;
- Fe-Zn compound formation dominated by solidification of the coating by δ phase (Fe-Zn intermetallic compound) formation;
- Fe enrichment of the coating via solid state interdiffusion of Fe and Zn.[13]

In the galvannealing process, the cooling tower is transformed into an annealing furnace either by introducing an induction furnace above the gas wiping jets and using a good part of the tower height as a holding furnace, or introducing a gas heating furnace above the gas knives.

On the one hand, bath temperature and dipping time, a result of line speed, are specific operating parameters that can be optimized to control efficient surface cleaning, strip heating and minimization of alloy layer growth during the immersion step.

On the other hand, in order to produce an optimized galvanneal product, it is important to control processing parameters such as heating rate, peak or hold temperature, and cooling rate, as they all affect the amount of alloying that will occur in the coating prior to reaching the tower roll.

Marder et al.[8] affirmed that good process control requires that the effects of heating rate, hold temperature and time, and cooling rate on the Fe-Zn reaction kinetics be well understood so that the optimum coating for the desired properties can be obtained. Besides

processing variables, variations in bath chemistry and substrate composition all contribute to the final microstructure.

Besides the variables associated with hot-dip galvanizing, e.g. bath temperature, substrate alloy content and bath composition, a major variable of the galvannealing process is the line speed, which will control the dependent galvannealing variables such as:

- Heating rate;
- Peak or holding temperature and time;
- Cooling rate.[8]

Furthermore, the water vapor content in the annealing atmosphere was expressed as the dew point value. For IF steels, Feliu et al.[4] reported that the annealing cycle consisted of a linear heating ramp (15 ^{0}C/s) up to 850^{0}C, holding the specimens at this temperature for 40 s and then immediately cooling them at a rate of 15 ^{0}C/s to room temperature.

2.4.1. FORMATION OF GALVANNEALED COATINGS

2.4.1.1. THE Fe-Al INHIBITION LAYER

During galvanneal processing, it was observed that the development of the coating microstructure can be divided into at least four distinct stages, as follows:

- Formation of the Fe-Al inhibition layer;
- Breakdown of the inhibition layer;
- Solidification of the coating by δ formation;
- Growth of Fe-rich phases via solid state interdiffusion of Fe and Zn.[14]

The inhibition layer was observed to be a layered structure of $FeAl_3$ and Fe_2Al_5. Other authors have found the layer to consist of Fe_2Al_5, $FeAl_3$ and/or an Fe-Al-Zn ternary compounds.[15] The formation and dissolution of the inhibition layer is an important issue because it sets the stage for the coating transformation that follows.[14]

Dionne et al.[16] postulated that the formation of an inhibition layer is dependent upon the ferrite grain substrate. They found that the regions associated with the emerging ferrite

grain boundaries showed deeper attack with no residual Al-rich layer, whereas a thin Al-rich layer was detected on the surrounding surfaces where the reaction was less advanced.[16]

Results achieved by McDevitt et al.[17] through TEM analysis show that the inhibition layer displayed two distinct morphologies each covering regions approximately 50 μm^2 in size. The first region was a flat continuous layer, and the second region was highly discontinuous where only 60% of the substrate was covered. Furthermore, it was observed that the structure of the inhibition layer was not strongly influenced by the chemical composition of the substrate steel.

Their TEM observations on three different steel substrates can be summarized as follows:

- After 1s of dipping, an Fe-Al inhibition layer formed on all three substrates and could consist of Fe_2Al_5, FeAl or and Fe-Al solid solution. On top of that layer, Γ_1, ζ or η-Zn was observed.

- After 3s, the dominant microstructure was a thin Fe_2Al_5 inhibition layer covered by a 50-150 nm thick Γ_1 layer, and occasional ζ crystals.

Additionally, electron diffraction on cross-sectional TEM samples identified the Al-rich layer as a structure consisting of Fe_2Al_5 at the steel interface and Γ_1 and ζ lying between the Fe_2Al_5 and the Zn outer layer. The presence of Γ_1 and ζ intermetallic compounds on top of the Fe-Al inhibition layer is quite surprising. It has been a widely held belief that the Fe-Al layer prohibits the formation of any such Fe-Zn compounds.[17]

Some studies reported that Fe_2Al_5 is the main constituent of the Al-rich layer when high Al (> 0.13 wt%) baths are used. However, more recent studies reported that the Al-rich interfacial layer is composed of two Fe-Al intermetallic phases: Fe_2Al_5 and $FeAl_3$. The sublayer in contact with the Zn overlay is mainly $FeAl_3$, while the Al-rich layer on Ti-IF and Ti-Nb-IF steels was composed primarily of Fe_2Al_5. The preferred orientation relationship between Fe_2Al_5 and the ferrite grains of the substrate was identified as $(011)_{Fe}//(001)_{Fe2Al5}$, $[-100]_{Fe}//[-310]_{Fe2Al5}$. It has also been reported that only 0.09 wt% Al is required to slow down the Fe-Zn reaction.[10]

Morimoto et al.[18] confirmed that the formation of an Fe_2Al_5 interfacial layer during galvanizing is the most widely accepted result of many experiments and had been reported by several authors. However, there are also reports apud Morimoto et al.[18] that the interfacial layer is composed of Fe-Al-Zn ternary compounds, mixtures of Fe_2Al_5 and $FeAl_3$, and some researchers Morimoto et al.[18] report observing Fe-Zn compounds instead of an Fe-Al interfacial layer.

They also stated that the Fe_2Al_5 was the primary phase in the interfacial layer and formed a continuous layer on the steel substrate. The Fe_2Al_5 grains could frequently be recognized by characteristic triangular-shaped grain cross-sections. A second Fe-Al intermetallic phase, $FeAl_3$, was observed to lie between the Fe_2Al_5 and the Zn layer. However, the $FeAl_3$ was not ubiquitous in the coating. The thickness of the layer of Fe_2Al_5 and $FeAl_3$ was confirmed to vary between 50 and 300 nm.[18]

Furthermore, at the grain boundary, the Zn composition was nearly twice that of the bulk grain due to the Zn enrichment at the grain boundary observed through a compositional profile across a grain boundary between two Fe_2Al_5 grains. There was a variation in Zn content from grain to grain in Fe_2Al_5. [18]

According to Lin and Meshii, the Fe_2Al_5 phase shows some pillar-like grains of Fe-Al-Zn ternary compound. On an ELC (<0.010 wt% C) steel substrate, they observed only the Fe-Al-Zn ternary compound.[18]

Regarding to selective competition between the formation of Fe-Zn intermetallic compounds and the inhibition layer, O'Dell et al. have observed that ζ phase can form epitaxially upon (111) orientated grains and a melting point of 530^0C. The ordered epitaxial nucleation of the ζ phase upon the substrate becomes energetically favorable due to the reduction in the energy barrier as a result of easy accommodation upon (111) oriented grains. Hence, the Fe-Zn intermetallic compound formation is energetically favorable over the Fe_2Al_5 inhibition layer.[19]

In order to prepare samples for inhibition layer characterization, many researchers have done so through selective dissolution of the Zn overlay by using fuming nitric acid (e.g. 90 vol% HNO_3 according to Baril et al.[10]). The nitric acid dissolved Zn and Zn-Fe compounds, leaving the Fe-Al phase untouched at the surface of the steel substrate.[10]

Regarding to microscopy analysis, it is important to mention that the Fe-Al layers that form in commercial coatings are generally too thin to be observed in cross-section using light optical microscopy or conventional SEM. Therefore, high intensity X-ray sources or parallel beam geometry diffractometers are necessary to detect diffraction peaks from the interfacial layer.[18]

TEM allows for superior spatial resolution and unambiguous phase identification using electron diffraction. SEM provides a broader view of the sample and a clear image of the morphology of the interfacial layer. X-ray diffraction offers the advantage of study from a statistically significant area of the sample. However, the results can be difficult to analyze due to the complexity of the phases in the Fe-Al-Zn system.[18]

With the exception of Lin et al. apud McDevitt et al.[15], who used electron diffraction in TEM, researchers have used either X-ray diffraction (XRD) exclusively or in combination with EPMA to identify the thin inhibition layer. McDevitt et al.[15] commented that there exists some ambiguity in results carried out by both XRD and EPMA analysis because:

- The XRD patterns are very complex and some authors did not precisely identify each diffraction peak;
- There is still some debate regarding the lattice parameters, and thus the correct location of diffraction peaks for Fe_2Al_5;
- The thickness of the inhibition layer can be small, such that the diffracted intensity from the layer is very weak;
- EPMA identification of a phase is only reliable if the layer has reached an equilibrium state. Supersaturation of one element in a phase can lead to incorrect identification of the phase.[15]

2.4.1.2. FORMATION OF THE Fe-Al INHIBITION LAYER

There are often conflicting results about the formation of initial inhibition layer. It is believed that many of the inconsistencies made in observations are due to the nonequilibrium nature of this process. In fact, it is very difficult to explain the decomposition of this inhibition layer because the Fe_2Al_5 is thermodynamically stable in the presence of liquid Zn. Many of the inconsistencies observed are believed to be caused by the differences between nonequilibrium and equilibrium conditions.[20]

It has become clear that the strict use of equilibrium arguments fails to describe the microstructural development observed in galvanneal coatings, especially early in the processing where the local chemical environment might deviate significantly from equilibrium, i.e., occurrence of Fe supersaturation in the Zn bath.[14]

Nevertheless, Tang showed that the formation of the inhibition layer is a two-stage process. The first stage, associated with a high rate of Al uptake at the coating/substrate interface, is controlled by continuous nucleation of Fe_2Al_5, followed by a second stage diffusion-controlled growth process.[8] Additionally, he suggested that the inhibition layer formed on the steel surface by precipitating from an Fe-supersaturated Zn liquid. This mechanism would therefore require the coprecipitation of FeAl and Fe_2Al_5 from the bath.

McDevitt et al. studied the steps of inhibition layer formation, growth and breakdown for three different steel substrates. In the first second of hot-dipping the majority microstructure on all three steel substrates consisted of an Fe-Al layer on the steel surface covered by layers of Γ_1 or ζ phases. Moreover, the inhibition layer was absent on approximately 15% of the steel surface after dipping for one second, in which case the substrate was observed in direct contact with either Γ_1 or ζ crystals. Furthermore, Fe_2Al_5 appeared to comprise approximately 85% of the inhibition layer.[14]

O'Dell et al. reported that the rapid formation of the inhibition layer, about 5 miliseconds, is due to Al's high affinity with Fe and also due to it small critical radius.[19]

2.4.1.3. GROWTH OF Fe-Al INHIBITION LAYER

McDevitt et al. reported that, after three seconds, the inhibition layer grew laterally on the substrate surface so that it covered at least 95% of the surface. At this point only Fe_2Al_5 was observed in the inhibition layer, and no Al was detected in the substrate adjacent to the Fe_2Al_5 layer.

Moreover, it appeared that substrate chemistry had little or no substantial influence on how the Fe_2Al_5 layer developed. The only slight substrate effect observed was that the ζ phase appeared more uniformly distributed on the P-added substrate than on the Ti-Nb IF or Ti IF substrates.[14]

Morimoto et al. added that, whenever the two phases Fe_2Al_5 and $FeAl_3$ coexist, Fe_2Al_5 was always observed in contact with the steel substrate. It is likely that the microstructure developed by $FeAl_3$ formed first on the steel substrate, followed by subsequent precipitation and growth of Fe_2Al_5. There would be a thermodynamic driving force to nucleate Fe_2Al_5 at the interface between $FeAl_3$ layer and the Fe substrate. Once nucleated, Fe_2Al_5 could grow by consuming $FeAl_3$ as Fe diffused into the layer. At the end of the day, one might say that Fe_2Al_5 is responsible for inhibiting the growth of Fe-Zn compounds.[18]

2.4.1.4. BREAKDOWN OF Fe-Al INHIBITION LAYER

Dionne et al. observed that the first step of the breakdown of the inhibition layer at the beginning of the galvannealing reaction is the enrichment of the inhibition layer with Zn. The second step in the breakdown of the inhibition layer is the transformation of the Zn-enriched Fe_2Al_5 phase into a layer of δ crystals.[16]

It has been thought by many authors that the mechanism that operates in the inhibition layer breakdown may be strongly influenced by the initial state of the compound layers.[14]

Marder et al. stated that the inhibition layer is a transient phenomenon in galvannealing coatings, explained by thermodynamic equilibrium between Fe_2Al_5 and the liquid. If some regions of overlay/substrate interface have little Al content, Zn atoms attack substrate through ferrite grain boundaries, which are short circuit paths for Zn atom diffusion. When Zn reaches the substrate, it reacts with Fe, nucleating Fe-Zn intermetallic phases at the

Fe_2Al_5 inhibition layer/substrate interface that bursts the layer apart into the surrounding bath. Since Zn atom diffusivity is too high, it diffuses back to the overlay forming outbursts, totally destroying the Fe-Al inhibition layer.[8]

Similarly, McDevitt et al. observed that substrate chemistry had little or no effect on the formation of the inhibition layer, but strongly affected the breakdown of the Fe-Al layer where the inhibition layer survived significantly longer on the P-added steel substrate. There was no evidence that the inhibition layer disappeared due to mechanical breakage by growth of Fe-Zn compounds in outbursts between the layer and the steel substrate on samples galvannealed at 500 ^{0}C.[14]

Therefore, they stated that the inhibition layer breakdown did not occur via outburst mechanism, rather it was eliminated by dissolution into the substrate and possibly by consumption by the Γ_1 phase. It was reported that the Fe_2Al_5 inhibition layer began to disappear upon removal from the Zn bath and heating to 500 ^{0}C. The layer was nearly completely dissolved on the Ti-Nb IF and the Ti IF substrates by the time the sample reached 500 ^{0}C.[14]

From three key observations regarding breakdown of the inhibition layer, McDevitt et al. proposed their theory:
The thickness of the inhibition layer decreased with processing time;
The composition of the inhibition layer changed;
The composition of the substrate originally in contact with the inhibition layer changed.[14]

Thus, it was assumed that there is direct evidence that the inhibition layer dissolved at least in part by Al diffusion into the steel substrate, according to the following statements:

The thickness of the inhibition layer decreased with processing time. The Al concentration in the substrate near the coating/substrate interface was observed to increase when the inhibition layer had disappeared, and the Zn concentration of the inhibition layer increased with processing time. These observations support a dissolution mechanism where the inhibition layer is dissolving by Al diffusing into the substrate at the substrate/inhibition layer interface.[14]

Al is expected to diffuse into the substrate as the chemical potential of Al in Fe is lower than in Fe_2Al_5 until the Al concentration of the Fe exceeds 17 wt%. However, due to the thickness of the substrate relative to that of the Fe_2Al_5 layer, there can not be enough Al available for the substrate to reach the equilibrium concentration of Al. There will always be an Al concentration gradient in the substrate such that Al will diffuse away from the Fe_2Al_5 inhibition layer, and the Fe_2Al_5 layer will continue to dissolve.[14]

Zn enrichment of the Fe_2Al_5 concurrent with the Al depletion is not unexpected as the system seeks an equilibrium condition. The combination of Al depletion and Zn enrichment lead to the disappearance of the inhibition layer by dissolution into the steel substrate and possibly simultaneous consumption of the inhibition layer by the existing Γ_1 phase.[14]

Finally, on non-P added substrates, a higher Al concentration was observed at Fe substrate grain boundaries. This observation indicates grain boundary and possibly interfacial diffusion, which are significantly faster than bulk diffusion, are operating in the present case of diffusion of Al into the substrate.[14]

Morimoto et al. also states that it is not likely that substrate grain boundaries play an important role in the breakdown of the inhibition layer, since no evidence that grain boundaries in the steel substrate were locations of enhanced formation of the inhibition layer, nor were the grain boundaries a site for the local breakdown of the inhibition layer. Substrate grain boundaries did not show penetration of Al or Zn indicating that their diffusion into the steel substrate is also not likely an important factor in the breakdown of the inhibition layer.[18]

In fact, the composition profile in the direction normal to the interface indicates that bulk diffusion of Zn into the inhibition layer may not be an important diffusion mechanism because the Zn concentration was unchanging with distance into the Fe_2Al_5 grain. In contrast, the profile across the Fe_2Al_5 grain boundary indicating that grain boundary diffusion of Zn through the inhibition layer may be important in the breakdown of this layer.[18]

On the contrary, Jordan et al. observed that the effect of substrate grain size on Fe-Zn phase formation and growth supports the mechanism that the Fe-Al inhibition layer is first attacked by liquid Zn at sites corresponding to substrate steel grain boundaries. This theory will be discussed in a further session where the outburst mechanism is more clearly explained. [2]

Finally, Guttman proposes a diffusion-assisted mechanism to explain the inhibition breakdown and the localization of the outburst. Indeed, the diffusion of Zn towards the steel substrate through the Fe_2Al_5 layer could be the mechanism that explains the destruction of the diffusion barrier, which is called the inhibition layer. The diffusion short circuits through Fe_2Al_5 may be the grain boundaries of the layer. [10]

2.2.1.5. EFFECT OF OPERATIONAL PARAMETERS ON THE INHIBITION LAYER

McDermid et al. reported that bath effective Al controls the formation of the η-$Fe_2Al_5Zn_x$ layer at the steel/coating surface such that, at low bath Al contents, the layer is thin and inhibition layer occurs rapidly, facilitating the galvannealing operation. On the other hand, at high bath Al contents, it promotes the formation of a thicker inhibition layer in which inhibition breakdown is prevented and a pure metallic coating results.[21]

Marder et al. reported that increasing the Al content or decreasing the bath temperature increases the stability of the Fe-Al inhibition layer. The stability of the Fe_2Al_5 interfacial layer is enhanced by high Al levels (> 0.15 wt% Al) inhibiting Fe-Zn phase formation in the short term, whereas Fe-Zn reactions are enhanced by low Al bath levels (< 0.15 wt% Al).[8]

Many researchers believe that there is a threshold bath Al level around 0.14 wt% below which no Fe-Al inhibition layer should form. However, Pelayo et al. presented results that conclusively show that an Fe-Al interfacial layer forms under the low bath Al content (0.14 wt% total Al), short dipping time (3 seconds) conditions of commercial hot dip galvannealing. Additionally, they observed that, as the dipping time in the Zn bath increased, the coverage of the substrate by the Al-rich layer increased.

Moreover, the surface of the Fe-Al interfacial layer was generally flat and compact. In contrast, the surface morphology of the inhibition layer formed in a 0.20 wt% Al bath was sharply faceted. Some of the differences in morphology and microstructure of the grains of the inhibition layer in coatings produced in a 0.14 wt% Al and 0.20 wt% Al baths may be a result of $FeAl_3$ being present on the surface for one processing condition and Fe_2Al_5 being present on the surface in the other processing condition. The difference in surface morphology may also result from different growth mechanisms of the Fe-Al layer in the low and high Al content Zn bath processing conditions.[15]

Morimoto et al. observed that, in long dipping experiments, the supply of Al to the interface is effectively unlimited and controlled only by the rate at which Al can diffuse within the molten Zn bath. In commercial production, the amount of Al is constrained as soon as the trip exits the bath to that present in any interfacial layer plus that in the liquid Zn layer exiting with the strip. This difference may have an important effect on the growth or subsequent dissolution of the interfacial layer.[18]

Baril et al. stated that Al content in the inhibition layer generally increases with immersion time and increased Al content in the bath. Furthermore, longer immersion times in the Al-containing Zn lead to a more complete Al-rich layer and thereby reduce the amount of Fe in the coating as a result of Fe-Zn reactions during cooling. Yet this is not uniform. Hence, longer immersion times also lead to an increase of the coating Fe, due to Fe-Zn reactions in some areas, while the Al-rich layer grows in other areas.

On the other hand, when the Al level in the bath is below 0.12%, the Fe/Al ratio is strongly related to the immersion time, which suggests that the rate of the Fe-Al reaction is lower than that which occurs for the intermetallic formation of Fe-Zn. Thus, for this relatively low Al content (0.12%), the Fe-Zn reactions and the formation of Al-rich layer take place concurrently.

They added that one major effect of rapid solidification and increased metastability is an extension of solid solubility limits. Consequently, more excess Zn can be present in the Fe_2Al_5, and the Zn content of the Al-rich layer should be between the $ZnFeAl_3$ phase and the stable Fe_2Al_5 phase. By its way, the Fe_2Al_5 crystals have a strong crystallographic

texture. X-ray diffraction using parallel beam optics showed a strong (513) reflection. This reflection had been related to (200) planes parallel to the surface of the substrate. In addition, this crystallographic texture of the Al-rich layer is related to the Al content of the bath. The interfacial layer studied was mainly constituted by Fe_2Al_5 with (200) planes parallel to the substrate surface.[10]

Reporting results related to the effect of substrate grain size upon the inhibition layer, Jordan et al. observed that substrate grain size is a more significant factor in Al-containing baths than in the 0.00 wt% Al-Zn baths, in which the Fe_2Al_5 inhibition layer does not form, negating any incubation time necessary for Fe-Zn phase nucleation and growth. A large grain seized ULC substrate promoted the stability the Fe-Al-Zn inhibition layer and delayed the formation of Fe-Zn phases.[2]

Faderl et al. reported that increasing the difference between the strip entry temperature and the Zn bath temperature increased the Al content of the interfacial layer.[15]

2.2.1.6. EFFECT OF SUBSTRATE CHEMISTRY ON THE INHIBITION LAYER

In order to determine how the different substrate compositions influence the beginning of galvannealing reaction, interrupted galvannealing treatments are performed to induce partial breakdown of the inhibition layer. [16]

Miyasaka et al. concluded that the acceleration or retardation of galvannealing reaction by the addition of C, P, Ti, Nb or B alloying elements was not caused through the change of the amount and/or structure of Fe-Al-Zn initial layer.[22]

Morimoto et al. observed that the grain size of the interfacial layer on the IF substrate sample was significantly larger (0.5 μm) in the lateral dimensions than on the P, Mn-added sample (0.2 μm), but both samples showed the same faceted morphology. Moreover, the grain size was the only difference observed between the two samples. The composition, thickness, and the constituent phases of the interfacial layer were the same for both substrates.

Nevertheless, the difference in grain size between Fe_2Al_5 formed on the two substrates suggests that the segregation of P and Mn on the substrate surface decreases the nucleation rate of the interfacial layer and delays the formation and growth of the inhibition layer. This result may be related to observations that the rate of the galvanneal reaction is slower on P-added steel substrates than on IF substrates.[18]

Really, Lin et al. apud Jordan et al.[23] proposed an alternative mechanism, whereby P segregates to the steel surface during recrystallization annealing, stabilizing the inhibition layer and retarding the rate of Fe-Zn phase growth reactions during galvanizing.

However, Jordan et al.[23] observed that, in a 0.00 wt% Al-Zn bath, the kinetics of the total alloy layer and individual Fe-Zn phase layer growth were not influenced by the ion implantation of P. The total layer growth as well as the individual phase layer growth followed the same growth-time relationships on both the P- and non-P-ion implanted surfaces. Coverage of the steel/coating interface by the total Fe-Zn alloy layer was complete on both surfaces, indicating the P-ion implantation did not retard or inhibit the overall Zn attack of the steel surface. Briefly, they concluded that P-ion implantation did not affect the composition of the Fe-Zn-Al reaction layer. However, the total thickness of the Fe_2Al_5 (Zn) layer was found to be slightly larger at all reaction times for the non-P-ion implanted surface.

Similarly, in a 0.20 wt% Al-Zn bath, growth kinetics of the Fe_2Al_5(Zn) showed a linear growth rate (n=1) for both surfaces, independent of P surface segregation. It appeared for them that the grain size of the substrate and its effect on the grain size of the Fe-Al-Zn inhibition layer are the dominant reaction mechanisms as compared to surface chemistry (P surface segregation).

Guttman et al. apud Jordan et al.[23] proposed a mechanism that liquid Zn diffusion is the most rapid at random high-angle boundaries of the Fe_2Al_5 inhibition layer, and these high-angle boundaries could correspond in location to the sites of underlying substrate steel grain boundaries. Thus, in contradiction to the suggestion by Lin et al., P segregation to substrate steel surfaces is not an important mechanism in the Fe-Zn reaction. Instead, substrate grain size dominates the nucleation and formation of Fe-Zn phases with P only

acting to retard Zn diffusion along substrate steel grain boundaries by segregating in these boundaries, in agreement with Allegra et al. apud Jordan et al.[23]

Lee et al. studied the influence of Ni additions upon the inhibition layer. They observed that, in the absence of Ni addition, Al is mainly concentrated at the interface between Zn coating and the base steel. As a result, a dense Fe-Al inhibition layer forms at the interface presumably acting as a diffusion barrier. In contrast, the Al concentration at the interface was remarkably reduced by the 0.15 wt% Ni addition, and the Al distribution over the interface is almost the same as that of Ni. This means that Ni strongly interacts with Al at the interface. Therefore, it seems that the inhibition layer of Fe_2Al_5 decomposes thermally and a new phase of Al-Ni intermetallics forms in the coating layer. These intermetallics presumably accelerate the Fe-Zn alloy reaction.[20]

Finally, Dionne et al. carried out Mn and Ti mapping of FIB cross-sections. They revealed numerous surface oxides located within the inhibition layer. The surface oxides did not affect the thickness of composition of surrounding inhibition layer phases and the Fe_2Al_5 phase was not alloyed with either Mn or Ti. [16]

2.4.1.7. EFFECT OF IF STEEL ALLOYING ELEMENTS ON THE INHIBITION LAYER

Bhattacharya et al. observed that Nb segregation to the surface may affect galvannealing in two ways. It may affect the diffusion of Fe into the Zn layer during galvannealing or it may affect the formation of the inhibition layer that, in turn, will influence the galvannealing process. In any case, their study proved that Nb segregation to the surface, in addition to grain boundary segregation, explains why the galvannealing behavior of Ti-Nb-stabilized IF steels is markedly different than Ti-stabilized IF steels.[1]

Similarly, Osman et al. reported that the breakdown of the inhibition layer for Ti-stabilized steels occurred randomly, but was more uniform for Ti-Nb-stabilized steels.[3]

However, Miyasaka et al considered that C, Ti and Nb did not affect the amounts and structure of Fe-Al-Zn barrier layer, but the influence of Ti and Nb was greater on the reduction of C_{eff} – whose formula usually is $C_{eff} = C – (Ti – N.48/14)/4 – Nb.12/93$ – and

presumably C segregated at the ferrite grain boundary, and resultant change in metal diffusion through grain boundary, than on the stability and protectability of the Fe-Al-Zn barrier layer.[22]

Meshii et al. supported the theory that, since the growth of the δ phase did not occur until Fe_2Al_5 layer had decomposed, it is suspected that the non-uniform growth can be contributed in part to non-uniform dissolution of the inhibition layer on the Ti IF and Ti-Nb IF substrates. Such behavior is expected because substrate grain boundaries acted as sites for enhanced Al dissolution from the Fe_2Al_5 into the substrate steel which should result in faster dissolution of the Fe_2Al_5 layer at the substrate grain boundaries.[13]

Dionne et al.[16] reported that the major phase in the inhibition layer was Fe_2Al_5 containing 7-11 wt% Zn for a Ti-stabilized IF steel and 5-14 wt% Zn for a Ti-Nb-stabilized IF steel. Moreover, for the Ti IF steel, a Fe-Al-Zn phase with 40-50 at% Al and up to 30 at% Zn was observed, suggesting that significant diffusion of Zn had taken place during galvanizing and/or during post-galvanizing cooling.

In previous studies, the $FeAl_3$ phase had been detected as a minor constituent of the inhibition layer on Ti-Nb and Ti-Nb-P IF steels galvanized in a hot dip simulator and in a continuous galvanizing line. A small amount of $FeAl_3$ in the inhibition layer would be unlikely to affect significantly the galvannealing response.

The size of the inhibition layer grains is of interest since it could have a significant influence on the kinetics of inhibition breakdown during galvannealing. In this respect, the Ti IF steel showed the thinnest minimum inhibition layer, of 30 nm, and the Ti-Nb IF steel a thickness of 45-50 nm.

Moreover, the breakdown of the Fe_2Al_5 layer in the case of the Ti- and Ti-Nb-IF steels was significantly faster in the regions surrounding the emerging ferrite grain boundaries than in the bulk of the grains.[16]

Pelayo et al.[15] studied the inhibition layer upon three different steel substrates. They carried out SEM analysis that convincingly demonstrate that a nearly continuous, Al-rich interfacial

layer forms and was present on a Ti IF, Ti-Nb IF, and P-added Ti IF steel substrates after dipping in a 0.14 wt% Al-bearing Zn bath for 3s.

Furthermore, the Fe-Al interfacial layer on all three substrates (Ti, Ti-Nb and P-added IF steels) was identified using electron diffraction as being composed primarily of Fe_2Al_5. Moreover, the Fe_2Al_5 layer had a nominal thickness of 30 nm on the Ti-Nb IF substrate and 10-20 nm on the P-added and Ti IF substrates.

They also observed that the Ti IF substrate exhibited the most continuous inhibition layer of the three substrates with 90–95% coverage of the substrate. The Ti-Nb IF substrate showed a compact Fe-Al layer covering approximately 80% of the substrate surface.

Finally, they concluded stating that their results showed an inhibition layer where Fe_2Al_5 is the dominant phase. Hot-dip galvanized samples were composed primarily of Fe_2Al_5, but minor amounts of $FeAl_3$ were also present in the layer. Moreover, in the early stages of development, the inhibition layer on the Ti and Ti-Nb IF substrates went through a transition from an Fe-Al solid solution or ordered phase to the Fe_2Al_5 phase.[15]

2.4.2. GROWTH OF Fe-Zn INTERMETALLIC COMPOUNDS

A reasonable understanding of the galvanneal process and final microstructure is strongly dependent upon the nucleation and kinetics of Fe-Zn intermetallic compounds formed in between the Zn layer and the steel substrate. Indeed, it is the formation and growth of the Fe-Zn intermetallic compound layers that ultimately controls the properties of galvanneal coatings.[13]

Table 1 shows the consensus among most part of the authors regarding to some features of the of Fe-Zn intermetallic phases:[8]

Table 1. Features of Fe-Zn intermetallic compounds.

Intermetallic Phase	**Fe (wt%)**	**Symbol**	**Crystal**	**Morphology**
ζ (Zeta)	5.7-6.3	$FeZn_{13}$	Monoclinic	Pillar-Like

δ (Delta)	7-11.5	$FeZn_{10}$	HCP	Columnar
δ_1 (Delta 1)	7.5-12	$FeZn_7$	HCP	Polygonal
Γ (Gamma)	23.5-28	Fe_3Zn_{10}	BCC	Columnar
Γ_1 (Gamma 1)	17-19.5	Fe_5Zn_{21}	FCC	-

Regarding to the usual chemistry range of Fe-Zn intermetallic compounds, Perrot et al. introduced the data shown in Table 2.[21]

Table 2. Usual chemistry range of Fe-Zn intermetallic compounds.

Intermetallic Phase	wt% Al	wt% Fe	wt% Zn	Fe/Al ratio
η-$Fe_2Al_5Zn_x$	37-46	31-37	18-25	0.7-0.9
δ-$FeZn_7$	1.5-3.5	2.2-9.5	87-93	1.55-5.30
ζ-$FeZn_{13}$	0.7-1.0	5.8-6.1	93.2	N/A

According to Marder et al.[8], the zeta (ζ) phase is formed from the peritectic reaction between the delta (δ) phase and liquid Zn at 530 +/- 10 ^{0}C. The delta (δ) phase is formed from another peritectic reaction, gamma (Γ) and liquid, at 665 ^{0}C. The gamma$_1$ (Γ_1) phase forms as a result of a peritectoid reaction between the gamma (Γ) and delta (δ) phase at 550 +/- 10 ^{0}C. The gamma (Γ) phase forms as a result of peritectic reaction at 782 ^{0}C between ferrite and liquid Zn.

Additionally, they classified the cross-section microstructure of galvanneal coatings as follows:

Type 0: Underalloyed coating containing predominantly ζ phase;

Type 1: Optimum alloyed coating with less than a 1 μm interfacial Γ layer and an overlay containing δ phase interspersed with a small amount of ζ phase.

Type 2: Overalloyed coating with a Γ layer > 1 μm and an overlay containing a δ phase with basal plane cracks perpendicular to the coating/substrate interface and an occasional top layer of ζ phase.

Moreover, the relative amounts of ζ, δ and Fe_2Al_5 phases depend upon:

- The substrate steel reactivity;
- Bath temperature;
- Immersion time.

Marder et al.[8] reported that the sequential nucleation of Fe-Zn phases occurs at the interface beginning with ζ phase layer, followed by δ phase layer, and after some incubation time, Γ phase layer. δ and Γ are the brittle phases in the Fe-Zn coatings, while ζ phase is the most ductile.

If the Zn melt is supersaturated with Fe, and there is sufficient nucleation of new crystals, numerous tiny ζ crystals can form in the melt, that are separated from each other by the solidified Zn η phase. It means that the morphology of ζ phase is a function of Fe supersaturation on Zn bath.[8]

Baril et al.[10] stated that ζ ($FeZn_{13}$) crystals are preferentially formed orderly on (111)αFe, whereas the precipitation of Fe-Zn intermetallics is retarded on (001)αFe and (101)αFe.[10]

Lin et al. [9] reported that the δ phase is the major phase in the commercial galvanneal coatings with the Fe content in the range of 10 to 12 wt%.

They also observed a two layer structure, one consisting of the δ phase with a small fraction of the ζ phase dispersed on the surface and Γ phases and another consisting of the δ and Γ_1 phases, was observed in the P-added IF steel sample substrate. On the other hand, a three-layer structure consisting of the δ, Γ_1 + δ, and Γ phases was observed on the IF steel sample substrate.

Referring to a controversy in earlier diffraction studies, they mentioned that it was wrongly speculated that the Γ_1 phase is not likely to form in commercial galvanized steels because of their short processing time. Finally, they stated that the existence of the Γ_1 phase in commercial galvanneal coating was then verified. The grain morphology of the Γ_1 phase was rather irregular in comparison with that of the Γ phase, which always exhibited a well-defined columnar grain microstructure.

The Γ phase, which shows a columnar grain structure, has an average columnar width of 0.25 μm, which is a small fraction of the average grain size of steel substrate. This suggests that no unique orientation relationship exists between the Γ phase and ferrite.[9]

According to some authors, e.g. Perrot et al, there are strong indications that the galvanizing bath is not at chemical equilibrium. Hence, the metastable phase diagram and not the chemical equilibrium is one of the most use to galvanizers for the calculation of effective Al (by displaying only δ-$FeZn_7$ and η-$Fe_2Al_5Zn_x$ phases, rather than the higher number of intermetallic species found over the same composition range showed in the equilibrium diagram).[21]

Finally, among the microscopy techniques used to identify the Fe-Zn intermetallic compounds, the electron probe microanalysis (EPMA) has been used to identify the phases revealed by chemical etching. The EPMA analyzer, whose best estimated spatial resolution is about 1 μm, is often unreliable in identifying a phase whose size is lesser than the spatial resolution of the analyzer (e.g. Γ phase with thickness lesser than 1 μm). The X-ray diffraction technique is frequently used to identify the phases in galvanneal coatings, but it cannot be used to determine their distribution neither to detect a phase with a small volume fraction.

The phase identification problem is especially pronounced for state-of-the-art high-tech-processed galvanneal steel coatings, since the coating thicknesses are dramatically reduced as compared to those produced during the early developmental stages of the galvanneal-processing technique.[9]

2.4.2.1. KINETICS OF Fe-Zn INTERMETALLIC COMPOUNDS

Marder et al.[8] reported that the incubation period (i.e. the time for Fe-Zn phases to form) increases with an increase in Al content in the bath and decreasing bath temperature.[8] Yet Miyasaka et al.[22] described the incubation time as the time between the start of heating and the onset of rapid increase in the emittance. Thus, emittance is strongly related to that time

when there is a change of the coating surface from the liquid Zn into the solid Zn-Fe crystalline phases, such as ζ and δ_1 phases.[22]

Studying kinetics of Fe-Zn intermetallic compounds becomes a complex issue because several interface reactions are occurring at the same time, including wetting of the solid substrate by liquid Zn, dissolution of the steel by the Zn, isothermal solidification of Fe-Al-Zn intermetallic compounds, solid state diffusional phase transformations, and solidification of the liquid Zn alloy.

Nevertheless, the former researcher proposed a time sequence model for galvanneal coating formation, as follows:

t_0: The steel develops an Fe-Al interfacial layer during hot-dip galvanizing which, depending on Al content in the Zn bath, inhibits the formation of Fe-Zn phases. The effectiveness of the inhibition layer depend on the Al content in the Zn bath, as well as time of immersion and bath temperature.

t_1: Fe-Al inhibition layer breaks down during annealing causing nucleation and growth of δ phase at the coating/surface interface. Outburst formation can also occur with accelerated growth of Fe-Zn phases. Simulated annealing of a galvanized coating in an environmental SEM shows the formation of outbursts at the interface. The rate of Zn attack will depend on the substrate alloy addition as well as the temperature profile in the annealing process (type 0 galvanneal microstructure).

t_2: As annealing continues, diffusional growth of δ phase in a columnar growth morphology occurs. Previously nucleated ζ phase transforms to δ phase. Additional ζ phase may nucleate due to oversaturation of Fe in the liquid η phase or upon cooling. An interfacial Γ phase forms at the coating/steel interface.

t_3: Zn depletion occurs with longer temperature exposure resulting in the complete consumption of η phase at the coating surface. Fe concentration increases in the coating as δ phase continues to form, pushing the ζ phase to the surface and maintaining a constant 1 μm thickness Γ phase. This has led many to rely on an Fe concentration measurement (approximately 10 wt%) as a requirement for the optimum galvanneal coating (type 1 galvanneal microstructure).

t_4: With longer times at temperature, δ phase diffusional growth continues towards the surface of the coating consuming the ζ phase, while maintaining a constant 1 μm thickness Γ phase.

t_5: Once the δ phase reaches the surface it serves as the Zn rich side of the δ phase Fe-Zn/steel diffusion couple, allowing for the continued growth of Γ phase at the expense of δ phase. Cracking occurs along δ phase basal planes parallel to the coating/steel substrate (type 2 galvanneal microstructure).[8]

Jordan et al.[2] reported that the total Fe-Zn alloy layer growth for two different grain sizes of an ULC steel substrate showed the same behavior over the reaction times studied. They used the power-law growth equation $Y = K.t^n$ to estimate the growth rate of each Fe-Zn intermetallic compound. By applying a logarithmic function in either side of the equation, it comes to log Y = log K + n.log (t), a plot of the log value of the total alloy layer thickness (Y) as a function of the log value of immersion time in the bath (t) can be fitted to the data to determine a line whose slope is defined as 'n', the growth rate time constant value. The growth rate time constant value is an indication of the type of kinetics controlling the growth. An n value of 0.5 is indicative of parabolic diffusion-controlled growth, while an n value of 1.0 is representative of linear kinetics in which growth is interface controlled.

For a 0.00 wt% Al-Zn bath, the data indicated a $t^{1/3}$ relationship, indicative of grain boundary diffusion of diffusion along grain boundaries during coarsening of the grain growth. The Γ layer growth followed a $t^{1/4}$ relationship, indicative of grain boundary growth kinetics of diffusion along grain boundaries of growing grains. The n values determined for Γ layer lie within the range of 0.10 to 0.50. Regarding to the δ layer growth, it was reported that the n range lies in between 0.49 to 0.65. Concerning to the ζ phase, the n range was reported to be in between 0.16 and 0.36. Limited Zn transport along the columnar boundaries of the ζ phase may be responsible for the observed $t^{1/3}$ kinetics.

It was observed that the ζ phase formed at the steel/coating interface first, followed in time by the formation of the δ phase between the ζ phase and the steel/coating interface and, last, a Γ phase layer formed between δ phase and the steel/coating interface.

Regarding to ζ layer growth, it is most likely not significantly affected by substrate grain size like the Γ and δ phase layers, which are more closely associated with the substrate steel/coating interface. On the other hand, the ζ phase is affected by the rapid growth of the adjacent δ phase layer, and its apparent consumption of the ζ phase layer also affects the growth-time relationship determined for the ζ phase.[2]

Jordan et al. added that the morphology of the liquid Zn/ζ interface was non-planar which could indicate that the kinetics of this growth reaction are governed more by the solidification transformation from liquid to solid, as opposed to solid state diffusion kinetics.[17]

On the other hand, for a 0.20 wt% Al-Zn bath, the presence of Al in the Zn bath causes the formation of a Fe_2Al_5(Zn) inhibition layer. According to Ghuman and Goldstein apud Jordan et al.[2], Fe-Zn phases are able to grow in Al-containing baths, while at the same time, Fe_2Al_5(Zn) is stable. δ phase formed first at the steel/coating interface followed by the formation of Γ at the steel/coating interface. The δ phase boundary furthest away from the steel/coating interface was in contact with the liquid Zn during immersion in the bath, and once solidified, the liquid Zn formed solid η phase.[2]

Horstmann apud Marder et al.[8] reported that there is an overall inward movement of the gamma ($\Gamma + \Gamma_1$) phase layer towards the Fe, whereas the ζ phase layer is displaced towards the Zn melt. The δ phase layer expands in both directions, but generally towards the Zn melt. Thus, as the $\Gamma + \Gamma_1$ phase layer grows into the Fe, it is also consumed by the growing δ phase layer. Similarly, the δ phase layer expands into the growing ζ phase layer that is advancing into the Zn melt. All of these transformations are governed by the diffusion of Zn into the Fe substrate.

Tang apud Marder et al.[8] suggested that the optimum Al composition for galvannealing is the transition from δ (or Γ) phase to the $Fe_2Al_5Zn_x$ (η) becomes an equilibrium compound in the bath. Al contents marginally higher than this level mean that the formation of the Fe_2Al_5 phase at the interface is practically impossible because of severe competition from the ζ and δ phases.[8]

From experiments carried out by McDevitt et al.[13], it was stated that the ζ phase formed in the bath and disappeared early in the galvannealing at 500 ^{0}C. During galvannealing, it was observed that the majority of the coating solidifies by δ formation from the liquid. The Γ_1 phase formed in the bath and grew during galvannealing until all the molten Zn solidified. The Γ phase nucleated upon dissolution of the inhibition layer as Γ_1 came into direct contact with the steel substrate.

The ζ phase generally grew in colonies of grains sharing a preferred orientation on the Ti-Nb IF and Ti IF substrates. The number of ζ crystals on the surface of the coatings on all substrates decreased substantially after the completion of 3s dipping. Concurrence with the disappearance of ζ, the presence of a thin, discontinuous layer of the δ phase was observed.

As the δ phase grew by consuming the Fe-supersaturated liquid Zn, the microstructure of the layer was a discontinuous mixture of δ crystals and surrounding Zn liquid – in these observations the Zn liquid has solidified upon quenching as the η phase. It appeared that the δ phase propagated by the continued formation of small grains from the liquid directly in front of the advancing solidification front. Even when δ grains had formed on the surface of the coating, liquid Zn remained trapped between grains within the δ layer. Continued galvannealing after this point resulted in the transformation of these regions of entrapped liquid into the δ phase thus resulting in a fully compacted δ layer after the 45 s galvanneal treatment. On the Ti-Nb IF and Ti IF substrates, this δ layer grew in thickness with the cube-root of galvannealing time.

After the initial period of non-uniform growth, the solidification front evened out and δ growth progressed invariably on all three substrates. However, as grains of the δ phase formed and grew, channels of molten Zn remained among the solidified grains. These liquid channels probably acted as avenues for fast mass transport of Fe to the advancing solidification front. The δ solidification front progressed with galvanneal time at a rate of thickness growth proportional to $t^{1/3}$. This rate is slower than either interface controlled (∞ t) or diffusion controlled growth (∞ $t^{1/2}$).

They finally concluded stating that solidification of the coating at 500 ^{0}C progresses by direct formation of δ from the liquid, instead of an intermediate step of ζ formation followed by transformation of ζ into the δ as is often observed in solid state Fe-Zn diffusion couples.

The higher Fe content Γ phase is the only Fe-Zn intermetallic compound that can exist in equilibrium with Fe and is predicted to form between Fe and Γ_1, but its formation must be controlled by nucleation kinetics. Moreover, a Γ_1/Fe interface is a thermodynamically unstable microstructure at 500 ^{0}C.[13]

2.4.2.2. EFFECT OF OPERATIONAL PARAMETERS ON Fe-Zn INTERMETALLIC COMPOUNDS

Several production parameters have a strong influence on the Fe-Zn reactions during the galvannealing process, as follows:

- Substrate chemistry;
- Steel pre-treatments (such as annealing);
- Zn bath composition;
- Bath temperature;
- Immersion time;
- Coating annealing temperature;
- Annealing time.[10]

Al is added to the Zn bath to improve corrosion resistance by either allowing for the formation of a pure Zn overlay for galvanic protection by inhibiting the formation of Fe-Zn phases or by introducing multiphase microstructures in the overlay coating.

However, Al control in the Zn bath is complicated by the fact that Al exists in two forms in the bath. Some Al is dissolved in the liquid Zn phase and the rest of Al is present in the intermetallic particles entrapped in the bath. It is the Al in liquid solution, commonly referred to as ‘active’ or ‘effective’ Al, which can perform the function of inhibiting the Fe-Zn reaction during galvanizing. Effective Al is also strongly dependent on the amount of dissolved Fe in

the bath, since supersaturated Fe can combine with Zn and Al to form Al-containing ζ, δ and $Fe_2Al_5Zn_x$ (η), further reducing the amount of Al in the liquid Zn.[8]

Baril et al. added that the Al addition in the galvanizing bath significantly reduces the rate of the Fe-Zn reactions during both the bath immersion and the galvannealing process. This phenomenon is called the inhibition and offers a superior way to continuously galvanize steel sheets and produce a single η-Zn phase coating. Furthermore, this improves control over the final alloyed coating during galvannealing.[10]

Perrot et al. stated that Al has been added to the galvanizing baths for many years. It improves the lustre of the coating, reduces the oxidation rate of the Zn bath and produces ductile layers by suppressing the growth of brittle Fe-Zn phases. However, the Fe-Zn interactions in presence of Al becomes unpredictable due to the highly exothermic nature of intermetallic compounds such as Fe_2Al_5 and $FeAl_3$, which occur as transient phases during the galvanizing process.[24]

Therefore, Al added to the bath is effective in inhibiting the formation of ζ phase in the bath and during the heating period and also in suppressing the growth of Γ phase. Morimoto et al. also confirmed that the volume fraction of ζ crystals decreased with increasing bath Al content.[14]

Jordan et al.[17], matching the results of most part of researchers, confirmed that 0.20 wt% Al-Zn baths delay the formation of Fe-Zn phases for immersion times greater than 300 s. Indeed, 0.20 wt% Al additions to the bath caused a non-planar growth condition of the δ/ζ phase boundary.

Moreover, they compared coatings that were produced with different Al contents in Zn bath. It was evident that Al in the bath reduces ‘n’ for Γ and δ layer growth.[17]

Pelayo et al. apud McDevit et al.[15] stated that a higher strip entry temperature can have a significant effect on the initial bath reactions because both chemical reaction rate and diffusivity depend exponentially on temperature.

Regarding to dipping time, McDevit et al. reported that there was no significant difference between morphologies of the Fe-Zn compound layer on samples dipped for 1s versus those dipped for 3s.[15]

Baril et al. found that Fe content in the coating increases with decreased Al content in the bath or with increased immersion time. For low Al bath contents (<0.12%), the effect of immersion time is more important. In such low Al content baths, it is largely reported that the growth of Fe-Zn intermetallic compounds is rapid, even during galvanizing. This was confirmed by the observation of large intermetallic crystals in metallographic cross sections of the coatings.[10]

According to Kanamura and Nakayama, the heating rate during galvannealing should be as high as possible to limit the growth of both ζ and Γ phases.[8]

Shindo et al. found that, by increasing the galvannealing temperature and suppressing the soaking time, the growth rate of the Γ-δ_1 mixture layer was increased. This leads to a rapidly increase in powdering. Ti and Nb, among other elements, are known for triggering off this behaviour.[25]

Meshii et al. observed the influence of galvannealing time on mechanical properties. While solidification progressed there was little increase in Fe concentration of the δ phase behind the solidification front. The use of this behavior could be important in production where coating mechanical properties can be optimized by producing a low Fe content δ coating. By controlling the galvannealing time, a δ coating with a low Fe content could be achieved.[13]

Dionne et al. studied the effect of cooling rate upon Fe-Zn intermetallic phases. They observed that the cooling rate after galvanizing could also affect phase formation. A slow cooling rate would provide time for diffusion of Zn into the phases already precipitated onto the strip, which could account for the Fe-Al-Zn ternary phase on the Ti-stabilized IF steel. On the other hand, fast cooling rates might promote the solidification of metastable phases such as the Al-rich δ crystals observed on the Ti-Nb-stabilized IF steel.[16]

Bhattacharya et al., unlike many authors, stressed the importance of carrying out experiments on work temperatures, instead of room ones. They explained that, since segregation to surface of surface-active elements is temperature dependent, it is important to perform analysis on samples quenched from the temperature at which steel enters the Zn pot and not on samples at room temperature. Therefore, only segregation at the real temperature of the steel during processing would yield true results.[1]

Finally, studying the influence of operational parameters on Fe-Zn-Al ternary system at 450 ^{0}C, Perrot et al. concluded that, generally, the stable Fe-Zn-Al diagrams obtained after long reaction time are characterized by less extended single-phase regions. For instance, the Zn solubility in Fe_2Al_5 and $FeAl_3$ decreases with increasing reaction time. As the reaction time proceeds, the system approaches an equilibrium state: the solubility of Zn in $FeAl_3$ and Fe_2Al_5, that of Al in δ and ζ, and that of Fe in the liquid are decreasing whereas that of Zn in ferrite is increasing. On the other hand, it is not certain that equilibria between solid phases are well established, even after 1000 h because of the low temperature (450 ^{0}C).[24]

2.4.2.3. EFFECT OF CHEMISTRY ON SUBSTRATE REACTIVITY AND Fe-Zn INTERMETALLIC COMPOUNDS

The literature has shown that substrate grain boundary cleanliness is the dominant steel substrate structural feature that controls the kinetics of Fe-Zn alloy phase formation in Al containing Zn baths.[8]

The control of interstitial species begins with steelmaking and casting techniques, which are primarily designed to minimize the amount of N and C in the steel. Subsequently, the stabilization of N and C via precipitation reactions will be determined by thermomechanical processing on the hot strip mill and during annealing.[3]

C was clearly found to retard growth rates of the δ and ζ phase layers, and have little effect on Γ layer growth.[17] Additionally, the presence of C in the steel substrate retarded the alloying between Fe and Zn, while P in the steel favored the formation of the Γ_1 phase over the Γ phase by its surface segregation in the steel substrate.

Lin et al.[9] have carried out TEM analysis that has clearly shown that alloying is more progressed in the coating on IF steel than that on ELC steel, which is galvannealed at a temperature about 5.6 ^{0}C higher than that used for galvannealing IF steel, indicating that the C in the steel substrate retards the alloying reaction between Fe and Zn. This trend of the observation is consistent with the early reports, indicating that solute C tends to segregate to ferrite grain boundaries during cooling after heat treatment and restrains the interdiffusion of Zn and Fe through ferrite grain boundaries.

They also mentioned that it was speculated that P has the same effect as C in retarding the alloying between Fe and Zn in spite of the facts that they have the opposite effects on intergranular fracture and that one is interstitial and the other is substitutional.[9]

Maschek et al. confirmed this direction. They observed that, since the onset temperatures of some galvannealing reactions are below the melting temperature of the Zn (419 ^{0}C), the observed intermetallic Zn-Fe growth at the interfaces has to be a solid state reaction. Therefore, it is assumed that the retarding effect of P is based on the difficulty for P to diffuse through solids at low temperatures.[26] Marder et al. added that P segregates to the grain boundary and slows the formation of Fe-Zn phases.[8]

Lin et al.[9] observed that the presence of P influences the nature of the inhibition layer and its longevity. In the coating on P-added IF steel, it is an Fe-Al compound (instead of an Fe-Al-Zn compound on IF and ELC steels) that forms, and tends to show enhanced stability.

Furthermore, it is suggested that strong-surface, instead of grain-boundary, segregation of P in ferrite has an important effect on the phase evolution of coating during galvannealing.[9]

Indeed, Maschek et al. mentioned that it is shared among most part of the authors that P inhibits the Zn diffusion in the grain boundaries of the steel substrate and therefore prevents the embrittlement of the steel substrate.[26]

Zhong et al. confirmed the work of the authors above, stating that the P solute segregated to the ferrite grain boundaries or to the steel surface can retard the Zn diffusion and reduce the Zn embrittlement.[27]

Allegra et al. found P to segregate to ferrite grain boundaries in LC steels (0.02 to 0.06 wt% C) containing at least 0.04 wt% P, blocking the diffusion of Zn along the grain boundary and lowering the thermodynamic activity. Mercer apud Allegra et al.[23] proposed that the P enrichment at the grain boundaries impeded Fe and Zn interdiffusion, thus lowering the amount of Fe in Zn galvanizing coatings on re-P steel. Therefore, P in the base steel acts as an inhibitor to Fe-Zn alloy growth primarily due to grain boundary segregation of P.[23]

Regarding to the influence of chemistry upon Fe-Zn intermetallic compounds, Shindo et al. reported that some elements such as Mn, Se, Cu, Ca and Ti are the ones that affect the growth of the δ_1 crystal when they precipitate as sulfides on the surface. Additionally, Ti has also been increased to predict its effect on the coating. Other elements like Nb and B affect the crystal shape of Zn-Fe alloy and are also reported to reduce the Γ crystal growth. Their results suggested that alloy elements added to the steel affected the Γ-δ_1 mixture layer, which developed between the substrate steel and δ_1 alloy layer. [25]

In order to enhance the reaction between molten Zn and the steel substrate, the addition of Ni to liquid Zn has been considered in the practices. The addition of Ni to the molten Zn has been made in batch galvanizing line to retard the growth of the ζ phase. This process has become known industrially as Technigalva.[20]

Regarding to the most used microscopy techniques to measure segregation, the X-ray photoelectron spectroscopy (XPS) technique is also proving to be an efficient and convincing tool for studying the segregation phenomena that take place on steel surfaces during annealing processes. A notable advantage of this technique is that it provides information on the chemical state of the elements present, though it presents the limitation of its low lateral resolution.

However, Feliu et al., performing experiments through XPS analysis, reported problems regarding to sample contamination when in contact with the laboratory atmosphere. They reported that, at room temperature, the surface of any metal, in contact with the atmosphere, irrespective of its composition, instantaneously becomes coated with a thin film of C-C/C-H groups (with a thickness less than 3 nm).[4]

In order to obtain more analytic information upon surface enrichment, GDOES-depth-profiles have often been made. Due to the high erosion rate of this method, caused by ion bombardment of the sample surface, it is possible to have a good idea about the chemical distribution from the top layer to the bulk within few seconds. In this case the disadvantage of low lateral resolution (analyzed area: 4mm in diameter) is more than compensated by an extreme high sensitivity of the system. Therefore, GDOES is useful to detect surface enrichments under different annealing parameters (also B and P) and not to differ between the chemistry of various particles.[28]

2.4.2.4. EFFECT OF IF STEEL ALLOYING ELEMENTS ON Fe-Zn INTERMETALLIC COMPOUNDS

Interstitial free (IF) steels have been found to have a more reactive behavior relative to other drawing steel alloys during Zn coating processing.[17] Ti added steels generally produce a clean substrate grain boundary for faster reactions. [8]

Lin et al. commented that is well known that C, Si and P in steel restrain the alloying reaction between Fe and Zn, whereas Ti and Nb promote the reaction between Fe and Zn. A popular explanation of the mechanism to explain the retarding effect by the alloy elements is that they segregate to grain boundaries and limit the short-circuit diffusion of Zn atoms into ferrite.[9]

Likewise, McDevitt et al. reported that P and C additions in the substrate are thought to reduce the rate of microstructural evolution of galvanneal coatings, while the addition of Ti is suspected to destabilize or increase the rate of development of the coating microstructure.[15]

Hisamatsu postulated that the chemical nature of IF steel grain boundaries increases their thermodynamic activity during hot-dip galvanizing, resulting in the preferential nucleation and growth of Fe-Zn phases at these sites. Further, he suggested that a finer grain size substrate is more reactive, because Fe-Zn phases are thought to first nucleate and grow at substrate steel grain boundaries. Therefore, as more grain boundary area is available for

reaction with the liquid Zn bath on a fine grain size steel surface, more rapid Fe-Zn phase growth results. Additionally, Jordan et al. reported that recent investigations had shown that as the grain size of a Ti-stabilized IF steel decreases, Fe-Zn reaction rates increased during post-dip annealing. [2]

Miyasaka et al.[22] observed that an increase in the amounts of Ti and Nb decreased the incubation time significantly, while on the other hand an increase in the amounts of C and P increased the incubation time. Since the amounts and crystallographic structure of the Fe-Al-Zn barrier layer were not affected by the above elements, the effects of the alloying elements on the galvannealing behavior were attributed to their influence on Fe diffusion at the ferrite grain boundary.

Therefore, the addition of Ti or Nb shortened the incubation time for galvannealing remarkably, though the change in the incubation time by the unit amount of Ti or Nb was greater with Ti addition than with Nb. The decrease in the incubation time by an increase of 0.01 wt% Ti was about 1.1s, that by an increase of 0.01 wt% Nb was about 0.5s. However, if we take into account that the atomic mass of Nb is 1.9 times as much as that of Ti, these results indicated that the Nb showed as much influence as Ti did when their contents were expressed in atomic percentage.[22]

According to Hisamatsu, Ti added sheet steel will alloy at 50-70 ^{0}C lower than a LC steel, both being galvanized in a 0.13% Al bath at 470 ^{0}C. Mercer found that Ti-stabilized steels were more reactive than Al killed steels for two different galvannealing temperatures. Maki showed that the Γ phase thickness was greater than Al killed steel for every annealing temperature studied, using a 0.11 wt% Al bath. Moreover, Ti steel inhibited the formation of a type 1 microstructure using a 0.10 wt% Al galvanizing bath, but accelerated the formation of type 1 with a 0.15 wt% Al bath, especially at higher galvannealing temperatures. Similarly, Ti-Nb IF steel galvanized at 0.14 wt% Al bath accelerated alloy formation.[8]

Seeking some differences between the Ti and the Nb behavior upon Fe-Zn intermetallic compounds, Pelayo et al.[15] stressed that the ζ crystals on the Ti IF and the P-added substrates grew without a noticeable preferred orientation, while on the Ti-Nb IF substrate

the ζ crystals grew in colonies of approximately 20-30 μm^2 where all the crystals within the colony had the same orientation.

On the one hand, the size of the ζ colonies on the Ti-Nb IF substrate were approximately the same as the grain size of the substrate, suggesting that the ζ phase growth is influenced by the orientation of the grains in the substrate. This implies intimate contact between the ζ phase and the substrate, or that all phases between the substrate and the ζ phase have an orientation relationship with the substrate grains. On the other hand, on the Ti IF steel substrate, the surface coverage with ζ was quite variable with an equal number of large regions (several hundred μm^2) of approximately 80% coverage and similarly sized regions with 40% coverage.[15]

Osman et al. reported that the initial formation of the ζ-phase (closer to the coating) for the Ti-stabilized steels occurred without a preferred orientation, while for Ti-Nb-stabilized steels grew in one direction and had a 'colony' size that was similar to the substrate grain size. It was found that nucleation of the ζ-phase in Ti-Nb-stabilized steels preferentially occurred over (111) α-Fe, resulting in a lower consumption of Fe and a correspondingly slower growth rate for the Fe-rich δ- (intermediate phase) and Γ-phases. After initiation of alloying, the presence of solute Nb at the grain boundaries may also serve to decrease the intergranular diffusion of Fe, thus assisting in the production of a more uniform alloy structure with a reduced Γ-layer thickness.[3]

Meshii et al.[13] observed that, once the Fe-Al inhibition dissolved and most of the ζ phase disappeared, the second stage of δ formation, growth of the δ phase by consumption of the liquid Zn, could begin. Initially, growth of the δ layer was non-uniform on the Ti-Nb IF and Ti IF substrates, but occurred more uniformly on the P-added substrate.

On the Ti-Nb IF and Ti IF substrates, propagation of the δ phase began immediately upon reaching 500 ^{0}C because the inhibition layer had already dissolved by this point in the processing. The start of δ propagation occurred sooner on the Ti-Nb IF and Ti IF substrates than on the P-added substrate, but the substrate chemistry had little effect on the growth rate of the δ phase or the Fe enrichment rate after the inhibition layer had dissolved.

Initially, growth of the δ phase on the Ti-Nb IF and Ti IF substrates was nonuniform. However, this nonuniform growth of the δ phase was not characteristic of an outburst structure.

Γ_1 grew during galvannealing, and on the Ti IF and Ti-Nb IF substrates the Γ phase nucleated and grew while the coating was solidifying. The increase in the average Fe content of the coating is due to all of these reasons. Growth of the Γ_1 phase continued until supply of liquid Zn was exhausted. At that point, on the Ti-Nb and Ti IF substrates, growth of the Γ_1 phase ceased and Γ grew by consuming the Γ_1 phase. These results indicate that the amount of liquid Zn remaining can play an important role in the course of the galvanneal reactions.

The Γ phase nucleated between the Γ_1 phase and the steel substrate shortly after the point in processing when the inhibition layer dissolved and the steel and the Γ_1 phase interfaced directly. On the Ti-Nb IF and Ti IF substrates Γ formation occurred within 3s at 500 ^{0}C, and even a few Γ grains were observed after 0s at 500 ^{0}C. On the P-added substrates, Γ phase formation was suppressed even after the inhibition layer disappeared suggesting that P affects the nucleation of the Γ phase at the Γ_1/Fe interface.[13]

Marder et al. added that Ti and Ti-Nb solute additions, which enhance grain boundary reactivity, resulted in more rapid growth kinetics of the Γ and δ phases than an ULC steel for a series of IF steels in Zn coatings containing an Fe_2Al_5 inhibition layer (Zn-0.20 wt% Al bath).[8]

2.4.2.5. EFFECT OF SURFACE OXIDES ON Fe-Zn INTERMETALLIC COMPOUNDS

Mn is the alloying element that is found in the greatest proportion on the annealing steel surface. According to the literature, it seems rather usual to find a continuous and thin film of Fe oxide over the steel surface, while Mn and Si oxides may be distributed in the form of an island.

The strong surface enrichment in Mn could be explained in general as due to equilibrium segregation and/or external selective oxidation. Selective oxidation of reactive alloying

elements appears to be a common phenomenon in the steel annealing treatments under vapor-containing protective atmospheres.

The increase in Fe^0 should be caused by the greater affinity of Mn for O, which could reduce the Fe oxides in the thin layer present on the outer surface of the steel. In accordance with the idea of Mn oxidation by the Fe oxides formed in the annealing process, Vanden Eynde et al., working in a nonreducing atmosphere (dry N), found that the reduction of these oxides did not come from the reactions between the annealing atmosphere and the steel surface but from the interchange of O between the Fe oxides and the alloying elements that segregate on the surface (Mn and Si).

Some authors apud Feliu et al.[4] have found a dear relationship between the inhibition of the growth of Fe-Zn intermetallic compounds and the fraction of the steel substrate surface covered by Mn oxides as a result of the annealing process.

The literature mentions a tendency toward the formation of outer layers of MnO during the annealing process of IF steels even in a reducing atmosphere. Feliu et al. reported that, on annealed IF steels (0.6 wt% Mn), the element that exhibited the greatest tendency towards segregation was Mn, which reached contents on the surface of close to 25%. The lower C content in the IF steel compared with the LC steel may increase the tendency for Mn to diffuse during the annealing process, in concordance with the observations of Zhang and Bensinger.[4]

Moreover, it is well known that the metallic alloying elements segregate toward the surface of IF steels in order to precipitate in the form of metallic oxides and hydroxides as a result of the annealing process. This segregation seems to inhibit the nucleation and growth of Fe-Zn intermetallic phases.[29]

Additionally, the Si contents in the bulk steels are lower than the contents of other alloying elements such as P, Cr, Al, Ni, etc., which are not detected by XPS on the outer surface of the annealed steels. This fact agrees with the great tendency of Si to precipitate on the surface of steels in the form of fayallite (Fe_2SiO_4) during some annealing cycles.[4]

Perez-Ravenga et al.[29] observed and studied the surface contamination of steel, which has endured the annealing operation and persists even after galvannealing treatment. It is as if the contamination had shifted during this treatment from the surface of the annealed steel to the outer surface of the galvanneal coating (Fe-Zn alloy phase), which had grown on that surface.

In the case of the galvanneal coating, the growth of the Fe-Zn alloy would push the contamination toward the outer surface of the coating, while on the galvanized coating it would remain at the Fe-Zn alloy/Zn interface, and thus be impossible to detect. This phenomenon is somewhat similar to other cases reported in the literature, e.g. that in Zn (Al) baths, the Fe_2Al_5 inhibiting layer is pushed into the melt during the formation of the galvanized coating.[29]

2.4.3. CRATER FORMATION

Marder et al.[8] pointed out that craters were found to be inherent to the galvanneal coating layer, causing major fluctuations in coating thickness and appear to be associated with outburst formation. They proposed the following mechanism to explain the relationship between outburst formation and the appearance of craters:

After an outburst of Fe-Zn intermetallic compounds occurs at the substrate grain boundary, rapid growth of these solid phases occurs into the liquid. The liquid Zn will remain present between the crystals, which enables very fast transport of Fe from the substrate. Capillary effects of the pores and channels between the crystals drain the nearby regions where no alloy reaction takes place, whereby ‘dry spots’ or craters are formed. Indeed, more craters were seen on the surface of galvanneal coatings for low Al baths, which were related to outburst formation.[8]

Faderl et al. reported that cratering occurs preferentially at low galvannealing temperatures as well as low ‘galvannealing-reactivity’ (re-P IF steel), and therefore indicates good adhesion of powdering performance. This is due to the formation mechanism of craters (which was explained by them as microscopic Zn transfer from ‘low-reactivity’ areas to ‘high-reactivity’ ones). Moreover, in several cases different coating formation (cratering)

was observed over the width for one coil but the powdering behavior was not influenced by cratering.[30]

van der Heiden et al.[12] pointed out that, though hard to recognize by SEM 2D photography, secondary electron 3D images clearly revealed that all the galvanneal surfaces were covered with craters – which they characterized as discontinuities. Typically, those craters covered 5-10% of the coating surface, as was quantified by measuring the thickness distribution by automatic image analysis. By applying SEM stereophotography, the columnar and compact crystals of the coating layer could be observed, in particular inside the craters on bottom and walls. No indications of fractured surface could be found inside the craters. Furthermore, SEM photographs and EPMA showed that there was always some Zn left on the bottom of the craters.

After became clear that the craters were not the result of sample preparation, it was wondered if skin passing might cause crater formation. However, craters were also found in samples from a coil that had not been skin passed. Even after 2% skin passing of this material on a laboratory mill, the same amount of craters was found. Indeed, only the surface was more flattened. Moreover, there were no fracture indications inside the craters. After studying many galvanneal products of several commercial lines, it turned out that craters are inherent to the galvanneal coating layer. It had become clear that they cause great differences in thickness on microscale and are formed during the galvanneal process itself.

One mechanism of crater formation was proposed by van der Heiden et al., as follows: Before the strip is entering the galvanneal furnace, an alloy layer of Fe_2Al_5 has been formed at the interface. This Fe_2Al_5-layer retards Fe-Zn alloying. When locally breaking up of this layer is promoted by a temperature rise, the Fe-Zn alloy reaction at this point proceeds very rapidly, leading to the appearance of the well known outbursts of Zn-Fe crystals. As suggested by Rensen and van Eijensbergen on the basis of the hot-stage microscopy experiments, liquid Zn remains present between the crystals, which enables very fast transport of Fe. Capillary effects of the pores and channels between the crystals will drain the nearby regions where no alloy reaction takes place, whereby ‘dry spots’ or craters are

formed. Obviously, at alloy/outburst locations, the interface moves inwards, as a result of Fe consumption.[12]

Finally, they concluded supposing that craters might have a positive effect on mechanical paint adhesion as well as on anti-powdering properties. The latter because powdering is the result of compressive stresses in the coating. The craters offer the possibility to prevent the build up of these compressive stresses to some extent. So the presence of craters has no negative influence on the product performance of galvanneal coatings.[12]

van Koesveld et al.[31] pointed out that the occurrence of outbursts along ferrite grain boundaries was shown to be the driving force for deep crater formation in the galvanneal coating. It causes, among other things, a non-uniform consumption of Fe from the substrate interface grains during galvannealing.

Through SEM back-scattered 3D electron images they were able to show very clearly the absence of fractured crystals on the wall and the bottom, indicating that the craters are not created by deformation like skin passing, confirming van der Heiden's assumption[12]. Consequently, their origin must be sought for in the galvannealing process itself.

Moreover, SEM and EPMA measurements could show that some residual Zn layer is always present at the bottom of the craters, which thus remain adequately protected against corrosion. Additionally, they found that free Zn remains present between the needle-like crystals of the outbursts. The latter crystals grow thicker than the surrounding residual liquid Zn, which is sucked into the open outburst crystal structure and on top of it by capillarity and surface tension effects. The outcome of this draining effect is the formation of craters.

They also mentioned about an additional crater formation mechanism, which had recently been put forward and will be explored following this by O'Dell et al. This theory is based on epitaxial relationships prevailing between ferritic substrate and galvanneal coating. Providing that coating Al content is high enough, Fe-Zn reactions are supposed to be slow on (111) surface ferritic grains, while they proceed faster elsewhere. According to this

mechanism, craters are then preferentially formed on (111) ferritic grains, the size of which controls crater dimensions.

Finally, they concluded also stating that craters have no negative influence on galvanneal product user's properties, including corrosion. On the contrary, the presence of craters has a positive effect on properties like coating adhesion.[31]

Similarly, O'Dell et al.[19] stated that the presence of craters within the galvanneal coating had been reported to reduce the amount of powdering experienced by the galvanneal coating. They reported that two different types of crater were observed, a light and a dark one. Within the light crater ordered crystals were seen at the base of the crater. The Zn content of these crystals is very similar to that found over the rest of the galvanneal coating. On the other hand, the dark crater shows a large presence of Fe. They also reported that, on all the samples analyzed by their study, no craters were found to be present after deformation through a standard cupping test.

Regarding to the influence of operational parameters upon the occurrence of craters, they found that the process parameters which have the most effect upon the crater coverage are the strip entry temperature (SET) and the temperature after dipping (TAD), which is defined as the lowest temperature the panel reaches after it has been dipped and prior to galvannealing. It was reported that an increase in the SET leads to an increase in crater coverage due to the improved nucleation ability of the ζ phase at these higher temperatures and the easier formation of the ordered ζ crystals during the initial dipping period. On the other hand, a decrease in the TAD promotes the formation of craters within the galvanneal coating because a lower TAD promotes the growth of the ordered ζ crystals resulting in a more compact and more stable structure.

They explained that diffusion of the Fe atoms into the ordered ζ crystals is limited by either the orientation relationship between the craters and the (111) substrate grains due to the persistence of an inhibition layer between the ζ crystals and the substrate. Moreover, the Zn above the ordered ζ crystals is drawn into the surrounding developing galvanneal coating so that the crater is created.

Briefly, as mentioned earlier, O'Dell et al.[19] pointed out that craters within the galvanneal coating help to reduce the powdering tendencies of the galvanneal coating by inhibiting crack propagation along the weak Γ/substrate interface. Indeed, they alleviate the compressive strains by the failure of the ordered ζ crystals, and therefore prevent the coating from powdering. Summarizing, they act as stress relievers for the galvanneal coating when subjected to compressive strains.[19]

2.4.4. EFFECT OF IF STEEL ALLOYING ELEMENTS ON GALVANNEALED COATING STRUCTURE

With the increased utilization of hot-dip galvanized coatings, IF steels became commercially viable since these grades did not require a pre- or post-anneal to prevent strain aging.

Today, hot-dip galvanneal coated IF steels processed through continuous galvanizing lines predominantly contain a combination of Ti and Nb for interstitial free stabilization. Additionally, some hot-dip galvanize coated sheets as well as batch annealed sheets (i.e., cold rolled or electrogalvanized sheets) contain Ti and Nb, especially higher tensile strength grades. The remaining IF steels currently produced rely upon Ti additions alone for interstitial stabilization.

Osman and Garcia have reported that, in addition to alloy phase development, Nb additions are also beneficial for reduction of 'woodgrain' appearance on the surface of the galvanneal sheet. The use of Nb for interstitial stabilization therefore reduces the necessary Ti content in the sheet, thus reducing the propensity for this type of surface appearance.[3]

2.4.4.1. STEEL SUBSTRATE REACTIVITY

Interstitial Free (IF) steels have been found to have a more reactive behavior relative to other drawing quality steel alloys during Zn coating processing. The reactive behavior of IF steels can lead to difficulty in controlling the degree of alloying that occurs during post-dip annealing. Rapid reaction times during hot-dip galvanizing and post-dip annealing can lead to overalloying and subsequent poor formability properties of the coating during press forming operations.[17]

Marder et al.[8] stated that because IF steels are more likely to form carbide, nitride, sulfide and phosphide precipitates in the grains, preventing segregation to the grain boundaries, the concept of excess Ti is very important and was introduced through the following formula:

excess Ti = total Ti – 3.99C – 1.49S – 3.42N – 1.55P

Where a positive excess Ti exists, it indicates a clean, carbide free and reactive grain boundary. A negative value of excess Ti would indicate that not all of the solute C is tied up and Zn diffusion down the boundaries would be blocked. Hence, the cleaner is the substrate grain boundaries, the easier Zn atoms diffuse along them.[8]

Hisamatsu apud Jordan et al.[17] confirmed that the substrate grain boundaries in IF steels are more typically reactive because they are essentially C free due to carbide and carbonitride formation that results from carbide stabilizing additions of Ti and or Nb. Indeed, according to his theory, the nucleation of Fe-Zn phases first occurs where the Fe-Al inhibition layer first breaks down, at a thermodynamically active steel substrate grain boundary.

Similarly, Jordan et al. affirmed the high reaction rates normally associated with IF steels may be related to their ultra low C content. They added that most of the research to date concerning substrate and Zn bath alloying additions had been conducted on pure Fe substrates.[17]

Dionne et al.[16] reported that C and P in the substrate are thought to have a retarding effect on the alloying reaction between Fe and Zn during galvannealing. It has been proposed that these elements segregate to the grain boundaries and limit the short-circuit diffusion of Zn atoms into the ferrite substrate. On the other hand, Ti additions promote the galvannealing reaction, possibly by reducing the concentration of free C.

Moreover, they found that the area fraction covered by δ crystals and the extent of reaction in the regions surrounding the emerging ferrite grain boundaries on Ti and Ti-Nb IF steels

partially galvanized for 4 s were similar, which indicates that the reactivity of both substrates at the beginning of the galvannealing reaction was comparable.[16]

Zhong et al.[27] explained that relatively slow lap shear strength for the Ti IF steel coatings tested is caused by the excess Ti in the steel. Since excess Ti results in clean grain boundaries by fixing all the C, S and N solute atoms within the ferrite grains, Zn diffusion along the ferrite grain boundaries is facilitated during galvannealing, and these atoms can lead to a substrate grain boundary embrittlement, thus reducing the bonding strength.

They added that, for Ti IF steel coatings, there are more ferrite grains being pulled-out, compared with the Ti-Nb IF steel coatings at a given coating Fe level. This proves that Zn embrittlement is the most severe in Ti IF steels, resulting in relatively low coating/steel bonding strength. With respect to failure, it was reported that Ti promotes flaking failure due to more severe substrate Zn embrittlement.[27]

van Koesveld et al.[31] pointed out that diffusion hampering by interstitials, through obstructing diffusion paths – dislocations and grain boundaries – with soluble C or N atoms, might take place in the Ti-Nb IF steel. Its chemistry sometimes corresponds to a ‘negative excess Ti’ suggesting that some limited amount of C and/or N can have been left free to segregate to ferrite grain boundaries.

They found that the weight losses observed in the case of Ti-Nb IF steel are systematically somewhat lower and less scattered than those of their Ti IF steel counterparts. Associated Rhesca simulation test results strongly suggested that this difference in performance derived from the very distinct surface reactivities of the two steel grades considered. Based on cup tests carried out on identically treated industrial products, it appeared that Ti-Nb IF steel grades exhibited a somewhat better and less scattered powdering resistance than Ti IF steel grades.

Furthermore, it was reported that in the case of the Ti-Si IF steel grades, galvannealing time had to be lengthened from 25 seconds to 40 seconds to produce the same degree of alloying as in its Ti IF steel counterpart, because of its lesser overall reactivity. Besides, in the re-P Ti-Nb IF steel, Zn penetration into ferrite grain boundaries is prevented by the

combined effects of TiFeP precipitation and interstitial atoms (excess Ti is even more negative). However, no surface analysis performed in their study confirmed other authors' assumption that P could segregate at the free surface and thus retard Fe-Zn reactions.[31]

Regarding to outburst formation on the surface of IF steel galvanneal coatings, Miyasaka et al. mentioned that it is well known that galvanneal of IF steel is prone to outburst microstructure and galvannealing of IF steels proceed rapidly compared with that of the conventional Al-killed steels.[22]

Marder et al. also reported that Ti-IF steels are more sensitive to outburst formation than Al-killed or even Nb-Ti steels. [8]

Osman et al. confirmed that while this outburst phenomenon occurs for both types of steels, Ti-stabilized IF steel grades exhibit a higher propensity for outbursts than Ti-Nb-stabilized IF steel grades. As a result, the growth of Fe-rich phases is more rapid for Ti-stabilized IF steels than for Ti-Nb-stabilized IF steels, resulting in a deleterious increase in the thickness of the Γ/Γ_1-layer (the phase closer to the substrate).[3]

Bhattacharya et al. mentioned that it has been suggested that since the affinity of Nb and P is lower than that of Ti and P, Nb does not scavenge P, as does Ti through the formation of FeTiP (Fe-Ti phosphides). As a result, some P is left reducing the outburst reaction. Moreover, they added that another school of thought is that the outburst reaction is higher in Ti IF steels because it has cleaner grain boundaries than Ti-Nb IF steels. This is a result of the segregation of Nb to the grain and sub-grain boundaries in Nb containing IF steels. Finally, one further idea is that Nb also segregates to the surface, thus affecting the formation of the inhibition layer and, in turn, the galvannealing behaviour.[1]

2.4.4.2. FORMATION OF OUTBURSTS

Galvannealing reactivity is the annealing time necessary to reach 8.5 % Fe in the coating.[30] It is significantly increased if the annealing is carried out below the recrystallization temperature, for high recrystallization annealing atmosphere dew points – known to lead to internal selective oxidation, with the formation of nodules below the surface - result in

increased reactivity.[31] Consequently, the rapid penetration of Zn at grain boundaries leads to the formation of outbursts, which are essentially regions of more rapid alloy growth.[3]

Guttmann apud Marder et al.[8] proposed that the Fe_2Al_5 diffusion short circuits would coincide with emerging substrate grain boundaries. Because of the Fe_2Al_5/substrate steel orientation relationship, the high angle boundaries between colonies of the inhibition layer could be coincident with random substrate grain boundaries. Oxide/Fe_2Al_5 interface short circuits may also be preferentially situated at substrate steel grain boundaries. Thus, both the effect of steel solute additions of ferrite grain texture and grain size can affect the rate of inhibition layer breakdown of outburst formation.[8]

Indeed, his studies meant that the Fe_2Al_5 inhibition layer that developed on the substrate during galvanizing forms epitaxially so that Fe_2Al_5 crystals develop colonies of the same orientation as the underlying substrate steel grain. The colonies form low-angle grain boundaries when contained within an underlying substrate grain interior and, therefore, Fe and Zn diffusion follow normal diffusion rates at these low-angle boundaries. However, at the location of a substrate grain boundary, two adjacent Fe_2Al_5 colonies of different orientation form a random high-angle boundary. This high-angle boundary can become a short circuit diffusion path for Fe and Zn interdiffusion, which leads to Fe-Zn alloy phase outburst formation (rapid Fe-Zn phase growth) at substrate grain boundary sites. Thus, the steel substrate grain boundary is expected to be indirectly related to outburst formation, because the steel substrate grain boundary fixes the location of the short circuit diffusion paths in the Fe_2Al_5 inhibition layer.[2]

According to Hisamatsu apud Marder et al.[8], Fe-Zn reactivity at grain boundaries of the substrate will depend upon the ability of the solute element to segregate to these sites. These alloying additions can be separated into elements that segregate to the grain boundaries (e.g. C, P), and those that will form compounds (e.g. Ti, Nb) that will precipitate throughout the grain, leaving the grain boundary ‘pure’ or ‘clean’. Clean grain boundaries will have no barrier to Fe-Zn compound formation, while segregated boundaries will reduce the thermodynamic activity at these sites, decreasing outburst and Fe_2Al_5 inhibition layer breakdown.[8]

Maschek et al. apud Marder et al.[8] also reported that P was found to retard the formation of outbursts and localized growth of the Fe-Zn phases.[21] Marder et al. complemented stating that P was found to segregate to ferrite grain boundaries in re-P LC steels, blocking the diffusion of Zn along grain boundaries and lowering the thermodynamic activity. They mentioned that it had also been proposed that P segregates to the steel surface during recrystallization annealing, stabilizing the inhibition layer and retarding the rate of Fe-Zn phase growth reactions during galvanizing.[8]

Regarding to IF steels, Maschek et al. found that they, in contrast to LC steels, tend to form outbursts preferentially at the grain boundaries of the steel substrate. The retarding effect of P is therefore explained by the formation of Ti-P-precipitates near the grain boundaries of the IF steel substrate. These precipitates consume a distinct amount of solute Ti and therefore compete with the formation of TiC in the steel substrate, allowing additional solute C to segregate at the grain boundaries, which will subsequently retard both the onset of the Fe-Zn reaction at the interface and the formation of outbursts. Other theories suggest that the P diffuses to the surface of the IF steel substrate or interacts with the Fe-Al-Zn inhibition layer after segregating to the grain boundaries in the steel substrate.[26]

Moreover, Marder et al. observed that outburst formation readily occurred in the 0.20 wt% Al baths due to the initial formation of the Fe_2Al_5 inhibition layer; however, increased grain size significantly retarded incubation time and promoted Fe_2Al_5 inhibition layer stability.[8]

Nevertheless, McDevitt et al.[14] affirmed that there was no observation of rapid Fe-Zn growth at the inhibition layer/substrate interface and no mechanical breaking of the inhibition layer has been observed under these conditions simulating commercial galvanneal processing. They said that it proves that outburst mechanism is not the sole means for inhibition layer breakdown during galvannealing. Additionally, they pointed out that if the outbursts mechanism is observed to occur under similar galvannealing conditions in the future, then it will be clear that the inhibition layer is subject to breakdown by either or both of the competing mechanisms.

In addition, the presence of Γ_1 on the inhibition layer prevents intimate contact of the molten Zn with the inhibition layer, which in turn may prevent outburst formation. On long dipping

time samples or on samples produced in higher Al content baths, less surface area of the inhibition layer is covered by Fe-Zn compounds so that the inhibition layer is less protected from direct attack by the liquid Zn, and outburst formation may occur.

Finally, they concluded affirming that their present results also demonstrated that phenomena related to substrate grain boundaries cannot be exclusively attributed to outburst formation as grain boundaries also played an important role in the Al diffusion into the substrate during inhibition layer dissolution.[14]

Meshii et al.[13] also confirmed that a correlation between formation of the Γ_1 phase and occurrence of outbursts exists. They started affirming that, in addition to the Fe-Al layer inhibiting the interaction between the substrate and the molten Zn, the Γ_1 layer may too have hindered molten Zn-substrate interaction and further formation of the Fe-Zn intermetallic compounds. The presence of the Γ_1 layer after the dipping process may in part explain why outbursts were not observed. Reporting to Hisamatsu, they concluded stating that the outburst phenomenon occurs by direct reaction of the galvanizing bath and the steel substrate through an Fe-Al-Zn ternary compound layer formed in the initial stage of immersion. Finally, as the Fe-Al inhibition layer broke down, the Γ_1 layer prevented interaction between the substrate and the molten Zn, which in turn deterred rapid localized growth of the Fe-Zn compounds.[13]

Baril et al.[10] stated that outbursts are more likely to form at the grain boundaries of the substrate. In fact, random high angle boundaries of Fe_2Al_5 are short circuit diffusion paths for Zn. They further observed that the formation of outbursts is expected to lead to a significant increase of the local Fe content in surrounding liquid Zn, which will tend to pump Al from the bath to form Al-Fe-rich compounds. This may explain the relatively large amount of Al in the coating for immersion time of 3.5 and 6 seconds, for an Al bath content of 0.10%.[10]

Through higher magnification analysis, van Koesveld et al.[31] reported that the presence of ferritic grain boundaries in the depressed areas was revealed, which correspond to initial outbursts. This substantiates that outbursts appear most generally along the ferritic grain

boundaries of IF steel substrates, thus accounting for the apparent relationship between ferritic grain and crater sizes.

Moreover, obviously enough for them, outbursts could only grow by consuming the Fe immediately underneath them, which results in an average interface depression of about 10% of the total coating thickness (thus accounting for the total amount of Fe needed for complete alloying). The corresponding enhanced Fe consumption along the grain boundaries increases the steel-coating interface roughness, which improves its shear strength.[31]

Regarding to the morphology of outbursts, Zuhr et al.[23] observed that it was similar to that found on other 0.20 wt% Al-Zn coatings and consisted of a thin Γ layer of approximately 1.0 μm at the interface and a thick 10- to 100-μm δ phase layer adjacent to the Γ layer. Similar to other 0.20 wt% Al-Zn coatings, the δ layer was in contact with the liquid Zn. Furthermore, the localized Fe-Zn phase growth was found to correspond directly to the location of a substrate grain boundary site, and the results show that nucleation of the outbursts occurred in the same grain boundary independent of P surface segregation.[23]

Jordan et al.[2] added that the Fe-Zn outbursts typically had trailing elongated tails of Fe-Zn phase that extended down along substrate grain boundaries. They also confirmed that the Fe-Zn outbursts also appear to consist of Γ and δ phase layers.[2]

2.4.4.3. FORMATION OF CRATERS

It was postulated that Ti addition to the IF steel gives superior mechanical properties compared to Nb added IF steel. Ti added IF steel produced in a very simple process exhibits superior mechanical properties. However, Ti addition tends to cause streaky surface defect, which appears after galvannealing as white band along rolling direction. The appearance of streaky defect is depressed with the decrease in Ti content of substrate. Therefore, the amount of Ti addition must be kept at lower level (about 0.025%).[32]

Miner et al.[33] reported that streaks are generally associated with Ti-stabilized IF steel substrates and are caused by differences in reflectivity associated with local variations in

coating morphology. Countermeasures for streaking include lower pot Al levels to promote more uniform alloying, lower Ti levels to avoid nonuniform scaling during hot rolling and better control of upstream processing to provide a more uniform surface for the galvannealing reaction. It was also affirmed that galvannealed steels are more susceptible to electroprimer cratering which can adversely affect pain line productivity and under some conditions can exhibit loss of the galvanneal coating during paint chipping.[33]

Finally, Parks et al.[11] studied the influence of ferritic rolling upon the occurrence of streaks. They pointed out that ferritic rolling of ultra-low C interstitial-free steels has a positive effect on Ti-streak surface defects that occur on Zn-coated products. They characterized this defect as associated with Ti-containing surface oxides that appear as dark streaks following galvannealing. While no quantitative data are available, it can be concluded that lower furnace temperatures result in fewer surface oxides.[11]

3. EXPERIMENTAL PROCEDURE

3.1. MATERIALS

Two IF steel grades were used for this project, a Ti-stabilized and a dual (Ti-Nb) stabilized IF steel grade. Table 4 features information on the steel samples used for this project.

Table 3. IF Steel substrates and conditions tested.

Steel Substrate	Condition	Code
Ti-stabilized IF steel	As received (cold rolled)	A
Dual-stabilized IF steel	As received (cold rolled)	B
Ti-stabilized IF steel	Galvanized (GA)	AG
Dual-stabilized IF steel	Galvanized (GA)	BG

120 x 200 mm cold rolled steel sheet coupons were received from two different suppliers, where the longitudinal axis corresponds to the rolling direction. The as-received coupons were immediately degreased with soap and dried off with ethanol, and a 50 x 50 mm central surface area was grinded and polished on each sample for the purpose of minimizing the surface roughness for further GD-OES surface analysis.

The chemistries for the two IF steel grades, obtained by the Jobin-Yvon/Horiba Quantum IQ V2.22 Glow-Discharge Optical Emission GD-OES in bulk composition mode, are shown in table 5.

Table 4. Chemistries for the Ti-stabilized IF steel grade and the dual-stabilized IF steel grade.

Steel Chemistries	Ti-stabilized IF Steel	Dual-stabilized IF Steel	Ti-stabilized IF Steel	Dual-stabilized IF Steel
	Steel A	Steel B	Steel AG	Steel BG
wt% C	0,003	0,002	0,002	0,002
wt% Mn	0,16	0,19	0,11	0,18
wt% P	0,008	0,005	0,015	0,009
wt% S	0,008	0,005	0,005	0,006
wt% Si	0,007	0,005	0,001	0,009
wt% Cu	0,020	0,018	0,008	0,020
wt% Ni	0,013	0,019	0,004	0,010
wt% Cr	0,02	0,02	0,01	0,05
wt% Mo	0,004	0,001	0,002	0,007
wt% V	0,002	0,001	0,010	0,001
wt% Nb	0,006	0,029	0,005	0,020
wt% Ti	0,052	0,020	0,043	0,030
wt% Sn	0,002	0,006	0,001	0,002
wt% Al (sol.)	0,03	0,035	0,030	0,060
wt% N	0,002	0,003	0,002	0,001
exc Ti* (%)	0.009	(0.013)	(0.002)	(0.004)

*** exc Ti = Ti – 3.99.C – 1.49.S – 3.42.N – 1.55.P**

3.2. TESTS PERFORMED

Table 6 features the tests the above mentioned steel samples were submitted to.

Table 5. Tests performed on the IF steels.

	Steel Code			
Characterization Tool	A	B	AG	BG
Sample Chemistry	X	X	X	X
HDG Simulations	X	X		
Interrupted Cycle HDG Simulations	X	X		
Glow Discharge Optical Emission Spectroscopy	X	X	X	X
Scanning Electron Microscopy	X	X	X	X
X-ray Photoelectron Microscopy		X		

Figure 1 features a chart displaying a comprehensive plot of the steps carried out by this research project including sample characterization as well as microscopy techniques used.

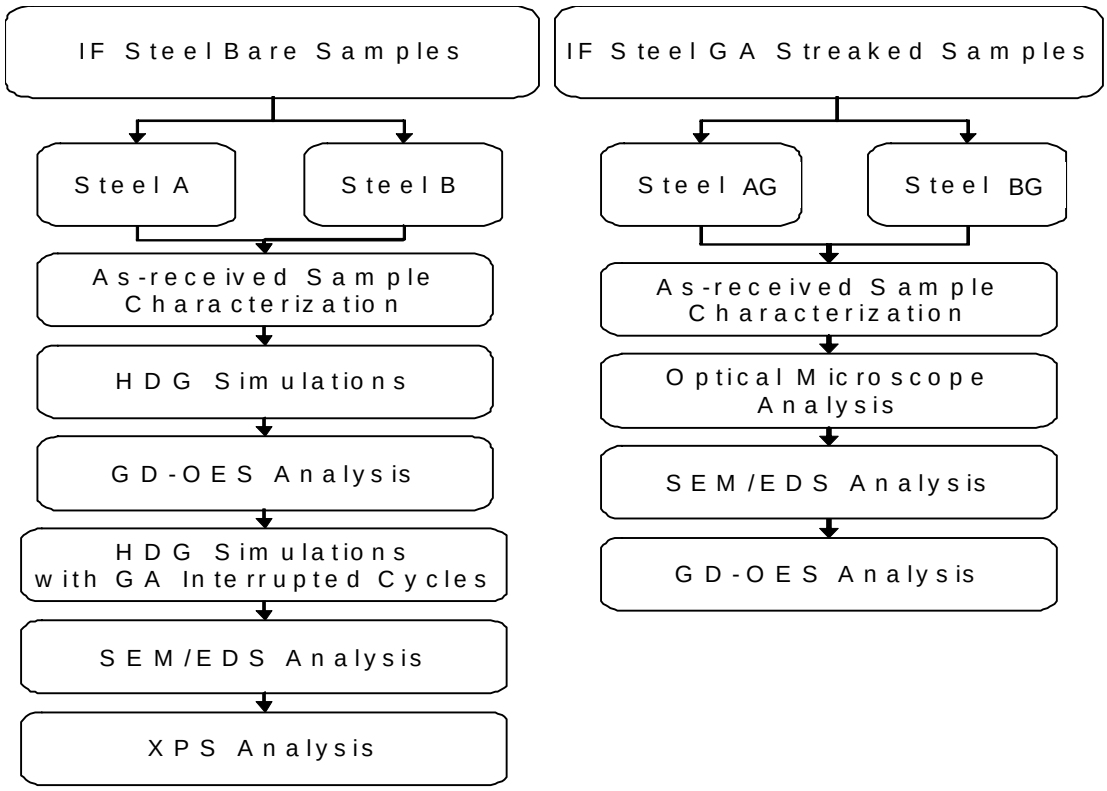

Figure 1. Flowchart of the steps carried out by this research project.

3.3. METALLOGRAPHIC CHARACTERIZATION OF AS-RECEIVED SAMPLES.

IF steel sheet coupons were sheared down to 10 x 10 mm-size samples and then mounted as three-piece cross section sandwiches in cold resin for the purpose of metallographic characterization. As soon as the resins solidified under vacuum environment, the samples were ground on Si carbide papers starting from 240- down to 600-grit papers in water. After that, the samples were polished on rounded Si carbide polishers starting from 800 down to 4000-grit papers, and then properly dried off to be taken to next sample preparation stage. The final fine polishing step was carried out by using both 3µ- and 1µ-grit diluted Al_2O_3 paste .

Etching was performed by immersing samples for 1 min in a 1% HNO_3-Ethanol (nital) solution. Next, the samples were taken to an optical microscope for their first characterization. For the purpose of measuring the average ferrite grain size, an imaging software attached to the Carl-Zeiss optical microscope was used. The methodology complied with the guidelines according to the Heyn Lineal Intercept Procedure described on the ASTM E 112 - 96 standard.

3.4. IF STEEL GA SAMPLES WITH STREAKS

Industrial IF steel GA samples with streaks were received from two different suppliers and correspond to both Ti- and dual-stabilized IF steel grades. GD-OES bulk composition mode was used to obtain the bulk steel chemistry of the samples.

Knowing the chemistries for the two sets of industrial streaked samples, next step carried out was the coating characterization, when GD-OES surface analysis method was used for that purpose. The author sought to establish comparisons between dark and light streaked areas for both Ti- and dual-stabilized IF steel GA samples.

Representative dark and light streaked areas on industrial samples supplied by two different suppliers were chosen for morphology characterization and chemistry analysis. The samples were degreased with soap and cleansed with ethanol, sheared to fit the GD-OES sputtering beam size and then stored in desiccators to keep them from excessive humidity.

3.5. HOT-DIP PROCESS SIMULATOR

GENERAL DESCRIPTION

In order to simulate the operating conditions of a commercial Continuous Galvanizing Line in a smaller scale, an Iwatani-Europe Hot-Dip Process Simulator, HDP, was used. This equipment is composed of an upper chamber for sample input/output and further cooling by faster rates. The infrared heat treatment furnace lies in the middle of the equipment, operating by either radiant or induction heating. Finally, the lower middle part of the equipment consists of a chamber for slower cooling rates, which is placed right above the 30 kg Zn-bath crucible.

The picture below displays the Iwatani-Europe Hot-Dip Process Simulator used to perform HDG simulations upon IF steel panels.

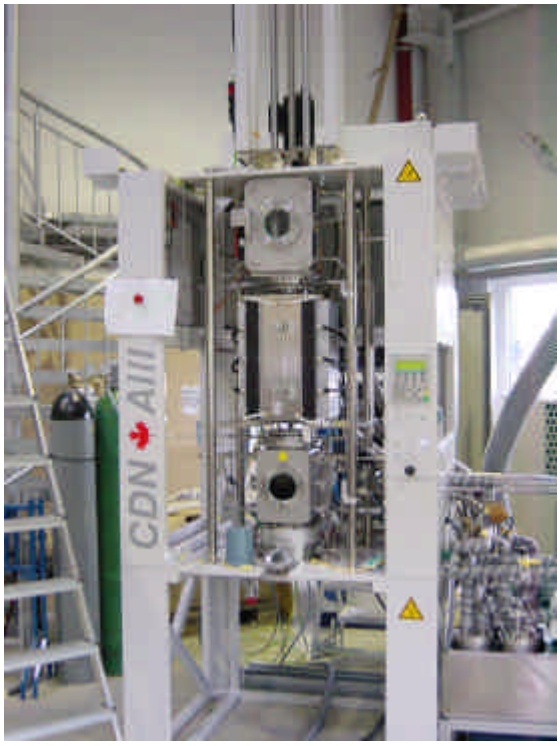

SAMPLE GEOMETRY

In order to fit the HDP simulator sample input chamber, the cold rolled IF steel sheets were cut off in several coupons 120 x 200 mm in area. Next, a 50 x 50 mm central area was polished in order to minimize the surface roughness of the samples.

SAMPLE PREPARATION FOR THE HDP SIMULATOR.

Industrial as-received cold rolled Ti-stabilized and dual-stabilized IF steel samples were received from steelmakers.

Due to dimensional restrictions given by the sample input chamber at the HDP simulator, the samples were sheared down to 120 x 200 mm coupons.

Furthermore, in order to prepare the sample surface for further HDP simulation, soap was used to remove grease as well as ethanol for contamination removal.

Moreover, tap water was used to wash residues away from the sample surface, followed by ethanol application on the sample surfaces in order to remove any contaminants.

Finally, fast hot-air cooling was performed in order to keep the sample surfaces from excessive ethanol residues.

3.5.1. DEFINITION OF HEAT TREATMENT CYCLES FOR Ti- AND DUAL-STABILIZED IF STEEL GRADES.

In order to set up the heat treatment cycles for both IF steel grades with a special focus on the galvanneal heat treatment parameters - GA temperature and soaking time -, trial dipping samples were run at the HDP simulator aiming to produce a fully-developed GA coating on top of the steel substrate.

3.5.1.1. EXPERIMENTS FOR SETTING GA TEMPERATURES AND SOAKING TIMES

The experiments were carried out by using the same effective Al 0.13 wt% in the Zn pot and same furnace controlling atmosphere 95% N_2 + 5% H_2 in the cooling chambers. The operating parameters were set up to produce a 1 μm-thick Γ layer close to the interface between the Zn coating and the steel substrate.

3.5.2. INTERRUPTED CYCLES FOR IF STEEL BARE SAMPLES

Once the thermal profiles for both IF steel grades were properly set up, interrupted cycles were run for bare samples from both IF steel grades, stopping the cycle at pre-determined spots along the thermal curve, and samples were taken out at each one of these spots along the thermal profile. The interrupted thermal cycles for both IF steel grades can be seen on graphics of Figure 3, whose main processing parameters are as follows:

Thermal cycle set up for samples of both IF steel grades are given according to table 7.

Table 6. HDG operating parameters carried out for setting up thermal cycles run on both IF steel grades during HDG simulations.

Operating parameter	Ti-stabilized IF steel grade	Dual-stabilized IF steel grade
Peak Annealing Temperature (PAT)	875 ^{0}C	830 ^{0}C
PAT Soaking Time	22,1 s	61,2 s
Zn Bath Temperature	465 ^{0}C	465 ^{0}C
Zn Bath Immersion Time	5,1 s	5,8 s
Galvannealing Furnace Temperature	510 ^{0}C	510 ^{0}C

Figure 2 shows plots of the thermal profiles employed.

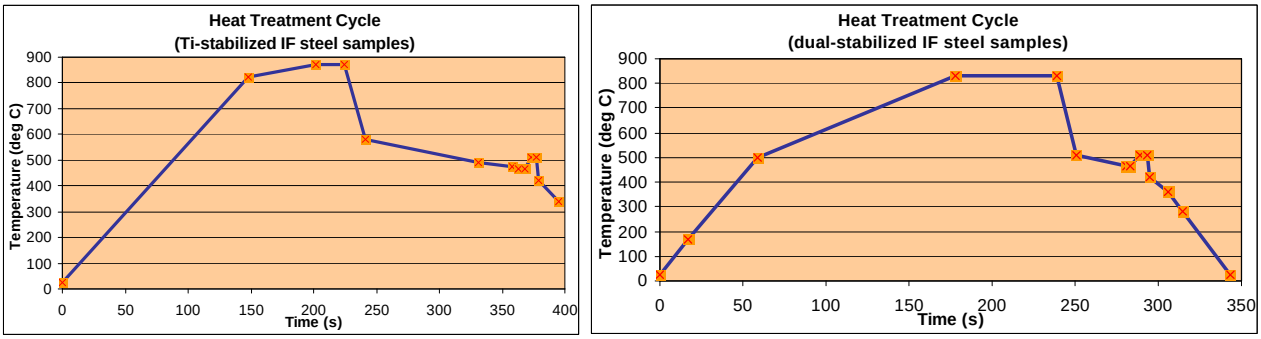

Figure 2. Thermal profiles set up for both IF steel grades at the HDP simulator. The markers show sampling conditions.

The purpose of this procedure was to observe how Ti and Nb surface concentrations evolve along the thermal profile for both Ti- and dual-stabilized IF steel grades compared with the as-received condition as well as to assess the effect of the annealing and galvannealing heat treatments upon the Ti and Nb surface segregation.

3.5.3. Ti-STABILIZED IF STEEL GRADE

12 (twelve) Ti-stabilized IF steel coupons were produced throughout the thermal profile set up for Ti-stabilized IF steels by interrupted cycles at the HDP simulator, one from each spot where the thermal cycle was purposely stopped for sample collection. As soon as the coupons came out of the HDP simulator they were soaked in isopropanol bath in order to keep them from excessive oxidation.

The polished surfaces on the coupons were then identified, dried off and sheared down to 20 x 120 mm slices to further fit the GD-OES sample chamber. Next, the slices were taken to GD-OES measurements, where a 4 mm-diameter rounded crater was carved on the surface to sputter and collect material for quantitative chemistry surface analysis.

3.5.4. DUAL-STABILIZED IF STEEL GRADE

12 (twelve) dual-stabilized IF steel coupons were produced throughout the thermal profile set up for dual-stabilized IF steels by interrupted cycles at the HDP simulator, one from each spot where the thermal cycle was purposely stopped for sample collection. As soon as the coupons came out of the HDP simulator they were soaked in isopropanol bath in order to keep them from excessive oxidation.

The polished surfaces on the coupons were then identified, dried off and sheared down to 20 x 120 mm slices to further fit the GD-OES sample chamber. Next, the slices were taken to GD-OES measurements, where a 4 mm-diameter rounded crater was carved on the surface to sputter and collect material for quantitative chemistry surface analysis.

3.5.5. POST-PROCESSING AND STORAGE OF EXPERIMENTAL COUPONS

As soon as the coupons passed through the heat treatment cycles and came out of the last cooling step of the thermal profile, they were soaked in an iso-propanol bath for the sake of keeping them from excessive oxidation.

Afterwards, the samples remained soaked in iso-propanol up to the point when they were taken out to be cut off down to 20 x 120 mm slices in order to fit the GD-OES sputtering chamber.

3.6. SAMPLE ANALYSIS TECHNIQUES

IF steel bare samples were analyzed by using the following image and chemistry analysis techniques: Scanning Electron Microscopy, Energy Dispersive Spectroscopy and Glow Discharge Optical Emission Spectroscopy.

The samples with streaks on top of GA coatings were supplied by two different suppliers. In order to establish comparisons between the areas featuring dark and light streaks, SEM was used for image analysis and EDS for chemistry measurements, on a Philips SEM 515 Scanning Electron Microscope, attached to a Link Analytical Pentafet Energy Dispersive Spectroscope micro analyzer.

SEM was also used as a tool for image analysis on samples with streaks on top of GA coatings as well as its attached EDS microanalyzer for the chemistry measurements. A new set of GD-OES profiles was run for the coated samples, this time aiming to identify the Fe-Zn intermetallic phases, determine the thickness of the Γ layer and also obtain the Ti and Nb concentration profiles through the GA coating, at the interfacial layer and into the steel substrate.

GLOW DISCHARGE OPTICAL EMISSION SPECTROSCOPY FOR SAMPLE ANALYSIS

A Jobin-Yvon/Horiba Quantum IQ V2.22 Glow-Discharge Optical Emission Spectroscope was used to obtain the surface chemistry profiles of the alloying elements for the as-received samples.

X-RAY PHOTOELECTRON MICROSCOPY FOR SAMPLE ANALYSIS

The X-ray Photoelectron Spectroscopy PHI Quantera SXM was used to identify the chemical state of Nb at the surface of IF steel substrates. The samples for the surface characterization of Nb compounds at the surface of dual-stabilized IF steel grade were taken from polished areas placed on the centre of the steel panels. The samples were then sheared down to 15 x 15 mm and wrapped in aluminum foil in order to keep them from external contamination. As the samples showed a slight C contamination when they were placed in the XPS stage chamber due to the higher C diffusivity and segregation enthalpy at lower temperatures ($T < 400\ ^{0}C$) relative to Si and P for example, Ar ion bombardment was used to sputter away the outer layers, therefore getting rid of the surface contaminants, among those mainly C.

CRATER AND STREAK CHARACTERIZATION OF GA COATINGS

Industrial GA samples coating Ti-stabilized IF steel substrates featuring dark and light streaked areas on top were received from steelmakers. Streak characterization was made by both optical and electron microscopy.

Therefore, SEM was used as a tool to perform crater identification, characterization and quantification. Furthermore, EDS analyzer was performed to assess the typical chemistries found for craters on bottom of light and dark streaked regions.

CHARACTERIZATION OF STREAKS AND CRATERS ON TOP OF GA COATINGS FOR INDUSTRIAL SAMPLES

Industrial GA samples with streaks on top were supplied by two different suppliers. The samples were degreased with soap and ethanol was used to clean them for further drying

off. Streaked spots across the surface were tactfully chosen, which further lead to cut offs for the Scanning Electron Microscope.

CHARACTERIZATION OF STREAKS AND CRATERS ON IF STEEL PANELS RUN UNDER SPECIAL COOLING CONDITIONS AT THE HDP SIMULATOR

Ti- and dual-stabilized IF steel GA panels were selected for special tests at the HDP simulator with the purpose of creating streaks on top of GA coatings. The thermal profiles were set up taking into account the cooling conditions after the GA heat treatment. In order to enable the operating conditions to create streaks, He gas was gushed in the fast cooling chamber instead of 5%H_2-N_2 in order to speed up the cooling rate.

The thermal cycles featuring faster cooling rates for both IF steel grades can be seen on Figure 3.

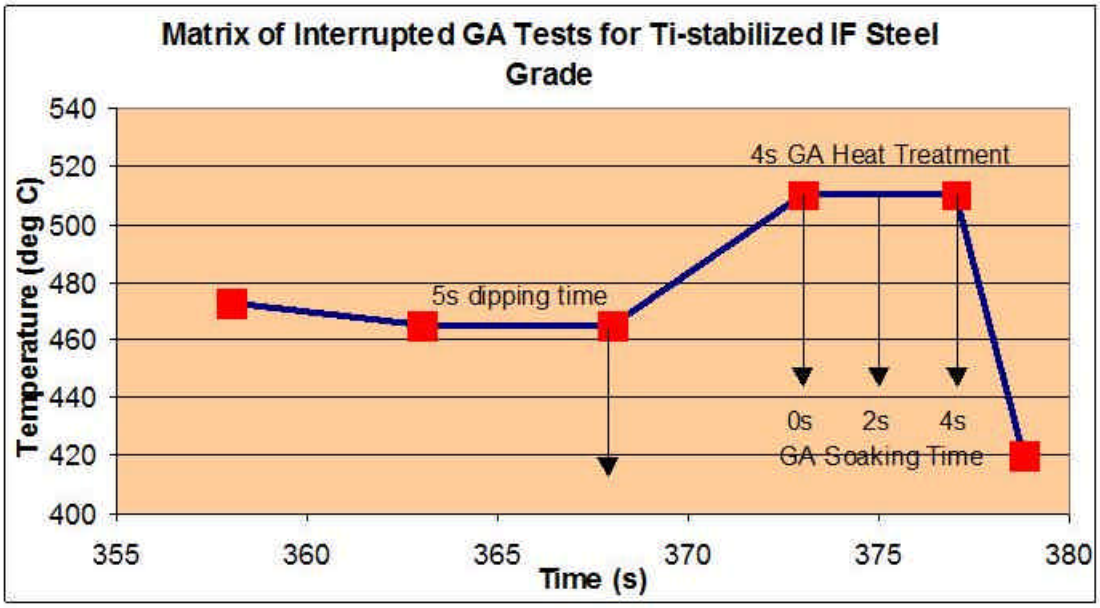

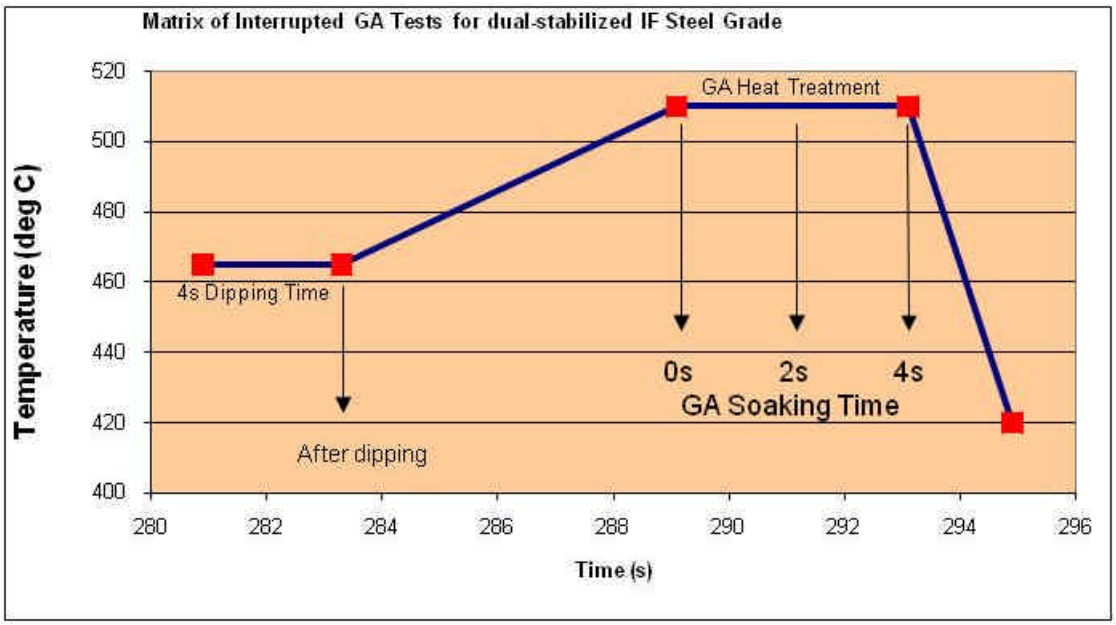

Figure 3. Thermal sequence for sampling with interrupted GA thermal cycles for both IF steel grades at the HDP simulator.

4. RESULTS AND DISCUSSION

4.1. MICROSTRUCTURE CHARACTERIZATION

The micrographs on Figures 4 and 5 show the typical microstructure found for the as-received, i.e. as-cold-rolled samples, for both Ti- and dual-stabilized IF steel substrates. The numbering of the Heyn Lineal Intercept Procedure for measuring the ferrite grain size is also shown.

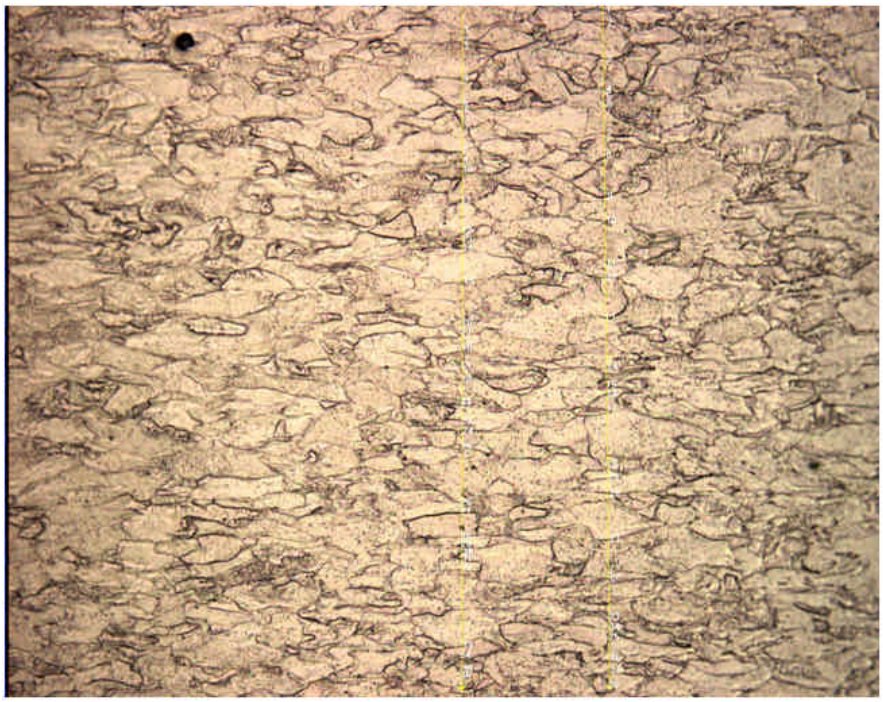

Figure 4. Micrograph featuring typical microstructures found for the as-received (as-cold-rolled) samples for Ti-stabilized IF steel substrate (optical microscope, magnification: 100X)

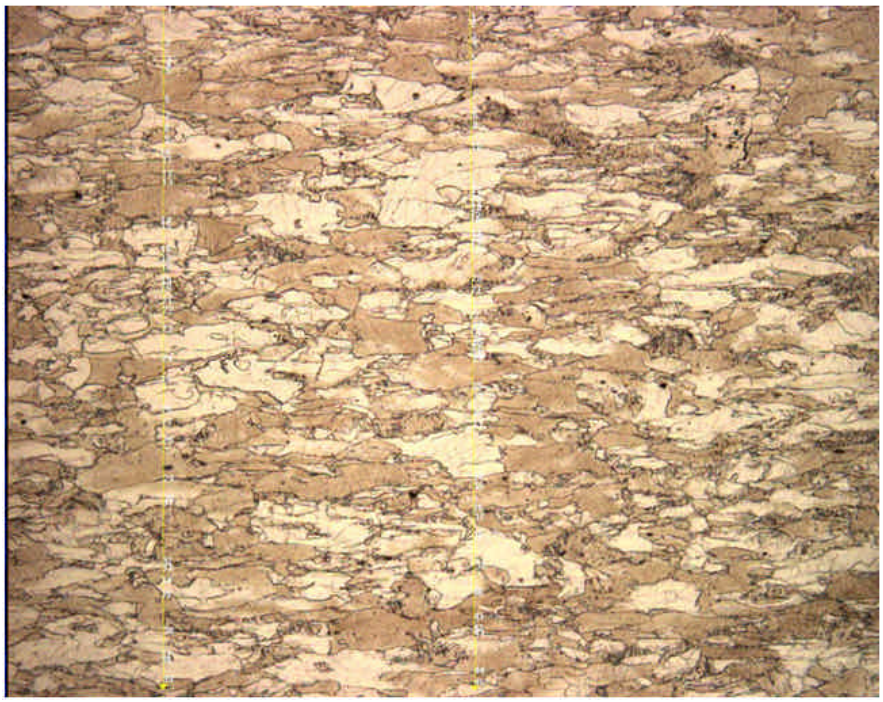

Figure 5. Micrograph featuring typical microstructure found for the as-received (as-cold-rolled) sample for dual-stabilized IF steel substrate (optical microscope, magnification: 100X).

The results carried out according to the Heyn Lineal Intercept Procedure for measuring the ferrite grain size described on the ASTM E 112 - 96 standard are on table 7.

Table 7. Ferrite average grain sizes of the IF steels studied before and after galvannealing.

IF Steel Grade	As-received	Galvannealed
Ti-stabilized	21.74 μm	34.48 μm
Dual-stabilized	15.15 μm	21.74 μm

4.2. CHEMICAL PROFILES ON Ti- AND DUAL-STABILIZED IF STEEL BARE AND COATED SAMPLES

The trial dipping samples ran at the HDP simulator in a 0.13 wt% effective Al in Zn bath and same furnace controlling atmosphere, 95% N_2 + 5% H_2, showed that, for a Ti-only-stabilized IF steel substrate, 8s at 510 ^{0}C were necessary to produce a fully-developed GA coating featuring a 1 μm-thick Γ layer. On the other hand, 15s were needed for the dual-

stabilized IF steel substrate to produce the same results at the same temperature, according to images shown on figure 6. Therefore, it can be concluded that a Ti-stabilized IF steel substrate is more reactive than a dual-stabilized IF steel substrate.

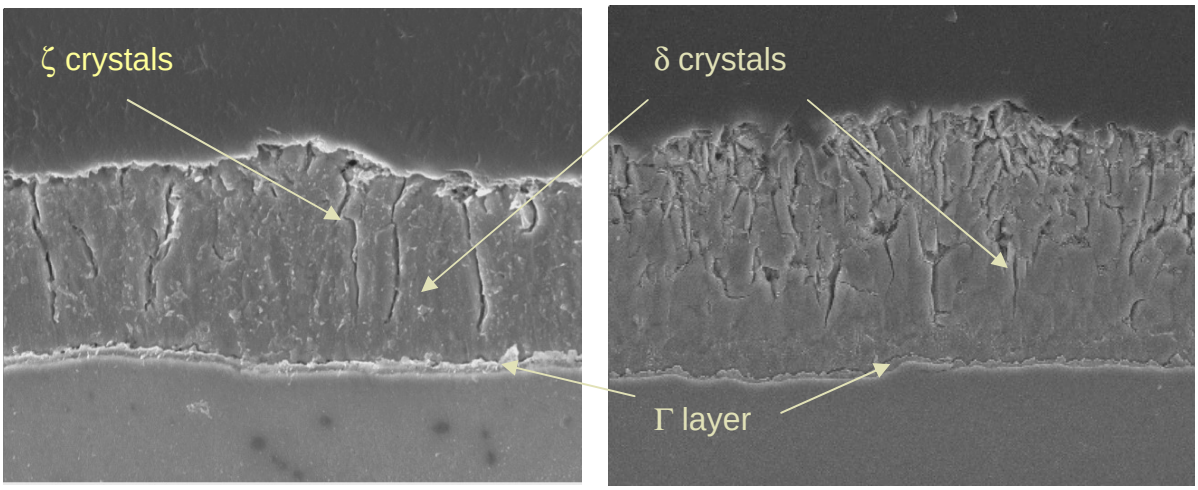

Figure 6. SEM images at 2100x and 2020x featuring the GA coating cross section for the Ti-stabilized IF steel grade (left-hand side) and the dual-stabilized IF steel grade (right-hand side).

GD-OES was used as a tool to assess the surface elemental chemistry on bare steel samples. As previously mentioned, 12 spots were chosen along the interrupted thermal profile curve, where the samples were taken out of the HDG simulator and their surfaces were assessed in order to understand the trend for both Ti and Nb surface concentrations along the thermal profile.

Figures 7 and 8 feature the spots chosen along the thermal profiles for both IF steel grades as well as the main areas of focus, i.e., the prior condition to sample dipping into the Zn bath.

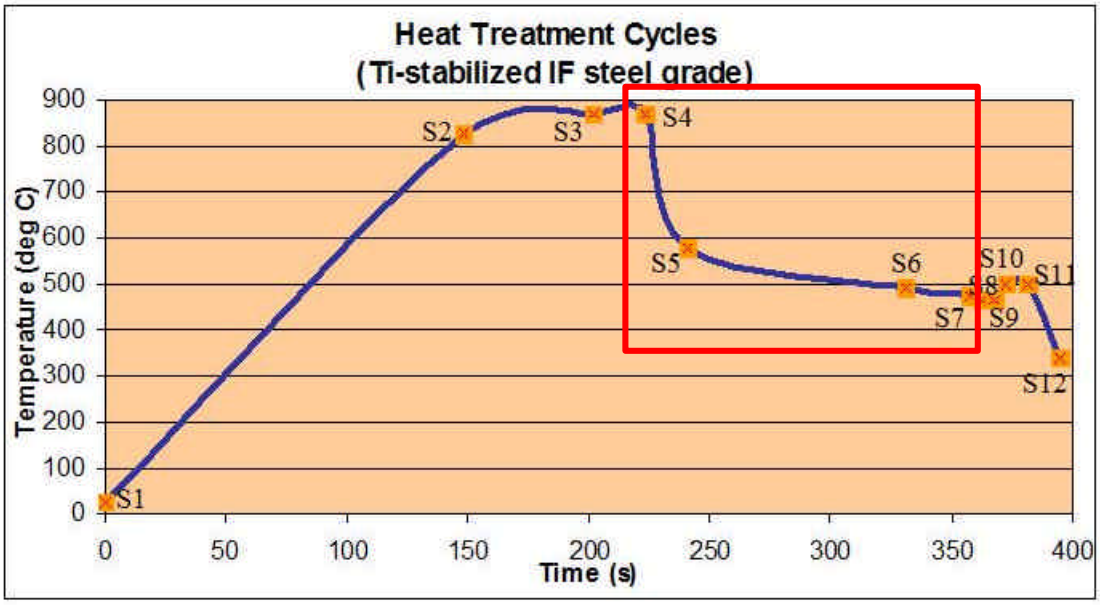

Figure 7. Spots chosen along the Ti-stabilized IF steel thermal profile. Region within the solid red square feature the prior condition to sample dipping into the Zn bath.

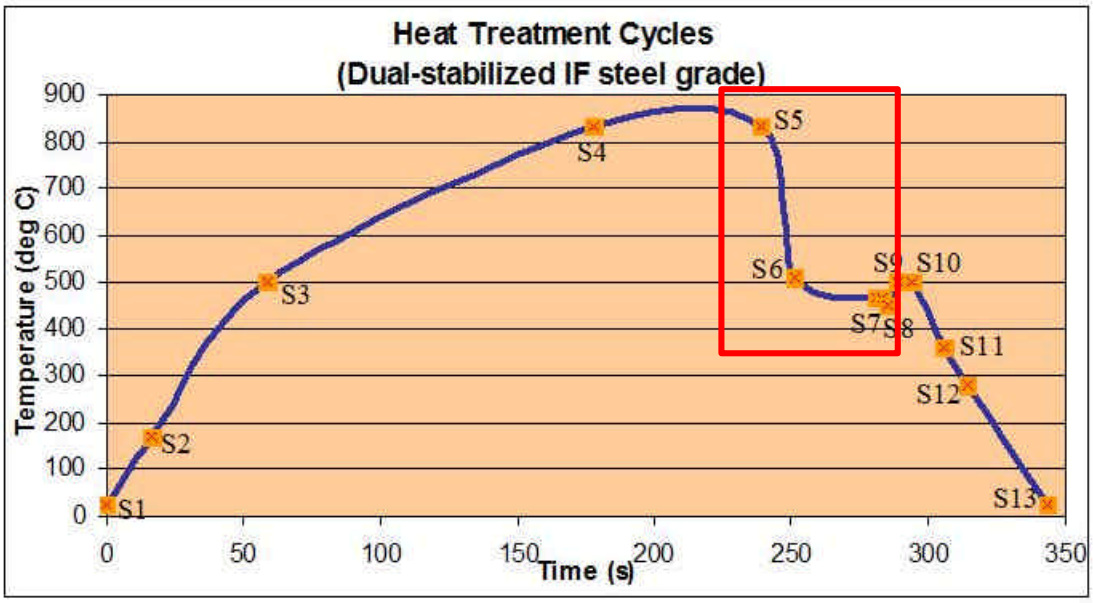

Figure 8. Spots chosen along the dual-stabilized IF steel thermal profile. Region within the solid red square feature the prior condition to sample dipping into the Zn bath.

Therefore, as soon as the samples were taken out of the HDG simulator along the interrupted thermal profiles mentioned above, their surface chemistries were assessed through GD-OES analysis.

Figures 9 to 12 show the Ti and Nb outermost surface concentration profiles along the thermal curves for both Ti- and dual-stabilized IF steel substrates found out for bare samples.

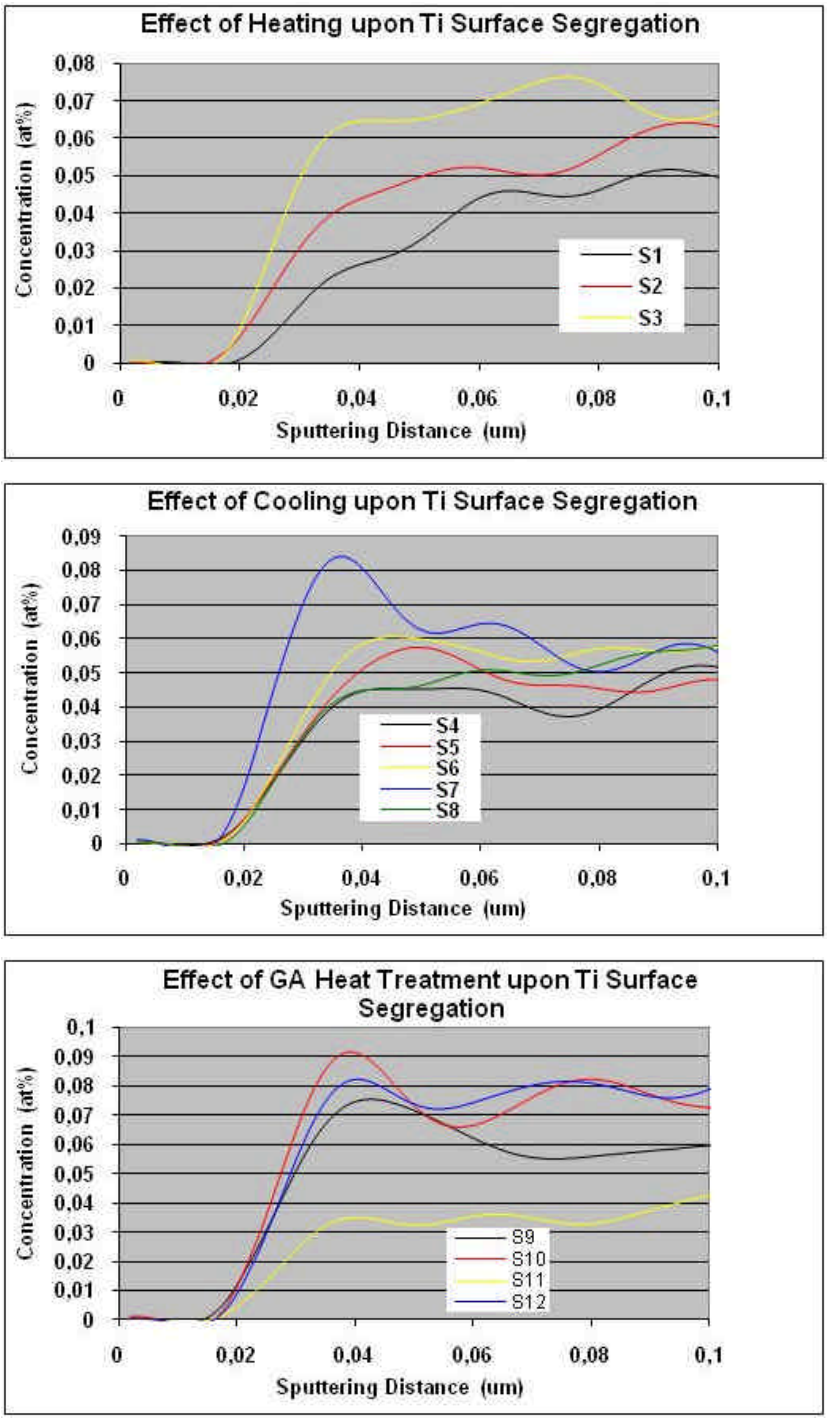

Figure 9. Ti outermost surface concentration along the spots where bare steel samples were taken out of Ti-stabilized IF steel thermal profiles. (S1 to 12 => temperature vs. time condition)

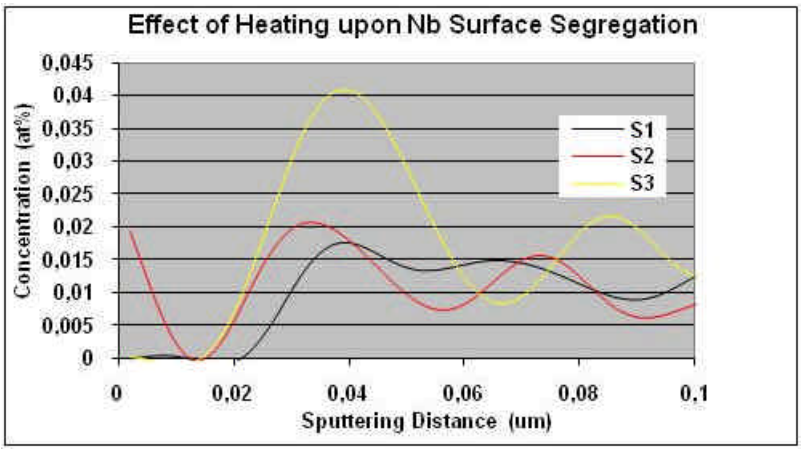

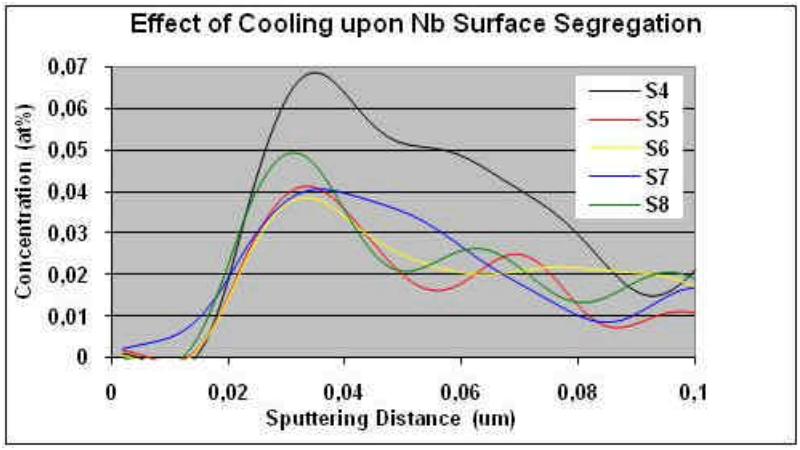

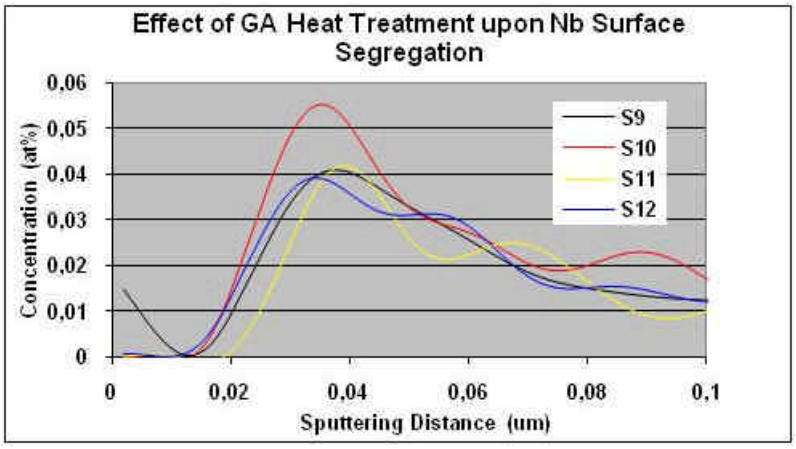

Figure 10. Nb outermost surface concentration along the spots where bare steel samples were taken out of Ti-stabilized IF steel thermal profiles. (S1 to 12 => temperature vs. time condition)

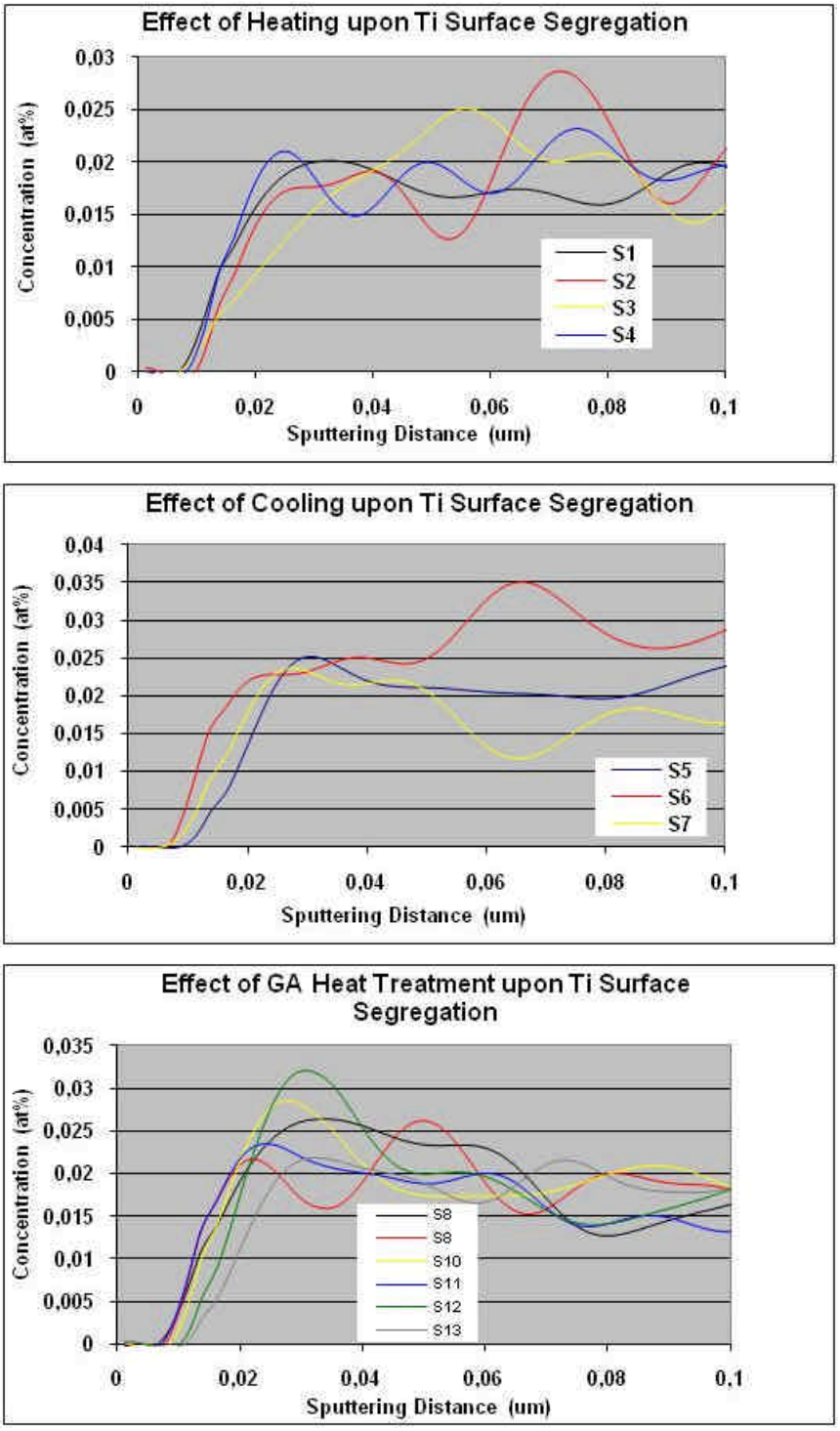

Figure 11. Ti outermost surface concentration along the spots where bare steel samples were taken out of dual-stabilized IF steel thermal profiles. (S1 to 12 => temperature vs. time condition)

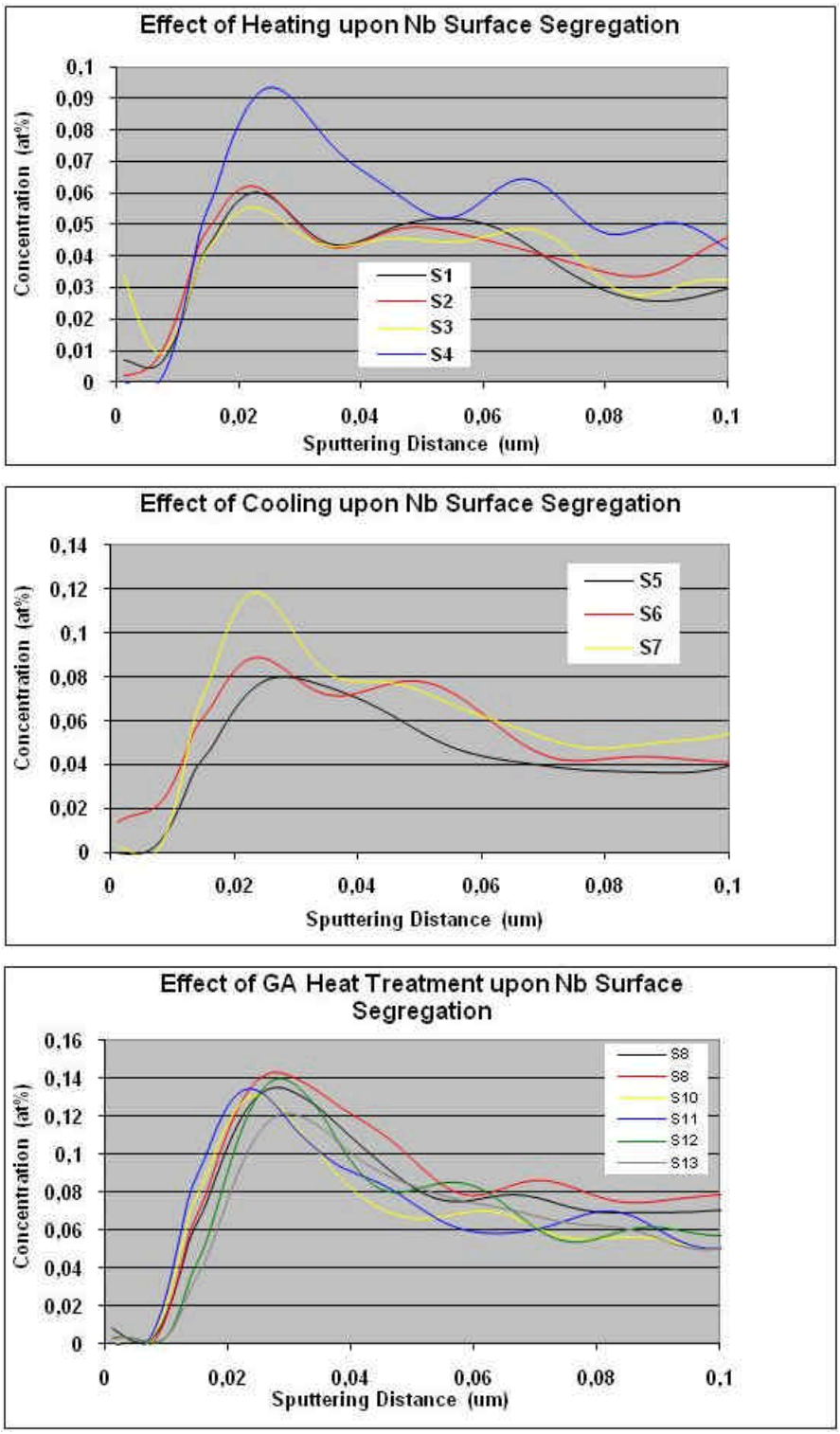

Figure 12. Nb outermost surface concentration along the spots where bare steel samples were taken out of dual-stabilized IF steel thermal profiles. (S1 to 12 => temperature vs. time condition)

Therefore, GD-OES results for bare samples on both IF steel grades showed that there is a Ti depletion at the outermost surface of both Ti- and dual-stabilized IF steel substrates. The influence of annealing and galvannealing heat treatments upon Ti surface segregation is

minimal and not remarkable. Up to a sputtering depth of 0.02 µm into the steel substrate, a Ti depletion was found on most samples along the thermal profile for both IF steel grades. Moving farther into the steel substrate - 0.1 µm – a slight Ti enrichment was found for most part of samples on both IF steel substrates. This enrichment is likely to be associated with a small amount of Ti that has not been previously tied up, therefore available in solid solution. According to excess Ti calculations based on the formula excess Ti = total Ti – 3.99C – 1.49S – 3.42N – 1.55P given by Marder et al., there are 90 ppm Ti left in solid solution and available for diffusion prior to the annealing heat treatment on the Ti-only-stabilized IF steel grade. GD-OES chemistry results for Ti can be seen on figure 13.

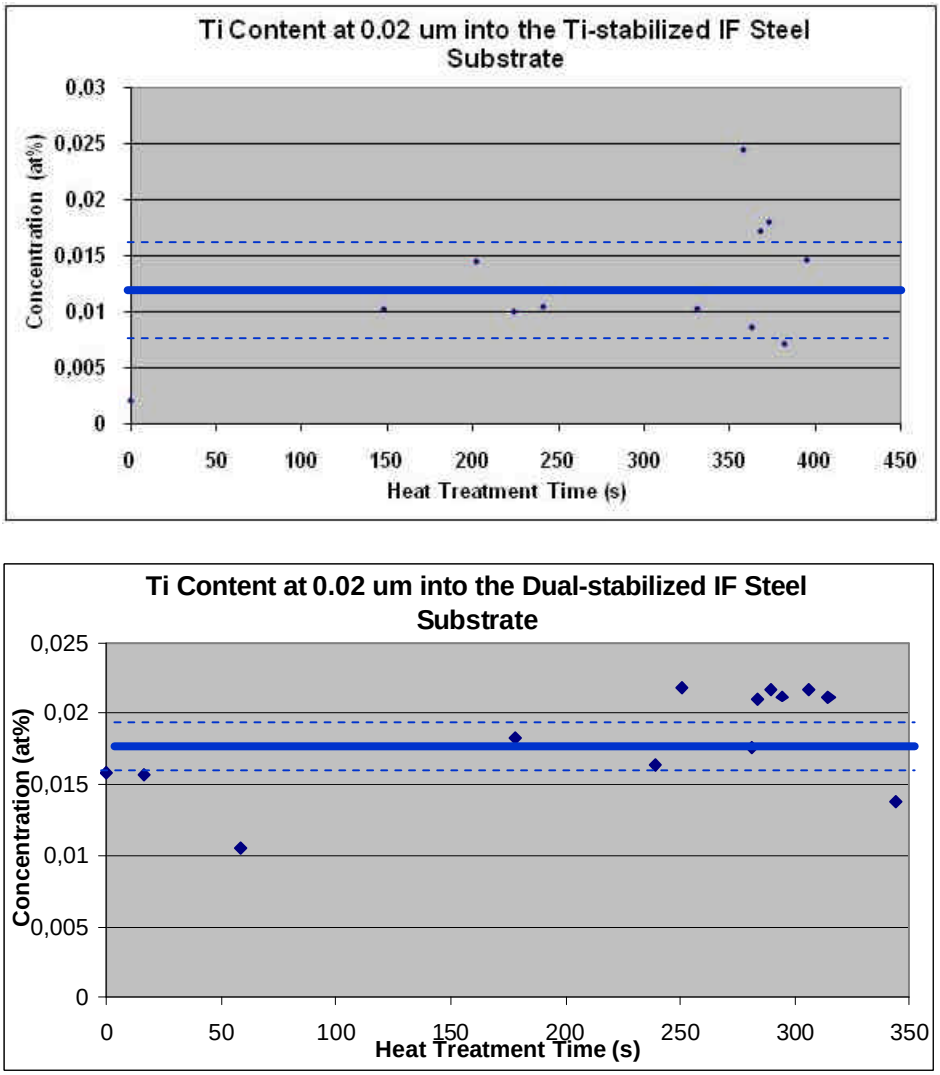

Figure 13. Ti surface concentration results at 0.02 µm into the Ti- and dual-stabilized IF steel substrates along the thermal cycles set up for both IF steel grades (Ti bulk concentrations are 0.062 at% and 0.024 at% respectively).

On the other hand, a strong Nb enrichment was found at the nearest surface on both Ti- and dual-stabilized IF steel substrates. As soon as the samples started to be heated upwards the annealing peak, part of Nb in solid solution starts to diffuse towards the outermost surface of the steel substrate, driven by the tendency of chemical potential uniformity for this element between the bulk of the steel substrate and the surface. In the wake of the annealing heat treatment, those high Nb concentrations remain at the nearest surface all the way through the end of the GA heat treatment cycle. Besides, during galvannealing heat treatment no remarkable effect has been observed upon the Nb surface segregation. Nb surface concentration profiles are featured on figure 14.

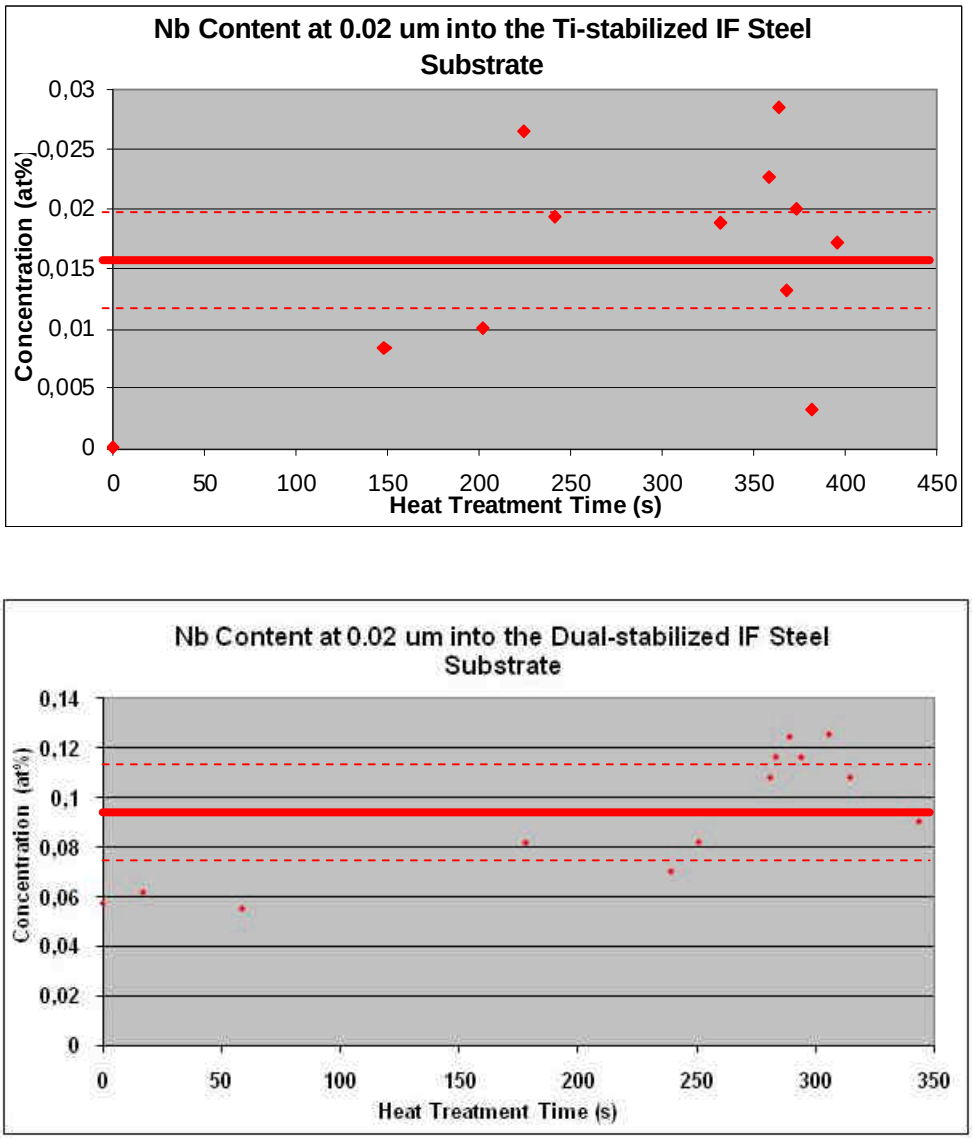

Figure 14. Nb surface concentration results at 0.02 mm into the Ti- and dual-stabilized IF steel substrates along the thermal cycles set up for both IF steel grades (Nb bulk concentrations are 0.005 at% and 0.029 at%, respectively).

XPS analyses were carried out aiming to assess the Nb chemical state for the as-galvannealed condition at the surface of IF steels. For this purpose, the samples chosen for such analysis were those taken at the threshold of the GA heat treatment, which represent the setting condition for the subsequent galvannealing heat treatment. The XPS results showed a characteristic Nb $3d_{3/2}$ peak, which corresponds to Nb oxides in the form of Nb_2O_5, as can be seen on figure 15.

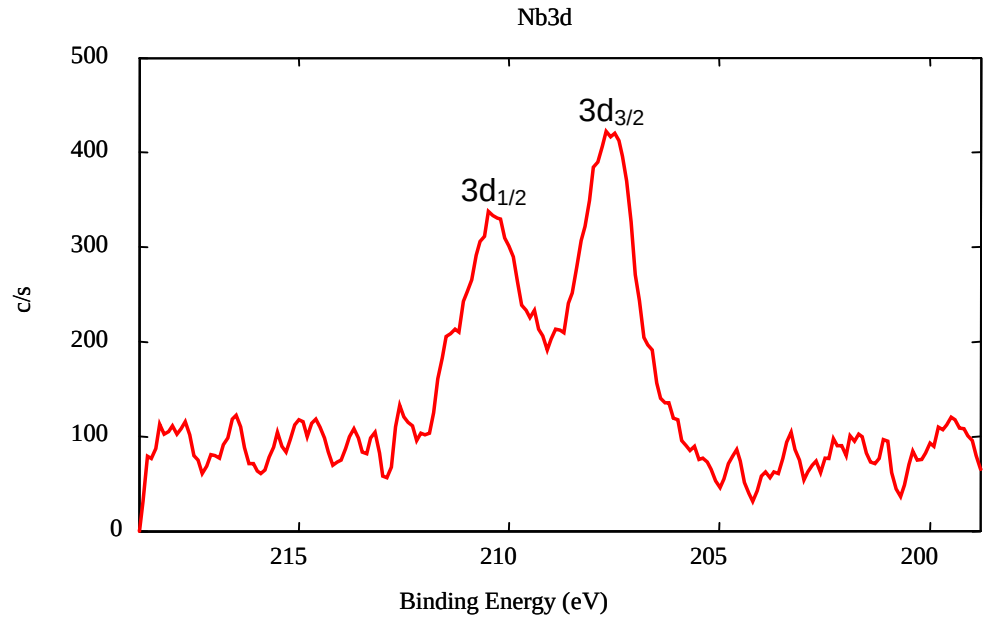

Figure 15. XPS surface analysis results for the dual-stabilized IF steel grade, featuring a Nb 3d3/2 peak whose binding energy is 207.4 eV), which corresponds to Nb^2O^5.

Therefore, it is possible that one of the reasons why the Ti-stabilized IF steel substrate is more reactive than the dual-stabilized IF steel substrate is that there are Nb oxides at the Zn coating-steel substrate interface blocking the Fe-Zn interdiffusion along the ferrite grain boundaries on the dual-stabilized IF steel substrate, whose Nb content is much higher than that for the Ti-only-stabilized IF steel substrate.

Regarding the setting up for GA heat treatment profiles for both IF steel grades, the GA heat treatment temperature chosen for the HDG simulator experiments was 510 ^{0}C. However, as the IF steel substrate reactivity depends on the Ti and Nb bulk concentrations, experiments were carried out in order to attain the GA heat treatment time necessary to produce a 1 µm-thick Γ layer on top of both IF steel substrates.

As indicated by the mainstream literature on IF steels, Ti-stabilized IF steel substrates are more reactive than dual-stabilized IF steel substrates. Therefore, the time necessary to produce a 1 µm-thick Glayer on top of a Ti-stabilized IF steel substrate (8 s) is shorter than for dual-stabilized IF steel substrates (15 s).

Figures below feature the GD-OES Fe, Zn and Al elemental concentrations across the GA coating for both IF steel substrates after GA heat treatment at 510 ^{0}C and GA heat treatment times mentioned above, according to the IF steel substrate.

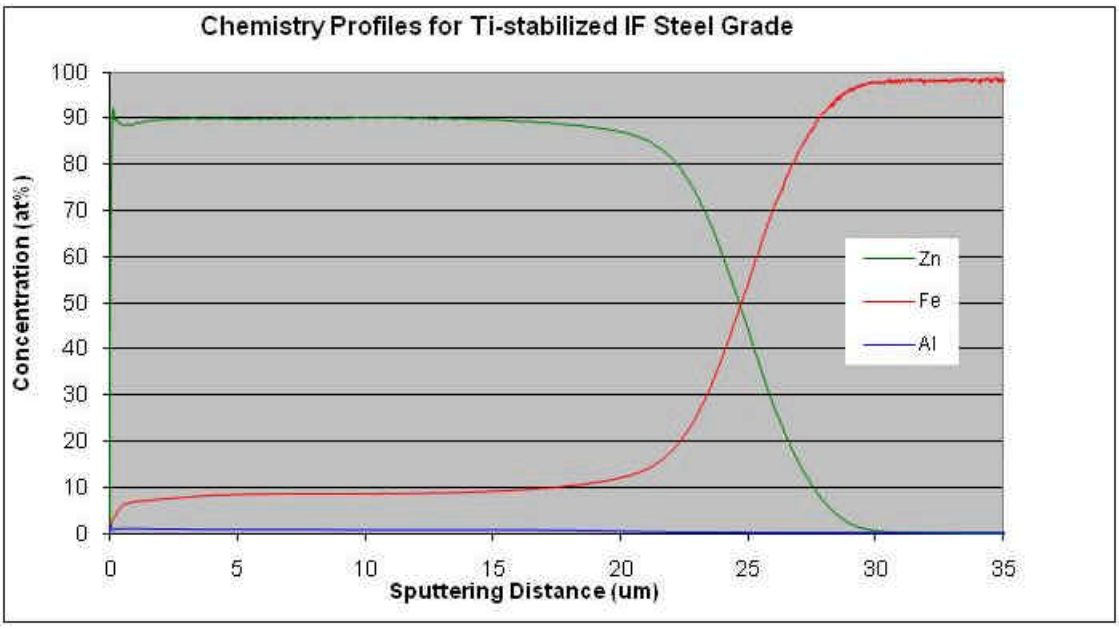

Figure 16. GD-OES Zn, Fe and Al atomic concentration across GA coating for a Ti-stabilized IF steel substrate.

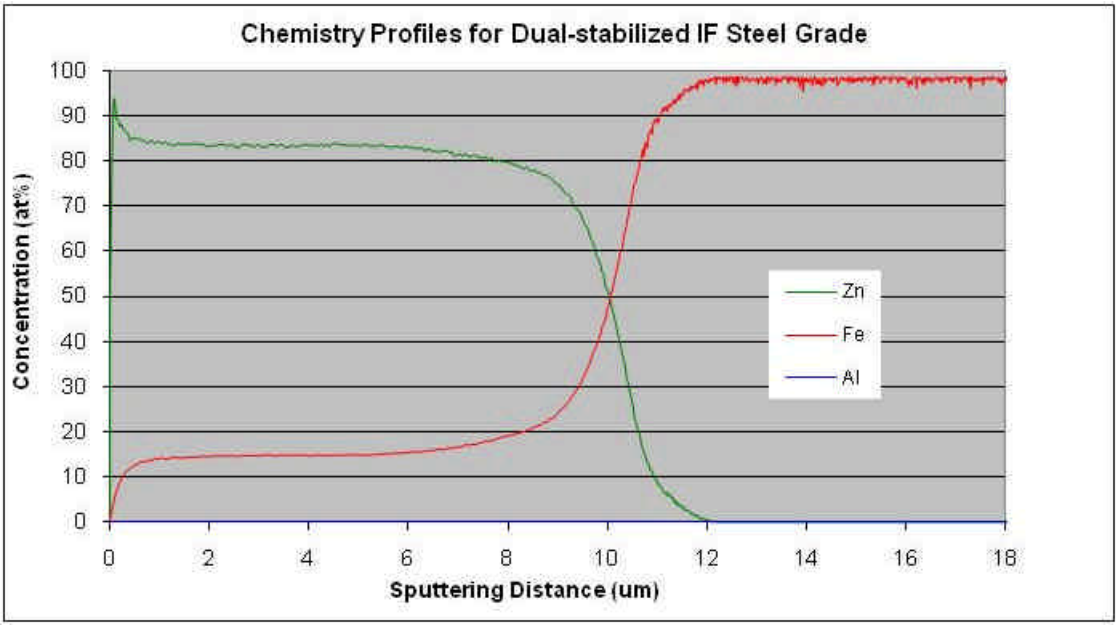

Figure 17. GD-OES Zn, Fe and Al atomic concentration across GA coating for a dual-stabilized IF steel substrate.

Even though the GA coating thicknesses observed for Ti- and dual-stabilized IF steels had not been uniform throughout the HDG simulation experiments, it is worth pointing out that the purpose of this project does not include setting up a uniform GA coating thickness, especially as it has neither straight correlation with IF steel substrate reactivities nor cratering formation mechanisms.

Regarding the surface concentration for alloying elements Ti and Nb across GA coatings for both IF steels, GD-OES experiments carried out on top of GA coated samples pointed out that both Ti outermost concentrations as well as Ti concentrations at the GA coating-steel substrate interface are significantly lower than those found at the bulk steel substrate, regardless of the IF steel substrate.

On the other hand, GD-OES elemental analysis for Nb have shown that both Nb outermost concentration as well as Nb concentrations at the GA coating-steel substrate interface are much higher than those found at the respective bulk steel substrate, regardless of the IF steel substrate.

Figures 18 and 19 feature the alloying element concentrations along the GA coating for both IF steel substrates.

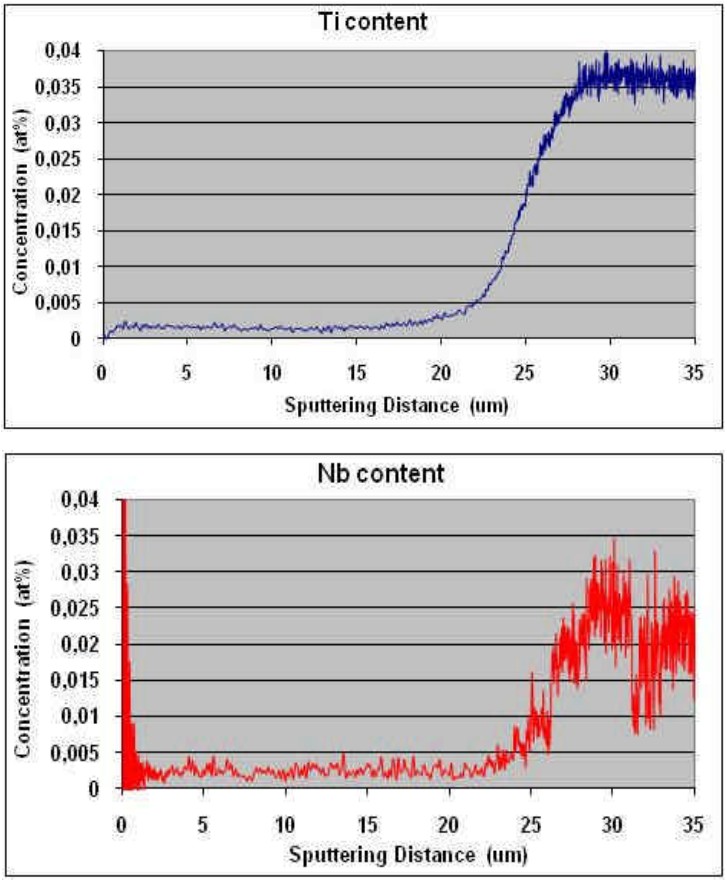

Figure 18. Ti and Nb concentrations along a 30 µm-thick GA coating on top of a Ti-stabilized IF steel substrate.

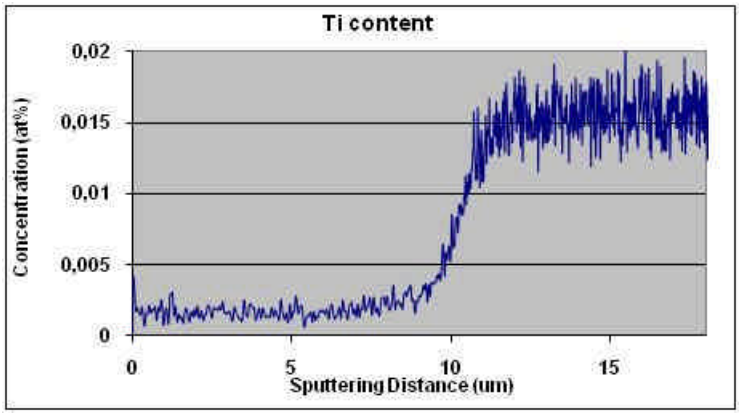

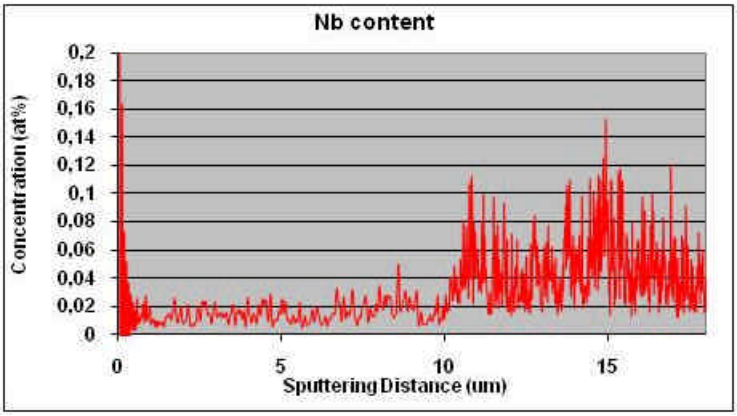

Figure 19. Ti and Nb concentrations along a 12 µm-thick GA coating on top of a dual-stabilized IF steel substrate.

4.3. CRATER ANALYSIS ON TOP OF GA COATINGS

4.3.1. CRATER ANALYSIS ON LIGHT AND DARK STREAKED AREAS FOR AS-RECEIVED GA COATINGS

Both light stereoscope and optical microscope micrographs were taken from the samples with streaks on top of GA coating. Two distinct types of streaks were found, a dark and a light one, which owe their distinctive features to differences in reflectivity and chemistry non-uniformity on top of the GA coating.

Figure 20 shows light stereoscope pictures featuring macro overviews of streaked regions on top of GA coatings.

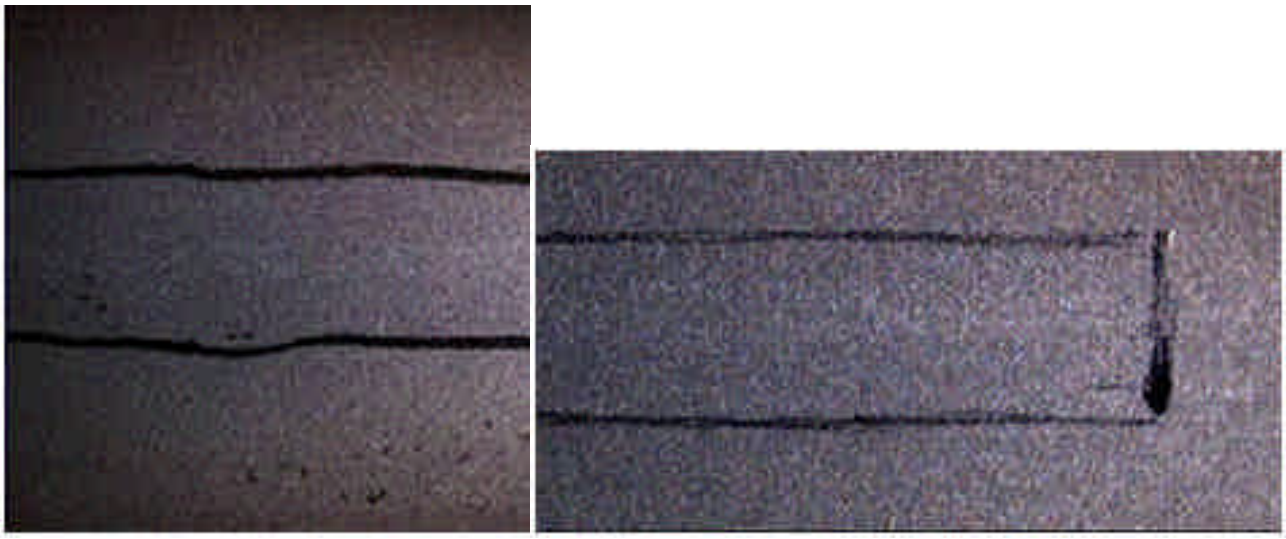

Figure 20. Stereoscope micrographs featuring light and dark streaked areas on top of GA coatings for Ti-stabilized IF steels. Magnification: 6.5 x.

After that, SEM image analysis was used to magnify the region on dark and light streaked areas, as can be seen on figure 21.

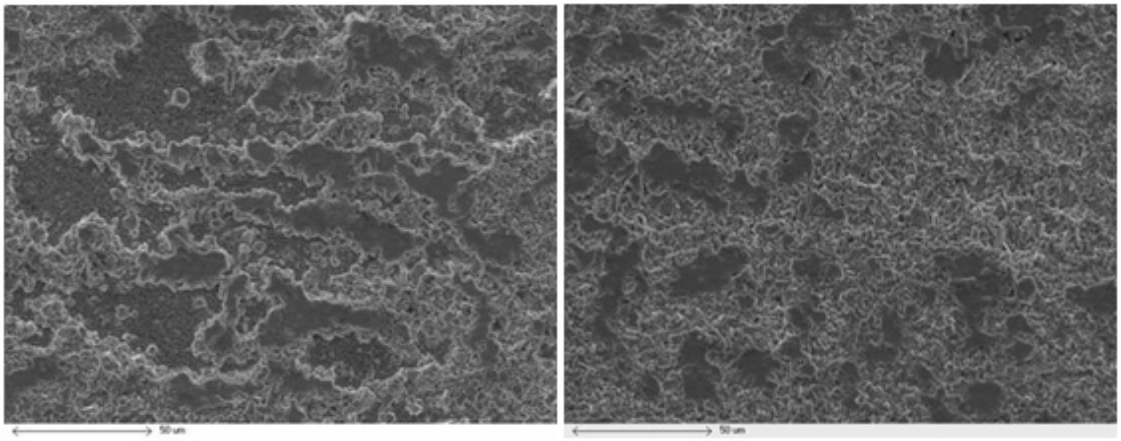

Figure 21. SEM micrographs featuring light (right-hand side) and dark (left-hand side) streaked areas on top of GA coatings for Ti-stabilized IF steels. Magnification: 573 x.

Furthermore, zooming in the SEM magnification within the light and dark streak areas, craters were found on the bottom of these regions. The areas featuring dark streaked areas showed a higher crater coverage when compared with the light streaked regions. EDS chemistry measurements were then carried out and showed that δ crystals were found on the bottom of craters on light streaked areas, whereas there is Γ layer on the bottom of craters on dark streaked areas. Therefore, the craters on dark streaked regions are deeper

than those on light streaked areas. Micrographs and typical chemistries found for both kinds of craters are shown on figure 22.

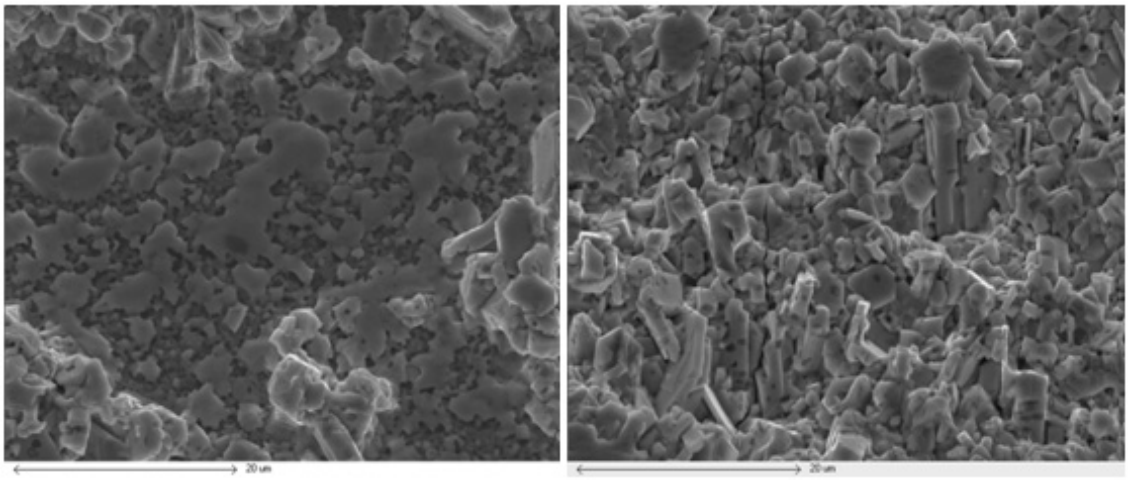

Element	wt%	at%
Al	1.91	4.35
Fe	21.39	23.54
Zn	76.70	72.11

Element	wt%	at%
Al	0.60	1.41
Fe	11.39	12.97
Zn	88.02	85.62

Figure 22. SEM images at 2300x featuring typical microstructures for a dark streaked area (left-hand side), whose EDS chemistry taken from the bottom matches a G phase, and light streaked area (right-hand side), whose chemistry is typical of a d phase.

4.3.2. SAMPLES RUN UNDER SPECIAL COOLING CONDITIONS AT THE HOT-DIP PROCESS SIMULATOR

Regarding the Ti- and dual-stabilized IF steel panels that run interrupted thermal cycles under special cooling conditions at the HDP simulator in order to reproduce the operating conditions for crater formation in a CGL, further SEM analysis and EDS chemistry results showed that craters were only found on top of GA coatings for Ti-stabilized IF steel substrates, no matter if the panels were heat treated for 0s, 2s or 4s. On the other hand, no craters were found for dual-stabilized IF steel samples, regardless of the GA heat treatment time. Therefore, contending the previous work by most part of authors, Ti-stabilized IF steel substrates are more prone to crater formation than dual-stabilized IF steel substrates. Figure 23 shows the overall GA coating surface for the panels run for both IF steel grades.

Figure 23. Pictures feature the overall look of Ti- (left-hand side) and dual-stabilized (right-hand side) IF steel panels that run interrupted GA thermal cycles under faster cooling rates.

Moreover, Ti-stabilized IF steel panels featuring light and dark streaked areas on top of their GA coating were taken to the Scanning Electron Microscope for the purpose of streak and crater characterization through SEM micrographs and EDS chemistry, whose results are shown on figures 24 and 25.

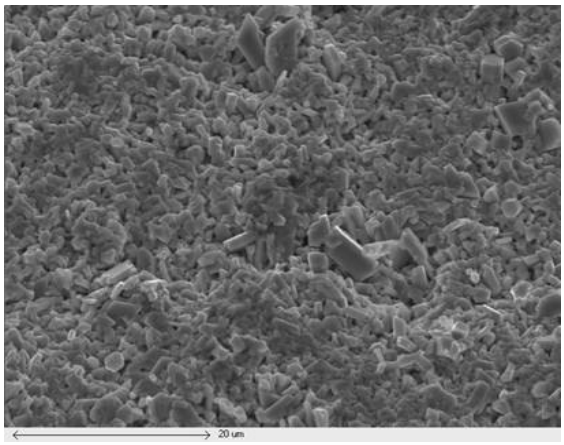

Panel Sampled after 2s GA Heat Treatment Time		
SEM Image – 2020x		
Element	Concentration (wt%)	Concentration (at%)
Al	2.11	4.89
Fe	9.28	10.39
Zn	88.61	84.72

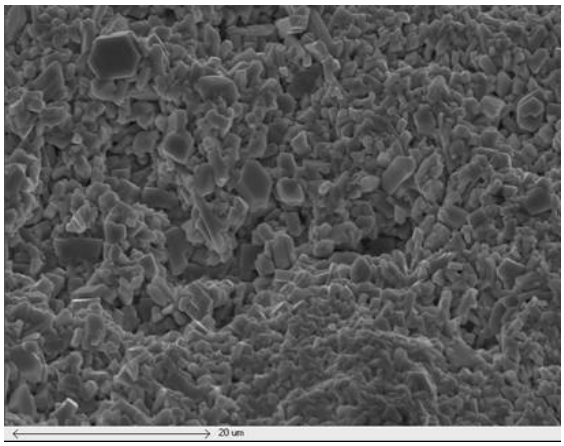

Panel Sampled after 4s GA Heat Treatment Time		
SEM Image – 2020x		
Element	Concentration (wt%)	Concentration (at%)
Al	0.25	0.60
Fe	10.89	12.47
Zn	88.85	86.92

Figure 24. SEM images and EDS chemistries for craters on bottom of light streaked areas at GA coatings on top of Ti-stabilized IF steel panels after running interrupted GA thermal cycles under faster cooling rates.

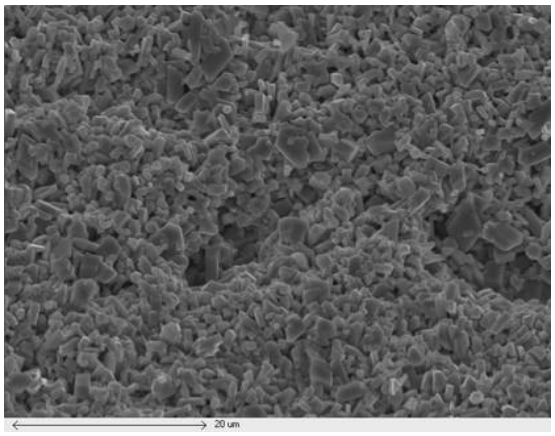

Panel Sampled after 2s GA Heat Treatment Time		
SEM Image – 2020x		
Element	Concentration (wt%)	Concentration (at%)
Al	0.68	1.61
Fe	12.05	13.69
Zn	87.27	84.70

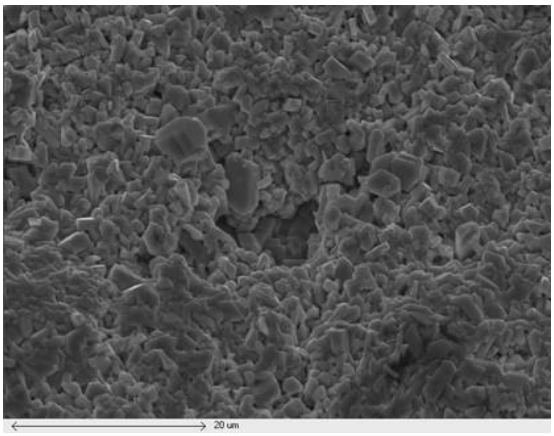

Panel Sampled after 4s GA Heat Treatment Time		
SEM Image – 2020x		
Element	Concentration (wt%)	Concentration (at%)
Al	0.29	0.67
Fe	19.14	21.61
Zn	80.57	77.72

Figure 25. SEM images and EDS chemistries for craters on bottom of dark streaked areas at GA coatings on top of Ti-stabilized IF steel panels after running interrupted GA thermal cycles under faster cooling rates.

The EDS chemistries found at the bottom of the craters proved that d crystals are connected with light streaked areas whereas Gphase is linked with dark streaked regions.

4.4. STEEL SUBSTRATE REACTIVITY ALONG FERRITE GRAIN BOUNDARIES ON Ti- AND DUAL-STABILIZED IF STEEL SUBSTRATES:

According to the literature, Ti-bearing precipitates, mainly TiN, segregate to regions far from the ferrite grain boundaries, for the reasons explained on previous sessions. Therefore, those compounds are responsible for “cleaning” the ferrite grain boundaries for speeding up further Fe and Zn interdiffusion along the ferrite grain boundaries by the time the steel sheet is immersed into the Zn galvanizing bath.

On the other hand, Nb-bearing precipitates, mainly NbC compounds, segregate to ferrite grain boundaries. Thus the Nb compounds get in the way of Fe and Zn interdiffusion along the grain boundaries as the steel sheet is immersed into the Zn galvanizing bath.

The results obtained by this research agree with the statements above. The galvanneal heat treatment time at 510°C necessary to end up with a 1 µm-thick G layer on top of the

steel substrate was longer for the dual-stabilized IF steel substrate when compared with shorter heat treatment times needed for Ti-stabilized IF steel substrate.

4.4.1. REGIONS OF HIGH REACTIVITY AND FORMATION OF OUTBURSTS

The absence of Ti precipitates, mainly TiN compounds, at the ferrite grain boundaries mean that the Ti-stabilized IF steel substrates are more reactive than the dual-stabilized IF steel substrates.

Therefore, Ti-stabilized IF steel substrates are more prone to outburst formation than dual-stabilized IF steel grades due to the faster Fe and Zn interdiffusion right after the steel sheet enters the Zn bath.

Furthermore, literature reports that craters are clusters of outbursts on top of the GA coatings, which blocks the nucleation and growth of Fe-Zn intermetallic phases on top of the steel substrate. Indeed, no craters were found amid the GA coatings on top of dual-stabilized IF steel panels, regardless of the GA heat treatment time.

4.4.2. REGIONS OF HIGH REACTIVITY AND FORMATION OF CRATERS ON LIGHT AND DARK STREAKED AREAS

Literature reports that the brightness differences on cratered regions on top of GA coatings are due to differences in reflectivity.

Indeed, the SEM as well as EDS results showed that there are two different kinds of craters on bottom of GA coatings, as follows: dark craters due to the presence of G layer on their bottom; light craters due to the presence of d crystals on their bottom.

Therefore, the research results agree with the literature.

4.5. THE EFFECT OF THE DIFFUSION OF IF STEEL ALLOYING ELEMENTS TOWARDS THE INTERFACE BETWEEN IF STEEL SUBSTRATES AND GA COATINGS ON CRATER FORMATION

The experimental results presented above have shown that IF steel alloying elements, namely Ti and Nb, feature distinctive characteristics at the GA coating-steel substrate interface.

The Ti and Nb free atoms in solid solution scattered across the typical ferrite microstructure of IF steels are bound to segregate as soon as the temperature is risen, therefore thermodynamics as well as kinetics play an important role when it comes to GA coating-steel substrate alloying element segregation.

Finally, based on the bulk chemistry given for each IF steel grade, useful formulas are frequently used in order to estimate the final free amount of Ti and Nb left in solid solution, taking into account the C, P, N and S contents at the bulk of the respective steel substrate.

4.5.1. Ti DEPLETION AT THE STEEL SUBSTRATE-GA COATING INTERFACE;

The experimental procedures carried out by this research have shown that the outermost surface of the steel substrates are free from Ti-bearing compounds shortly before the strip enters the Zn pot.

The statement above has been proved by suddenly stopping the thermal cycle at the HDG simulator and taking the steel coupon at the spot whose temperature and time set the conditions for Zn bath entrance for both IF steel substrates i.e. the surface condition upon which the steel substrate is submitted to Zn wetting.

As mentioned before, GD-OES elemental analysis were carried out for bare IF steel samples, and those representing the setting condition for the Zn bath immersion featured no Ti contents whatsoever above the average Ti content found in the bulk of the steel substrate.

Therefore, the Ti depletion at the surface of both IF steel substrate means that Ti-bearing compounds have no influence whatsoever on the Fe-Zn interdiffusion rates along the interface between the steel substrate and the GA coating, even for short circuit paths for diffusion i.e. ferrite grain boundaries.

4.5.2. Nb ENRICHMENT AT THE STEEL SUBSTRATE-GA COATING INTERFACE

The experimental procedures carried out by this research have shown that the outermost surface for both IF steel substrates at the time of strip entrance into the Zn bath feature a Nb concentration significantly higher than the Nb contents found in the bulk of both IF steel substrates.

The statement above has been proved by suddenly stopping the thermal cycle at the HDG simulator and taking the steel coupon at the spot whose temperature and time set the conditions for Zn bath entrance for both IF steel substrates i.e. the surface condition upon which the steel substrate is submitted to Zn wetting.

As mentioned before, GD-OES elemental analyses were carried out for bare IF steel samples, and those representing the setting condition for the Zn bath immersion featured higher Nb concentrations than those found at the bulk of both IF steel substrates.

Furthermore, XPS analysis have shown that the Nb-bearing compounds at the surface of steel coupons taken from the HDG simulator correspond to Nb oxides in the form of Nb_2O_5.

Therefore, the Nb enrichment at the surface of both IF steel substrate means that it affects the steel substrate reactivity, thus Nb oxides get in the way of Fe-Zn interdiffusion rates along the interface between the steel substrate and the GA coating by slowing down the Fe and Zn diffusivities across the interface.

Moreover, as typical bulk Nb contents are much higher for dual-stabilized IF steel grades when compared with those for Ti-stabilized IF steel grades, the effect of Nb surface

enrichments upon the reactivity of dual-stabilized IF steel grades is much improved when compared with Ti-stabilized IF steel substrates.

Indeed, the longer GA heat treatment times necessary to produce a 1 µm-thick G layer on top of dual-stabilized IF steel substrates when compared with the shorter ones necessary for Ti-stabilized IF steel substrates are enough to prove the statement above.

4.5.2.1. MECHANISMS FOR DRIVING Nb OXIDATION AT THE STEEL SUBSTRATE-GA COATING INTERFACE.

After cold-rolling to final thickness, steel sheets need to be recrystallized in order to recover intrinsic ductility for cold forming and drawing applications. This annealing treatment is performed either by batch-annealing of tight coils for long soaking times at intermediate temperatures or by continuous annealing of steel strip at higher temperature for shorter times, the later being the case carried out by this Master's thesis.

Therefore, a protective atmosphere based on either N_2-H_2 mixed gas or pure hydrogen is present in the furnace. This atmosphere is surely reducing for Fe but very often oxidizing for more reactive alloying or residual elements present in the steel, depending on the residual oxygen content and dew point of the concerned protective atmosphere.

In such conditions, it is anticipated that selective oxidation of alloying elements will take place at the steel surface producing extremely different surface chemistries for steel sheets, what results in different chemical reactivities in subsequent finishing treatments, for instance Zn coating by hot-dipping.

Wagner et al.[68] have put forward the theoretical basic principles of a mathematical model describing selective oxidation in ideal single crystal binary alloys where it is assumed that selective oxidation is governed by the interdiffusion of reactive species.

Moreover, both the localization of the reaction and precipitation front relative to the free surface depends on the balance between the inward oxygen and outward oxidizable solute

element flows. For well balanced flows, reaction as well as oxide precipitation are observed beneath the free surface and selective oxidation is called internal.

On the other hand, external oxidation can be treated like a particular case of the internal mode, when selective surface oxide precipitation, resulting from inward and outward flow balance is predominant enough as to obstruct all oxygen diffusion paths.

However, the complexity of the steel chemistries and the possibility to form complex or mixed oxides made the use of the Wagner's model quite difficult. For instance, the Wagner criterion cannot account for the grain boundary oxidation process observed in specific cases. Indeed, it is proposed to take account of selective oxidation at grain boundary by rewriting the Wagner criterion in such a form that the accelerated diffusion flows of oxygen and alloying element along these grain boundaries are considered.

However, due to the complex chemistry of steels, predictions based on relations derived from Wagner's criterion applied to bulk or grain boundary diffusion are generally far from accurate.

Regarding the Nb selective oxidation, it is considered by Birks and Meier[69] as a system with significant scale cracking. The high temperature oxidation of Nb is characterized by inward diffusion of oxygen through the scale. Initially, a protective layer is formed but, as the scale grows, the formation of oxide at the scale-metal interface stresses the oxide resulting in scale cracking and a breakaway linear oxidation.

Indeed, finding out the driving mechanisms for surface Nb oxide formation has not been the concern of this Master's thesis. As mentioned earlier XPS analysis on the bare surface for dual-stabilized IF steel substrates whose samples were taken at setting conditions for hot-dipping into the Zn bath has found Nb-bearing compounds namely Nb_2O_5.

Further recommendations for the follow up of this work include the following issues to be addressed focusing on further assessing the Nb oxide formation mechanisms:

- Transmission Electron Microscopy as a tool to spot the right location of Nb oxides on top of the dual-stabilized IF steel samples i.e. whether they are placed at the ferrite grain boundary intersections or along the bulk of the ferrite grains;

- Attaining a mathematical model in order to assess the mechanisms upon which free Nb has been driven outwards and tying up with oxygen as well as the thermodynamics (temperature and pressure conditions) behind the driving force for such mechanism.

4.5.3. EFFECT OF Ti AND Nb SURFACE SEGREGATION ON CRATER FORMATION

Literature in general has stated that craters on top of galvanneal coatings are formed due to the presence of liquid Zn close to ? crystals right after the strip entrance to the Zn bath. Provided the reactivity of the steel substrate is quite high, i.e. high Fe-Zn interdiffusivity along the ferrite grain boundaries, the liquid Zn is drained towards the outbursts formed at the GA coating-steel substrate, thus creating the streaks, which are clusters of craters on top of GA coatings.

Furthermore, some authors have found that high Ti contents at the IF steel substrates are prone to streak formation, thus proving the statement above.

The first task of this research toward craters was to provide its thorough characterization through optical microscope analysis, SEM microanalysis as well as EDS chemistry analysis on industrial samples taken from Ti-stabilized IF steel substrates.

Sample microanalysis carried out through optical microscope found that there are two basic types of streaks, i.e. cluster of craters on top of GA coatings, light and dark streaked areas.

Moreover, SEM analysis proved that the craters found on the bottom of light streaked areas are different than those found on the bottom of dark streaked areas when it comes to crater density and chemistry.

Therefore, the average crater density for dark streaked areas is significantly higher than for light streaked areas. Additionally, the EDS analysis carried out for both types of craters concluded that the chemistry for the bottom of craters on light streaked areas is similar to d Fe-Zn intermetallic phase, whereas the chemistry for the bottom of dark streaked areas is similar to GFe-Zn intermetallic phase.

Having said that, we can now point out that craters on dark streaked areas are deeper than those found on light streaked areas.

In order to replicate the industrial condition at the HDG simulator, bare samples were spared for both IF steel substrates, taking into account the thermal profiles set up thus far. However, the GA heat treatment was suddenly interrupted at three different spots and then cooling rates right after GA heat treatment were changed in order to enhance the kinetics towards crater formation by using He gas in a special cooling chamber.

Results from this experimental procedure pointed out that craters were only found at GA coatings on top of Ti-stabilized IF steel substrates regardless of the GA heat treatment time. On the other hand, no craters were found at GA coatings on top of dual-stabilized IF steel substrates regardless of the GA heat treatment time.

Therefore, as agreed with the literature in general, Ti content indeed plays an important role on streak and crater formation on top of GA coatings.

5. CONCLUSIONS

Ti depletion was found at the outermost surface on both IF steel grades, whereas this region features a strong Nb enrichment.

According to XPS analysis, this Nb surface enrichment corresponds to Nb oxides (Nb_2O_5). The presence of Nb oxides at the surface of dual-stabilized IF steel substrates may block the Fe-Zn interdiffusion along the ferrite grain boundaries.

Simulations under special cooling conditions at the Hot-Dip Process Simulator found streaks only on Ti-stabilized IF steel substrate.

There is higher crater density on dark streaked areas when compared with light streaked regions of IF galvannealed steels.

δ crystals were found on the bottom of craters on light streaked areas, whereas there is Γ phase on the bottom of craters on dark streaked areas. Also, the craters on light streaked areas are shallower than those on dark streaked areas.

Due to the presence of Nb oxides at the interface between the Zn coating and the dual-stabilized IF steel substrate, the Ti-only-stabilized IF steel substrate is more reactive and consequently more prone than the dual-stabilized IF steel substrate to the formation of outbursts, and consequently craters.

6. ACKNOWLEDGEMENTS

We would just like to say many thanks to each and every person who have been in some way connected with the experimental procedures as well as the results presented on this research project. Among them it is noteworthy to include the sponsors for the Master's project whose framework this work comes from i.e. CBMM as well as ArcelorMittal Tubarão's Customer Service and HR personnel, especially for the necessary support throughout my two-year stint as a Master's student at McMaster University in Canada. Besides them, special acknowledgments must be made to the supervisors whose valuable coaching has been paramount towards the soundness of the results attained, as such Dr Fernando Gabriel Araújo at Redemat/UFOP as well as Dr Joseph McDermid at McMaster University, also including MSE faculty, staff and alumni.

7. BIBLIOGRAPHY

1. Bhattacharya, D. and Cheng, C. *Mechanism of the Effect of Nb on the Galvannealing Behavior of IF Steels.* Proceedings of the 6th International Conference on Zinc and Zinc Alloy Coated Steel Sheet (GALVATECH'04), pp. 509-516, Chicago, 2004

2. Jordan, C. E. and Marder, A. R. *Effect of Substrate Grain Size on Iron-Zinc Reaction Kinetics during Hot-Dip Galvanizing.* Metallurgical and Materials Transactions A, volume 28A, December 1997, pp. 2683-2694, 1997

3. Osman, T. M. and Garcia, I. *Niobium-Bearing Interstitial-Free Steels: Processing, Structure and Properties.* Pittsburgh, USA: Basic Metals Processing, Research Institute

4. Feliu, S. and Perez-Revenga, M. L. *Effect of the Presence of Alloying Elements in Interstitial-Free and Low-Carbon Steels on their Surface Composition after Annealing in Reducing Atmospheres (Dew Point = -30^{0}C).* Madrid, Spain: CENIM (CSIC), 2003

5. Edwards, C.A.; Phillips, D. L.; Jones, H. N.; *The Influence of Some Special Elements Upon the Strain-Ageing and Yield-Point Characteristics of Low-Carbon Steels.* J. Iron and Steel Institute, 142, pp. 199-236. 1940.

6. Codd, I.; Petch, N.J. *Dislocation-Locking by Carbon, Nitrogen and Boron in a-Iron.* Phil. Mag. 5, pp. 30-42. 1960

7. Hook, R.E. *The Effect of Quench-Ageing on Inhomogeneous Yielding of Steels with Very Low Interstitial Solute Content.* Metallurgical Transactions, pp. 85-92. 1970.

8. Marder, A. R. *The Metallurgy of Zinc-Coated Steel.* Progress in Materials Science 45 (2000) pp. 191-271, 2000

9. Lin, C. S. and Meshii, M. *The Effect of Steel Chemistry on the Formation of Fe-Zn Intermetallic Compounds of Galvanneal-Coated Steel Sheets.* Metallurgical and Materials Transactions B, volume 25B, October 1994, pp. 721-729, 1994

10. Baril, E. and L'Esperance, G. *Studies of the Morphology of the Al-Rich Interfacial Layer Formed During the Hot Dip Galvanizing of Steel Sheet.* Metallurgical and Materials Transactions A, volume 30A, March 1999, pp. 681-695, 1999

11. Parks, W. H.; Haggerty, C. S. and Rock, T. R. *Ferritic Rolling of Interstitial-Free Steel.* Iron and Steel Engineer, October 1997, pp. 35-36, 1997

12. van der Heiden, A.; Burghardt, A. J. C.; van Koesveld, W.; van Perlstein, E. B. and Spanjers, M. G. J. *Galvanneal Microstructure and Anti-Powdering Process Windows.* The Physical Metallurgy of Zinc Coated Steel, pp. 251-263, 1993

13. McDevitt, E. T. and Meshii, M. *Microstructural Evolution During Galvannealing. Part II: Formation and Growth of the Fe-Zn Intermetallic Compounds.* Proceedings of the 4th International Conference on Zinc and Zinc Alloy Coated Steel Sheet (GALVATECH'98), Chiba, Japan, The Iron and Steel Institute of Japan, 1998

14. McDevitt, E. T.; Morimoto, Y. and Meshii, M. *Microstructural Evolution During Galvannealing. Part 1: Formation and Breakdown of the Fe-Al Inhibition Layer.* Chiba, Japan: The 4th International Conference on Zinc and Zinc Alloy Coated Steel Sheet (GALVATECH'98). The Iron and Steel Institute of Japan, 1998

15. McDevitt, E. T.; Pelayo, L; Morimoto, Y. and Meshii, M. *Investigation of the Fe-Al Inhibition Layer Formed During Hot-Dip Galvannealing.* 39th MWSP Conference Proceedings, ISS, vol. XXXV, pp. 127-135, 1998

16. Dionne, S.; Charest, M.; Botton, G. and Goodwin, F. *Influence of Substrate Characteristics on the Inhibition Layer Breakdown and Galvannealing Kinetics.* 44th MWSP Conference Proceedings, vol. XV, pp. 405-415, 2002

17. Jordan, C. E. and Marder, A. R. *Alloy Layer Growth During Hot-Dip Galvanizing at 450^{0}C.* Proceedings of The 5th International Conference on Zinc and Zinc Alloy Coated Steel Sheet (GALVATECH'95), pp. 319-325, Chicago, USA, 1995.

18. McDevitt, E. T.; Morimoto, Y. and Meshii, M. *Microstructural Characterization of the Fe-Al Inhibition Layer on Commercial Hot-Dip Galvanized IF Steel.* 39th MWSP Conference Proceedings, ISS, vol. XXXV, pp. 215-223, 1998

19. O'Dell, S. P.; Charles, J. and Randle, V. *The Formation of Craters Within the Galvanneal Coating and their Effects on Processing Properties.* 44th MWSP Conference Proceedings, vol. XL, pp. 1299-1307, 2002

20. Lee, H. J. and Kim, J. S. *Effect of Ni Addition in Zn Bath on Formation of Inhibition Layer During Galvannealing of Hot-Dip Galvanized Sheet Steels.* Journal of Materials Science Letters 20, pp. 955-957, 2001

21. McDermid. J. R.; Baril, E. and Thompson, W. T. *Fe Solubility in the Zn-Al-Fe System for Use in Continuous Galvanizing and Galvannealing.* Hamilton, ON, Canada: Department of Mechanical Engineering, McMaster University

22. Miyasaka, A. and Matsumura, K. *Influence of Alloying Elements in Steel on Galvannealing Behavior of Interstitial-Free (IF) Steels.* Proceedings of The 4th International Conference on Zinc and Zinc Alloy Coated Steel Sheet (GALVATECH'98), pp. 186-189, Chiba, Japan, The Iron and Steel Institute of Japan, 1998.

23. Jordan, C. E.; Zuhr, R. and Marder, A. R. *Effect of Phosphorus Surface Segregation on Iron-Zinc Reaction Kinetics during Hot-Dip Galvanizing.* Metallurgical and Materials Transactions A, volume 28A, December 1997, pp. 2695-2703, 1997

24. Perrot, P; Tissier, J. C. and Dauphin, J. Y. *Stable and Metastable Equilibria in the Fe-Zn-Al System at 450^{0}C.* Villeneuve d'Ascq, Cedex, France: Laboratoire de Metallurgie Physique, Universite de Lille, 1992

25. Shindo, Y. *Effect of Different Alloying Elements in Steel on Galvanneal Coating Formation.* Ispat Inland Research and Development

26. Maschek, W.; Hayes, S. P. and Marder, A. R. *Cross Sectional Studies of Zinc Iron Phase Growth in an Environmental Scanning Electron Microscope.* Proceedings of The 5th International Conference on Zinc and Zinc Alloy Coated Steel Sheet (GALVATECH'95), Chicago, USA, 1995.

27. Zhong, W.; Ng, H. F. and James, J. M. *Correlation Between Adhesion Properties and the Interfacial Bonding Strength of Galvanneal Coatings.* Proceedings of the 4th International Conference on Zinc and Zinc Alloy Coated Steel Sheet (GALVATECH'98), Chiba, Japan, The Iron and Steel Institute of Japan, 1998

28. Angeli, G.; Deinhammer, H.; Faderl, J.; Angeli, J.; Papst, I. and Wolpers, M. *Distribution and Composition of Surface Oxides on High Strength IF-Steels after Recrystallization Annealing.* 44th MWSP Conference Proceedings, vol. XL, pp. 825-832, 2002

29. Feliu, S.; Perez-Revenga, M. L. and Barranco, V. *Persistence of Superficial Contamination of Rolled Steel during Successive Treatments up to the Formation of a Galvanneal Coating.* Metallurgical and Materials Transactions A, volume 35A, July 2004, pp. 2185-2187, 2004

30. Faderl, J.; Strutzenberger, J. and Fischer, W. *Galvannealed Steel Sheet: 10 Years of Experience on Product and Process Improvement.* Linz, Austria: Voest Alpine Stahl

31. van Koesveld, W.; Lamberigts, A.; van der Heiden, A. and Bordignon, L. *Coating Microstructure Assessment and Control for Advanced Product Properties of Galvannealed IF Steels.* Proceedings of the 3rd International Conference on Zinc and Zinc Alloy Coated Steel Sheet (GALVATECH'95), pp. 343-354, 1995

32. Hashiguchi, K.; Yasuda, A.; Hanazawa, T; Ohori, M. and Ichida, T. *Galvannealed Sheet Steel with Excellent Press Formability.* La Revue de Métallurgie – CIT, Mars 1990, pp. 277-283, 1990

33. Miner, R. E. and Butler, J. F. *Comparison of Product Characteristics of Electrogalvanized and Galvannealed for Exposed Automotive Applications.* Proceedings of The 5th International Conference on Zinc and Zinc Alloy Coated Steel Sheet (GALVATECH'95), pp. 407-412, Chicago, USA, 1995.

34. Elias, C. N.; Alcala-Vela, J. and Maestri, C. *Microstructural Analysis of Galvannealed Coating by Grazing-Incidence X-Ray Diffraction.* Volta Redonda, RJ, Brazil: Escola de Engenharia Metalúrgica de Volta Redonda

35. Ebrill, N.; Durandet, Y. and Strezov, L. *Dynamic Wetting and its Influence on Interfacial Resistance during Hot Dip Galvanizing.* Shortland, Australia: BHP Minerals Technology

36. Zhong, W.; Ng, H. F. and Ichikawa, M. *Effect of Coating Characteristics on Powdering Performance of Galvanneal Coatings.* Proceedings of the International Symposium held at the TMS Annual Meeting, San Antonio, Texas, 1998

37. Wilmotte, S.; Fischbach, J. P. and Hardy, Y. *Control of the Galvannealing Process.* CRM-Belgium, SEGAL-Belgium

38. Lamberigts, M.; Beguin, M.; Dubois, M.; van der Heiden, A. and Verhoeven, G. *Kinetics of Fe-Zn Reactions During Galvannealing.* CRM, Segal, Cockerill Sambre, Hoogovens Groep B.V, N. V. Sidmar. Belgium. The Netherlands

39. Divinski, S. V.; Geise, J.; Rabkin, E. and Herzig, Chr. *Grain Boundary Self-Diffusion in α-Iron of Different Purity: Effect of Dislocation Enhanced Diffusion.* Z. Metallkd. 95 (2004) 10, pp. 945-952, 2004

40. Faderl, J.; Pimminger, M. and Schönberger, L. *Influence of Steel Grade and Surface Topography on the Galvanneal Reaction.* Voest-Alpine Stahl Linz GmbH

41. Drillet, P.; Dulcy, C.; Pazsko, F.; Mangelinck, D.; Gas, P.; Clugnet, G.; Bergman, C. and Vaughan, G. *Real Time Synchrotron Analysis of the Initial Stages of the Galvanization Process in Al Containing Zn Baths.* La Revue de Métallurgie-CIT, Janvier 2005, pp. 75-78

42. Rege, J. S.; Hua, M.; Garcia, C. I. and DeArdo, A. J. *The Segregation Behavior of Phosphorus in Ti and Ti + Nb Stabilized Interstitial-Free Steels.* ISIJ International, vol. 40 (2000), no. 2, pp. 191-199, 2000

43. Nassar, A.; Vipond, R. and Mintz, B. *Influence of Intercritical Annealing on Strength and Impact Behavior of Niobium Containing Steels.* Materials Science and Technology, August 1991, vol. 7, pp. 699-706, 1991

44. Alaoua, D.; Larere, A.; Lartigue, S. and Priester, L. *Interfacial Segregation in Ultra-Low Carbon Steels.* Materials Science Forum vol. 126-128 (1993), pp. 185-188, 1993

45. Olefjord, I.; Leijon, W. and Jelvestam, U. *Selective Surface Oxidation During Annealing of Steels Sheets in H_2/N_2.* Applications of Surface Science 6 (1980) pp. 241-255, 1980

46. Alaoua, D.; Lartigue, S.; Larere, A. and Priester, L. *Precipitation and Surface Segregation in Low Carbon Steels.* Materials Science and Engineering, A189 (1994), pp. 155- 163, 1994

47. Hua, M.; Garcia, C. I. and DeArdo, A. J. *Precipitation Behavior in Ultra-Low-Carbon Steels Containing Titanium and Niobium.* Metallurgical and Materials Transactions A, volume 28A, September 1997, pp. 1769-1780, 1997

48. Angeli, G.; Deinhammer, H.; Faderl, J.; Angeli, J.; Papst, I. and Wolpers, M. *Distribution and Composition of Surface Oxides on High Strength IF-Steels after Recrystallization Annealing.* 44th MWSP Conference Proceedings, vol. XL, pp. 825-832, 2002

49. Jordan, C. E. and Marder, A. R. *Fe-Zn Phase Formation in Interstitial-Free Steels Hot-Dip Galvanized at 450 ^{0}C.* Journal of Materials Science 32 (1997), pp. 5593-5602, 1997

50. Feliu Jr., S. and Pérez-Revenga, M. L. *Correlation between the Surface Chemistry of Annealed IF Steels and the Growth of a Galvanneal Coating.* Acta Materialia, March 2005

51. Guttman, M. *Diffusive Phase Transformations in Hot Dip Galvanizing.* Materials Science Forum vols. 155-156 (1994), pp. 527-548, 1994

52. Fujibayashi, N.; Kyono, K.; Kato, C. and Morito, N. *Influence of Carbide-Forming-Elements in Substrate Steels on Galvannealing Behavior.* Proceedings of the 4th International Conference on Zinc and Zinc Alloy Coated Steel Sheet (GALVATECH'98), Chiba, Japan, The Iron and Steel Institute of Japan, 1998

53. Cheng. C. *Galvannealing Behavior and Coating Performance of Ti-Nb and Nb-Ti-IF Steels.* 42nd MWSP Conference Proceedings, ISS, vol. XXXVIII, pp. 255-263, 2000

54. Shindo, Y. *Influence of Precipitates in IF Steel on Galvanneal Coatings Structure.* 42nd MWSP Conference Proceedings, ISS, vol. XXXVIII, pp. 265-276, 2000

55. Miner, R. E. and Butler, J. F. and Dunbar, F. C. *Comparison of Product Characteristics of Electrogalvanized and Galvannealed for Exposed Automotive Applications.* Proceedings of the 3rd International Conference on Zinc and Zinc Alloy Coated Steel Sheet (GALVATECH'95), pp. 407-412, 1995

56. Jordan, C. E. and Marder, A. R. *Inhibition Layer Breakdown and Outburst Fe-Zn Alloy.* Zinc-Based Steel Coating Systems: Production and Performance, pp. 115-126, 1998

57. DeArdo, A. J. *Physical Metallurgy of Interstitial-Free Steels: Precipitates and Solutes.* IF Steels 2000 Proceedings, ISS-AIME, pp. 125-136, 2000

58. Kino. N.; Yamada, M.; Tokunaga, Y. and Tsuchiya, H. *Production of Nb-Ti-added Ultra-Low-Carbon Steel for Galvannealed Application.* Metallurgy of Vacuum Degassed Steel Products, pp. 197-213, 1990

59. Tither, G.; Garcia, C. I.; Hua, M. and DeArdo, A. J. *Precipitation Behavior and Solute Effects in Interstitial-Free Steels.* Physical Metallurgy of IF Steels, ISIJ, pp. 292-322, 1994

60. Puente, J. M.; Alonso, F.; Andrés, L. and Prado, M. *Influence of an Adequate Surface Conditioning on the Final Characteristics of GI for Exposed Panels Use on Automotive Sector.* Proceedings of the 6th International Conference on Zinc and Zinc Alloy Coated Sheet Steels (GALVATECH'04), pp. 457-463, Chicago, 2004

61. Chen, T. R.; Hua, M.; Garcia, C. I. And DeArdo, A. J. *Role of Niobium on the Segregation Behavior of Phosphorus and Manganese in High Strength IF Sheet Steels for Automotive Use.* Developments in Sheet Products for Automotive Applications, Materials Science & Technology 2005, pp. 163-171, 2005

62. Grabke, H. J.; Leroy, V. and Viefhaus, H. *Segregation on the Surface of Steels in Heat Treatment and Oxidation.* ISIJ International, vol. 35 (1995), no. 2, pp. 95-113, 1995

63. Leprêtre, Y.; Mataigne, J. M.; Guttmann, M. and Philibert, J. *Reactive Interdiffusion in the Fe-Al-Zn System: Reaction Mechanisms during Hot-Dip Galvanizing.* Zinc-Based Steel Coating Systems: Production and Performance, pp. 95-106, 1998

64. Misra, R. D. K. *Temperature-Time Dependence of Grain Boundary Segregation of Phosphorus in Interstitial-Free Steels.* Journal of Materials Science Letters 21, pp. 1275-1279, 2002

65. Tang, N. Y. *Thermodynamics and Kinetics of Alloy Formation in Galvanized Coatings.* Zinc-Based Steel Coating Systems: Production and Performance, pp. 3-11, 1998

66. Giorgi, M. L. and Guillot, J. B. *Modeling of the Kinetics of Galvanizing Reactions.* Proceedings of the 6th International Conference on Zinc and Zinc Alloy Coated Steel Sheet (GALVATECH'04), pp. 703-711, Chicago, 2004

67. Leroy, V. *Surface Reaction of Steels in Batch Annealing: Relation with Residual Carbon Contamination and Partial Selective Oxidation.* 1st Internal Conference HICON-H_2. Linz, 1992.

68. Wagner, C. *Elektrochemie*, 63 (1959), 772.

69. Birks, N. and Meier, G. H. *Introduction to High Temperature Oxidation of Metals.* Edward Arnold Publishers. London, 1983.

70. Kaushik, P; Kruse, D.; Ozgu, M. *Assessment of Castability Issues in Interstitial Free Steels.* La Revue de Metallurgie - CIT, Février 2008, pp. 92 – 101.

71. Bordignon, L.; Vanden Eynde, X. *Zinc Wetting During Hot Dip Galvanizing.* La Revue de Métallurgie-CIT, Juin 2007, pp. 300 – 307.

72. Mizui, N. *Precipitation Control and Related Mechanical Property in Ultra-Low Carbon Sheet Steels.* International Symposium on Modern LC and ULC Sheet Steels for Cold Forming: Processing and Properties. Vol. 1, pp. 169-178. Aachen, 1998.